An Evaluation of Digital Methods in Reverse Engineering Using Selected Medical Applications

Andrew Mark Parrott

A dissertation submitted to the Faculty of Engineering, University of the Witwatersrand, Johannesburg, in fulfilment of the requirements for the degree of Master of Science in Engineering.

Johannesburg, October 2004

Declaration

I declare that this is my own, unaided work. It is being submitted for the Degree of Master of Science in Engineering of the University of the Witwatersrand, Johannesburg. It has not been submitted before for any degree or examination in any other University.

_____

Andrew Mark Parrott

Signed this _____ day of _____, 2004

Acknowledgements

Abstract

This dissertation investigates the use of digital modeling methods for selected medical applications. The digital methods include the design of a cranial implant, auricular prosthesis and the duplication of an oral prosthesis. The digital process includes imaging, image processing, design and fabrication steps. Three types of imaging used are contact and non-contact measurement systems and CT scanning. The investigation uses a Phantom haptic device for digital design. The implants and prostheses are fabricated using a Thermojet printer and investment casting. Traditional and digital processes are compared using four case studies on selected criteria. The conclusions of the investigation are that a digital process can be used and is equal to or better than traditional methods in prosthesis and implant design.

Table of Contents

List of Figures

List of Tables

Notation

CAD   Computer Aided Design

CAM   Computer Aided Manufacturing

CCD   Charge Coupled Device

CMM   Coordinate Measuring Machine

CNC   Computer Numerically Controlled

CT   Computerised Tomography

DICOM   Digital Imaging and Communication in Medicine

FDM   Fused Deposition Modelling

HU   Hounsfield Units

ICPM   Iterative Closest Point Matching

MDCT   Multi-Detector Row Computerised Tomography

MJM   Multi Jet Modelling

MPT   Miniature Projection Technique

MRI   Magnetic Resonance Imaging

NM   Nuclear Medicine

NURBS   Non Uniform Rational B-Spline

PC   Personal Computer

PET   Positron Emission Tomography

PMMA   Poly-methyl-methacrylate

RE   Reverse engineering

RP   Rapid Prototyping

SDCT   Single-Detector Row Computerised Tomography

SLA   Stereolithography Apparatus

SLS   Selective Laser Sintering

SPECT   Single Photon Emission Computed Tomography

STL   Stereolithography file format

2D   Two Dimensional

3D   Three Dimensional

1   Introduction

1.1 Background

This dissertation uses digital technologies for the design and manufacture of custom cranial implants and prostheses for human patients. Prosthodontists (prosthetic dentists) traditionally make prostheses by carving them from a block of wax. The prosthodontist uses investment casting to convert the wax model into a silicone prosthesis. Plastic surgeons use a similar process to make cranial implants, except normally *in-situ,* during an operation and using acrylic instead of silicone. The traditional methods rely on the artistic ability of the surgeon or prosthodontist, and in the case of an implant, are made during surgery at significant cost to the patient[1].

Recent investigations for the customisation of implants use medical scanning systems such as computerised tomography (CT) to obtain a digital model of the human anatomy from which custom implants and prostheses can be manufactured using technologies such as rapid prototyping (RP) (D'Urso *et al,* 2000, p. 201). These investigations lack a digital design step in the method and are more expensive (Choi *et al*, 2002, pp. 23-24). D'Urso *et al* (2000 p. 203) estimates the price of an RP cranial model at more than $1000 (US) per model. Figure 1-1 illustrates an RP model and cranial implant.

---

[1] Currently, operating room or theatre costs of R30 per minute at a private hospital are common in South Africa.
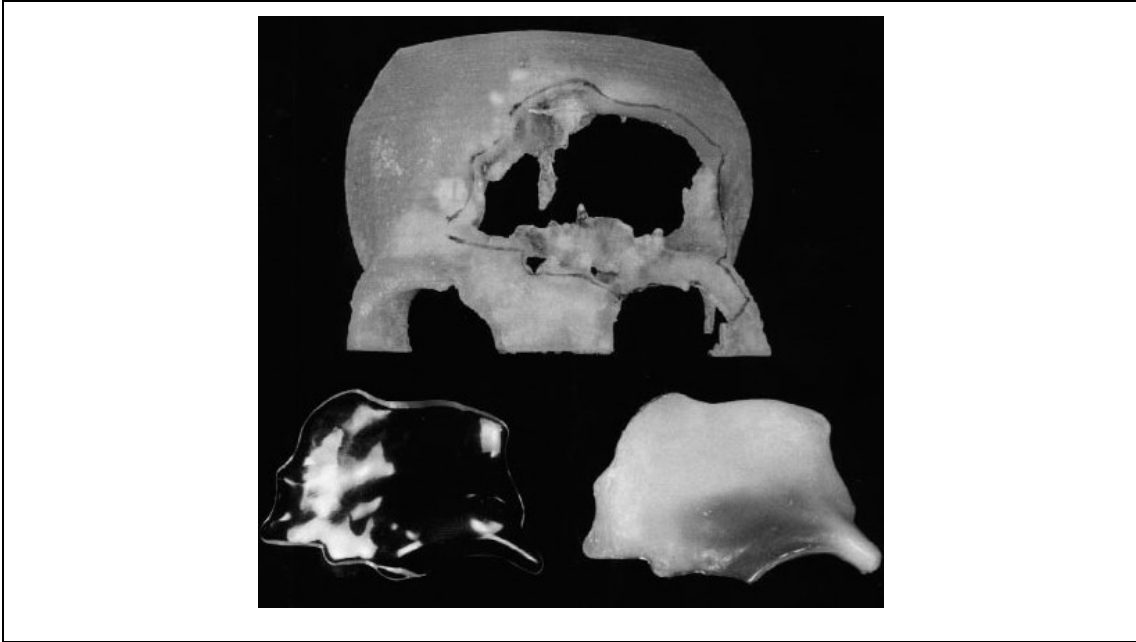
Figure 1-1: RP cranial model and implant
(D'Urso *et al,* 2000, p. 201)

The RP bureau service market was estimated at between $40 million to $60 million (US) worldwide in 1993 and this figure increases every year (Wohlers, 1995, p. 5). Much focus of RP is placed on its medical applications including custom implants and pre-operative models for planning. These medical applications come with the large cost associated with the Stereolithography (SLA)[1] process.

Increased customisation of implants and prostheses is a driving force behind using RP as a medical manufacturing process, as almost any shape can be manufactured, including internal anatomical features. Design input and editing is important in the creation of customised implants and prosthetics. Advances in computer processing power allow the use of high resolution scanning systems and haptic design devices for reverse engineering (RE) applications that include a design step.

Traditionally, computer design is restricted to two dimensional input devices, such as a keyboard and mouse. Haptic interaction devices can use a three-dimensional workspace and the sense of touch that may enhance design applications.

---

[1] The first commercially available RP system and uses resin as a build material

1.2 Problem statement

Traditional methods for both implant and prosthesis design require the artistic ability of a surgeon or prosthodontist. These implants and prostheses are either cast from a hand carved wax master or modelled directly onto the patient depending on the application.

The human body exhibits a degree of symmetry which can be used as a reference for unilateral injuries or defects. D'Urso *et al* (2000, pp. 200-204), Webb (2000, pp. 149-153) and Petzold, Zeilhofer and Kalender (1999, p. 278) use RP for duplicating human anatomy in several applications. The applications use prototypes either in pre-operative planning or moulding a prosthesis or implant. Large prototypes are costly as the cost of rapid prototyping is proportional to the physical size of the model.

Designing an implant or prosthesis digitally, may reduce cost and enhance a patient's treatment as only the implant or prosthesis is prototyped. A digital process including design still requires an imaging source and design software. A digital fabrication method, such as that offered by rapid prototyping, is also required.

For the purposes of this dissertation, the "digital process" stands for the technologies involved in the acquisition of a digital model, the design and modification of the digital anatomy and the manufacture of the required implant or prosthesis. The digital process includes: scanning, image processing, design and manufacture of the desired product. The "investigation", includes the apparatus, methods and subsequent data processing in this dissertation to achieve the objectives stated in section 1.5.

1.3 Importance of conclusions

A proven digital process allows surgeons and prosthodontists to fabricate custom implants and prostheses before surgery takes place. The production of a custom implant before surgery may reduce operating theatre time, with a direct impact on reducing costs. A digital process is compared to traditional medical procedures on selected points to determine additional benefits from using a digital process. Patients

requiring a facial prosthesis may benefit from increased aesthetic appeal that digital designs offer.

1.4 Description of the dissertation

The dissertation is divided into eight chapters. Chapter one introduces concepts in medical modelling and states the problem that is investigated and the research objectives. Chapter two examines existing literature on topics such as imaging, image processing, design, rapid prototyping, casting, medical topics and evaluation criteria. Chapter three describes the major apparatus in this investigation. Chapter four describes the method used during the course of the investigation and illustrates both a general process method, and a specific method for applications. Chapter five presents both the qualitative and quantitative results obtained from the investigation. Chapter six discusses the results with respect to the objectives stated in Chapter one. Chapter seven draws conclusions on the research performed and the results obtained. Chapter eight makes recommendations for future research work, expanding on what is presented in this dissertation. The appendices at the end of the dissertation contain additional information for readers including, but not limited to, technical specifications of apparatus and materials and additional figures.

1.5 Objectives

The three objectives related to this investigation are to:

1. Create a process for the design and duplication of selected prostheses and implants.
2. Use case studies in implant design, prosthesis design and prosthesis duplication. Each case study is to use the proposed digital process.
3. Compare the prosthesis design and duplication case studies to the traditional processes on selected points namely:
   a. accuracy;
   b. aesthetics;
   c. cost;
   d. and speed.

1.6 Major limitations in the dissertation

This dissertation is limited by the medical ethics and processes that could be used. In some cases the dissertation uses only portions of a digital process, and terminates before the full process is followed and simulates a human patient using cast anatomical models.

2   Literature Review

2.1 Literature Review Introduction

A digital process for the design and manufacture of customised anatomical implants and prostheses requires the use of several systems and steps. The outline of the literature follows the generic process of reverse engineering and manufacture (Cooper, 2001, pp. 166-167). The generic process using rapid prototyping typically consists of imaging, image processing, design, rapid prototyping and manufacture.
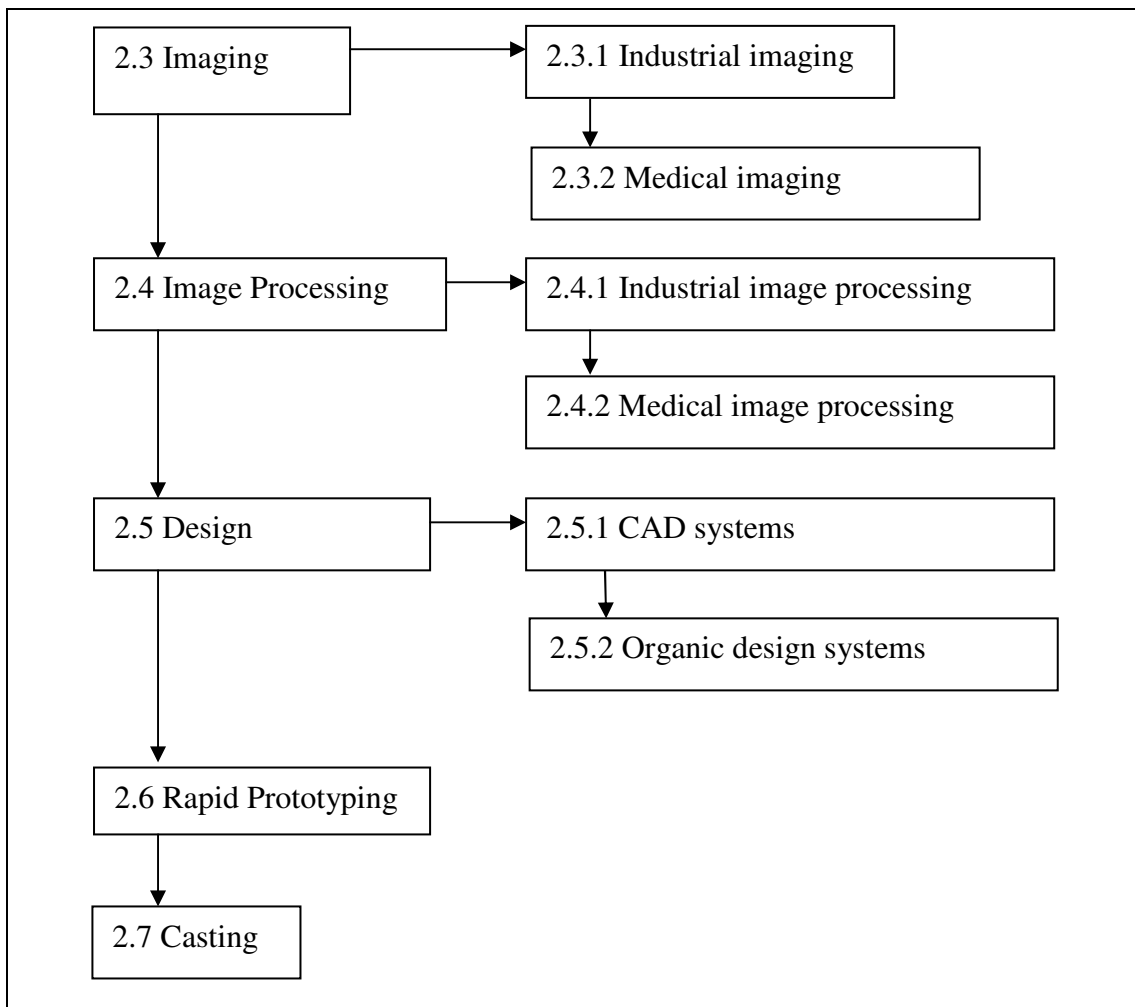
Figure 2-1: Literature layout of the digital process

Figure 2-1 shows the layout of the literature survey with respect to the generic process of reverse engineering. Section 2.2 describes the reverse engineering process and its definition. Section 2.3 deals with industrial imaging, followed more specifically by medical imaging techniques. This includes the various aspects of imaging and methods that are employed during the course of the investigation. Section 2.4 discusses the processing of scanned data and the conversion of medical image data to an industrial format. Section 2.5 describes and compares traditional computer aided design (CAD) and organic design methods. Section 2.6 discusses the processes and equipment related to RP technology. Section 2.7 briefly discusses casting methods and its application in the investigation.

Topics not illustrated in Figure 2-1 are sections 2.8, 2.9 and 2.10. Section 2.8 discusses traditional medical techniques and new technologies that enhance them. Section 2.9 discusses evaluation criteria and its application to the investigation. Section 2.10 draws conclusions from the literature and its application to the objectives stated in section 1.5.

2.2 Reverse engineering

There are many definitions for the term "reverse engineering". Varaday, Martin and Coxt (1997, p. 255), report it as the process of creating a CAD model from a prototype or model. Cooper (2001, p. 166), describes it is a process used to reproduce a component when designs are not accessible. Cooper further substantiates that reverse engineering using rapid prototyping (RP) technologies refers to the process of regenerating a physical object back to a digital form and then producing direct or modified copies of the original object using RP.

From the statements above, reverse engineering is a generalised term used when an object requires a digital or paper representation for the purposes of archiving designs or for physical duplication and modification using a selected manufacturing technology.

2.3 Imaging

Imaging is a starting point for a digital reverse engineering process and allows one to obtain a digital copy of existing geometry in three dimensions. Imaging can be broadly divided into industrial and medical processes. Both industrial and medical imaging processes offer several techniques and systems that are discussed in this section. Techniques are compared to one another using resolution (the absolute spacing of pixels), uncertainty (how close the pixels are to the correct position), speed and capital cost.

Imaging is divided into three sub-sections. Sub-section, 2.3.1, deals with generalised industrial imaging systems and sub-section 2.3.2 examines medical imaging devices that are available and routinely used in hospitals and clinics. Sub-section 2.3.3 summarises the industrial and medical imaging techniques.

2.3.1 Industrial imaging

Broadly speaking, industrial imaging can be broken into two system types; contact and non-contact imaging systems (Wang, Chang and Yuen, 2003, p. 241). A contact imaging system is usually mechanical in nature; whilst non-contact imaging systems generally use optical methods. The methods examined are:

1. Contact
   a. Manual Measurement
   b. Coordinate measuring machines (CMM)
2. Non-contact
   a. Time/Light in flight
   b. Moiré fringe patterns / structured light
   c. Digital photogrammetry systems

<u>Contact measurement systems</u>

Manual measurements are the simplest technique to employ for reverse engineering. Measurements of an object are made by hand, using a vernier or micrometer, and plotting these points into a suitable CAD or digitising package. This technique is used when few points are required and no complex surfaces exist. This method relies on humans and errors in both resolution and uncertainty are in the millimetre range. The capital cost of this technique is minimal compared to the automated systems discussed below.

A coordinate measuring machine, (CMM) is computer numerically controlled (CNC) device, used for measuring surfaces and boundaries, and the extraction of point coordinate data. A CMM is a contact system and uses a probe for digitising. Automotive manufacturing plants use CMM's extensively for quality control applications (Miguel and King, 1994, pp. 48-49). A CMM can be programmed to extract points from a known location, and check if a component is within tolerance.

A CMM operates by running the touch probe in a line over a surface and extracting data points at predefined intervals. Upon completion of a run, the probe steps over a predetermined distance and scan again (Bardell, Balendran and Sivayoganathan, 2003, p. 27).
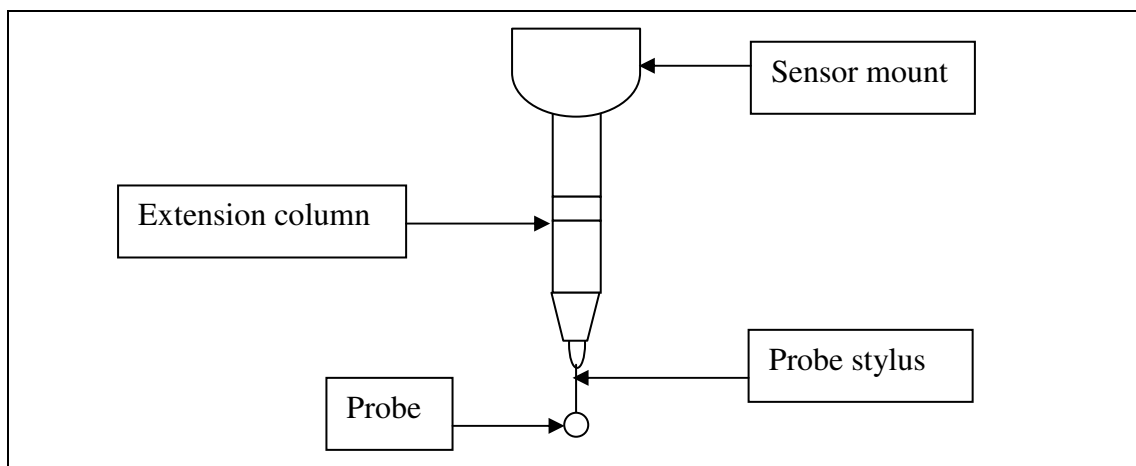
Figure 2-2: Touch probe components

(Adapted from Bardell, Balendran and Sivayoganathan, 2003, p. 27)

Figure 2-2 shows the major components of the touch probe for a CMM machine, the probe can be part of a dedicated scanning system, such as a Renishaw Cyclone scanner, or mounted onto a standard CNC machine.

CMM's use software algorithms to slow down at areas with high curvature; this obtains greater point density at a curve, but speeds up on flat areas. Bardell, Balendran and Sivayoganathan (2003, pp. 27-28), report when using a physical probe, one has to take into account the diameter and probe geometry and offset this against the digitised surface using the surface normal.

The Renishaw Cyclone has a resolution of 7µm and its uncertainty is also in that range, manufacturer's specifications for the Renishaw Cyclone are displayed in Appendix A. Newer models of CMM's are available with a laser option instead of a physical stylus. Bradley (1998, p 116) describes one such system, the Hymark 3D vision system which has a greater resolution than the physical probe, due to the width of the laser and an uncertainty of 25µm. CMM's provide more accurate data faster than using a manual method. The CMM's digitising time is dependent on the resolution, and object size.

Non-contact measurement systems

Non-contact measurement systems typically use a stereo technique for digitising. The stereo technique typically consists of a camera (Charge coupled device (CCD)) and projection unit. The projection unit uses either a light or laser source and includes the following methods:

1. Time / light in flight
2. Moiré fringe patterns / structured light
3. Digital photogrammetry systems

The time/light in flight method is based on the direct measurement of the time of flight of a laser or other light source pulse. During imaging, an object pulse is passed back to the sensor and a reference pulse is passed to the sensor through an optical fibre. The time difference between the two pulses is converted to a distance. The typical resolution of such a system is around 1mm (Chen, Brown and Song, 2000, p. 11). Time in flight systems use a charge coupled device, (CCD) to capture the

reflected light. Scanning systems such as the Cyberware Desktop scanner (http://www.cyberware.com 05 January 2004), are capable of capturing 14×10^3 points per second.

The Moiré technique uses two gratings, one is a master grating and the other is a reference grating, from which contour fringes can be resolved by a CCD camera. A light source is shone through these gratings for digitisation. Using Fourier transforms, and known calibration constants, depth and area can be determined. The Moiré technique is faster than the time/ light in flight method, as an entire surface can be digitised in a single scan. The structured light method is similar to the Moiré technique, but only uses one grating. The depth information is encoded into a deformed sinusoidal fringe pattern, detected by a CCD (Chen, Brown and Song, 2000, pp. 11-12).
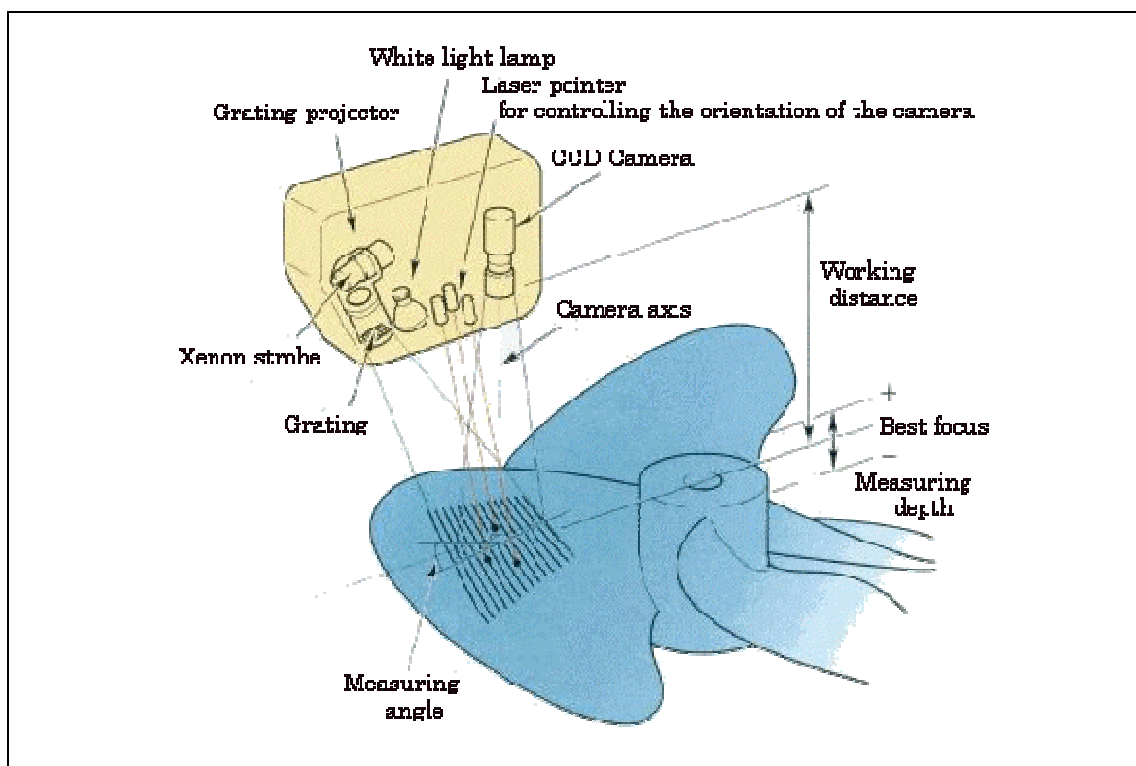
Figure 2-3: Structured light technique
(http://www.opton.co.jp/techrep/md/md1_1/mde1_1.html, 08 February 2004)

Figure 2-3 shows a system employing the structured light technique, with the grating projected onto the part. The structured light image digitised by the CCD camera, is used to calculate both the depth and shape from known calibration constants. A

combination of image size detectable by the CCD and the angle between the grating projector and CCD, determines the working distance and measuring depth for a single scan. The working distance is the centre of the scanning volume, and the volume extents lie between the best focus distances.

It is possible to have multiple scan volumes on one system employing either the Moiré or structured light technique. The scan volume is varied by altering the distance and angle between the CCD and projector. Scan volumes range from $1mm^3$ to specialist scanners with over $1m^{3.}$ The resolution of Moiré or structured light techniques is between 50µm and 3-4mm, with uncertainties in the range from 10µm to 1mm. One can expect a system with a maximum volume of 100 x 100 x 100mm (WxHxD) to have a resolution of 100µm and an uncertainty of 30µm.

Digital photogrammetry typically employs a stereo camera technique to measure 3D data. Bright markers are placed on an object such as retro reflective painted dots, and these are measured by the stereo camera set up (Chen, Brown and Song, 2000, p. 12). The markers of known dimensions are digitised and compared to theoretical values to aid in surface reconstruction and image registration, (discussed in sub-section 2.4.1). The resolution of such systems is similar to the Moiré technique, but a larger uncertainty exists as the dimension of the markers also has an associated uncertainty.
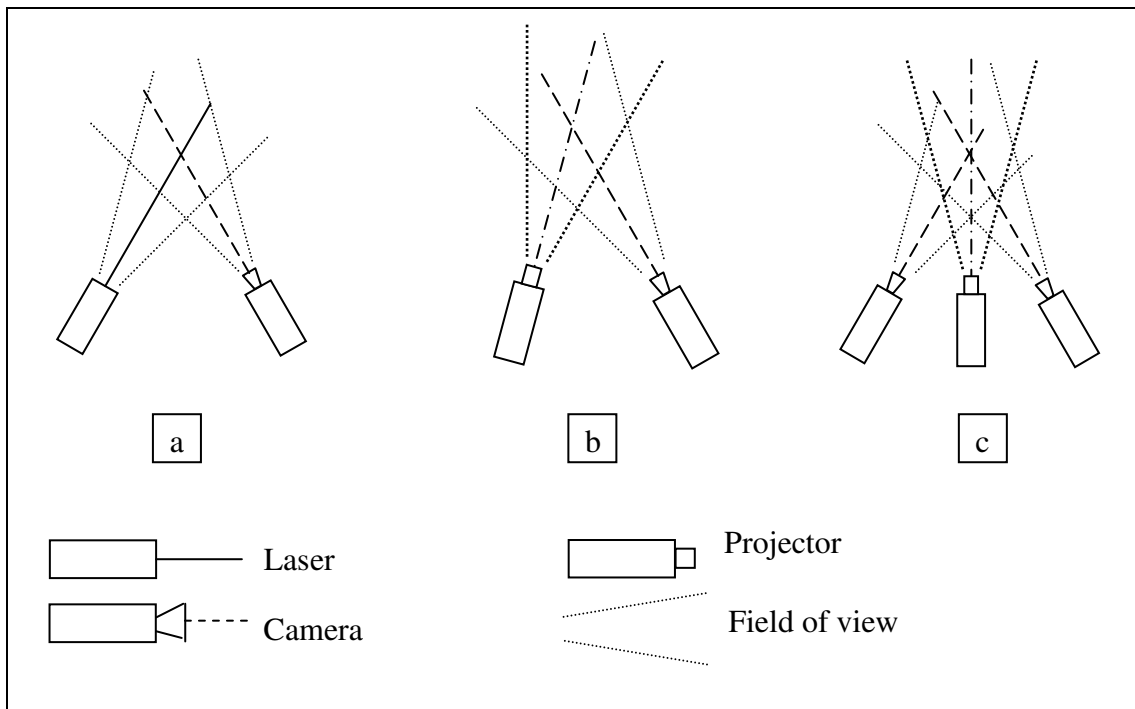
Figure 2-4: Optical stereo 3D scanner configurations
(Siebert and Marshall, 2000, p. 219)

Figure 2-4a, b and c, show stereo configurations of optical scanning systems that can employ the time/light in flight, Moiré, structured light and digital photogrammetry techniques. There are currently many commercially available scanning systems that employ a wide variety of triangulation-based 3D sensing techniques employing: laser-camera baselines (a), camera-projector baselines (b) and camera-projector-camera baselines (c), (Siebert and Marshall, 2000, p. 219).

An advantage of using optical scanning methods, is the ability to capture colour (Xu, Ye and Fan, 2002, pp. 495-499 and Siebert and Marshall, 2000, p. 225), using a colour CCD. The principle of a colour system uses a colour camera to take a 2D picture of the object. A laser or light projection source, and CCD camera are used to obtain the 3D information. The 3D and 2D colour information are merged to give a 3D colour model. Breuckmann GMBH has recently developed a colour optical scanner employing the structured light and digital photogrammetry techniques. Colour can be advantageous for prosthesis design as it is an external product

2.3.2 Medical imaging

Medical imaging goes beyond the techniques and methods presented in industrial imaging (Sub-section 2.3.1). A fundamental difference between industrial and medical imaging techniques is that medical techniques are designed for patient diagnosis and obtained from a lower resolution imaging system when compared to those presented in sub-section 2.3.1.

Several medical imaging systems are commonly used in clinical applications and include: magnetic resonance imaging (MRI), positron emission tomography (PET), single photon emission computed tomography (SPECT) and computed tomography (CT), (Meinzer *et al*, 2002, p. 311). Each medical imaging system has a specific application, and an area where it excels.

The resolution and uncertainty of medical scanners differs somewhat to the industrial scanners. A medical scanner is typically designed for internal imaging, obtained in slices that are stacked to form a 3D volume. There are different resolutions associated with the 2D image and 3D stacked images. Modern medical scanners typically use either a 512x512 or 1024x1024 pixel matrix, giving a resolution between 0.5mm and 1mm for each 2D image or slice. The slice distance determines the second resolution and is between 0.5mm and 10mm.

MRI and CT obtain geometric information about tissue structure or the location and description of bone fractures, whilst PET and SPECT usually find application in body metabolism and functions. Brief descriptions of MRI, PET and SPECT are provided, followed by a more specific and detailed examination of CT scanning.

MRI[1] functions on the premise that materials with an odd number of protons or neutrons posses a weak magnetic moment. The nuclear moments are randomly orientated, but align when placed in a strong magnetic field. MRI measures the moment of the protons or neutrons while they oscillate in the strong magnetic field.

---

[1] Also known as nuclear magnetic resonance imaging (NMRI)

MRI differentiates soft tissue such as the brain very well, but liquids such as blood and solids such as bone are problematic (Bronzino *et al*, 2000, p. 63-2, Meinzer *et al,* 2002, p. 312). MRI images are taken as a series of slices and are stacked to form a digital 3D volume.
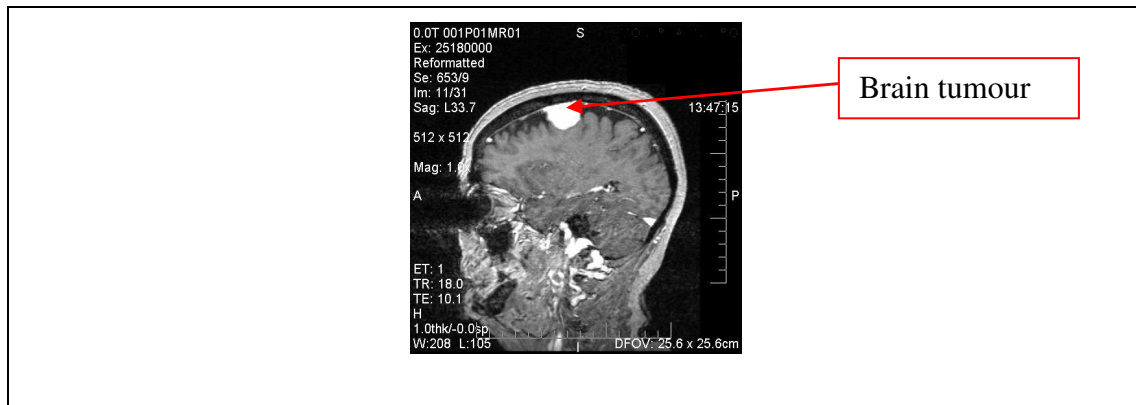
Figure 2-5: An example of an MRI image
(http://sprojects.mmi.mcgill.ca/braintumor/section2/subsection4/default.htm, 11 January 2004)

Figure 2-5 shows an MRI scan, where the patient has a brain tumour, depicted by the white area at the top of the cranium. The various structures of the brain are also depicted and show the level of tissue detail one can see with MRI.

PET scanning has an advantage over MRI in that it is reportedly more sensitive for dynamic studies such as metabolism. PET uses the high energy photons, produced by the annihilation of the positron from positron emitting isotopes (e.g. ^{11}C, ^{13}N, ^{15}O, or ^{18}F), to describe in 3 dimensions the physiologic distribution of tagged chemical compounds (Bronzino *et al*, 2000, p. 67-7). Metabolic activity is used for detection and location of cancerous areas in a patient amongst other applications (Meinzer *et al*, 2002, p. 312).

Figure 2-6: An example of a PET image

(PettiJohn, 1999, http://www.dushkin.com/connectext/psy/ch02/pet.mhtml)

Figure 2-6 shows a PET scan of brain activity whilst the subject is involved in mental activity. The subject is given a radioactive glucose injection, and the PET scan monitors areas of the brain that use glucose for energy. The image is viewed in a dynamic state on a computer monitor, and printed as in Figure 2-6 for reference purposes.

SPECT combines conventional nuclear medicine (NM) imaging techniques, such as PET and MRI, with CT methods. SPECT uses radioactive labelled pharmaceuticals (radiopharmaceuticals) that distribute in different internal tissues and organs, instead of an external x-ray source. Radiopharmaceuticals are a class of radioactive substances that are used for medical applications (Bronzino *et al*, 2000, pp. 64-10).
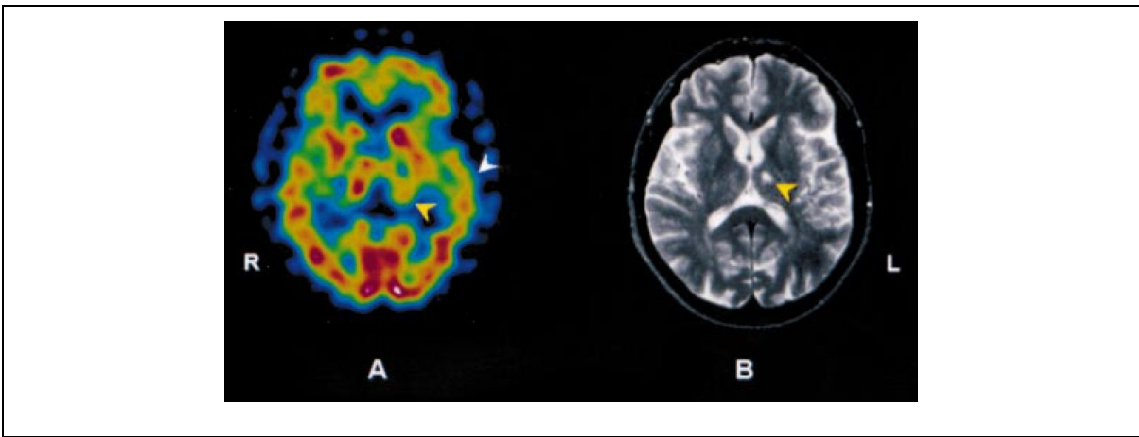
Figure 2-7: An example of a SPECT image

(Catafu, 2001, p. 260)

Figure 2-7 shows a SPECT image on the left and an MRI image on the right. The SPECT image, comparable to PET, shows brain activity, whilst the MRI image shows structural information. The SPECT images, like PET are suitable for dynamic applications and may only find limited use in the manufacture of custom anatomy. MRI may be used for reverse engineering purposes especially in soft tissue applications.

Computed Tomography[1] (CT) scanning was one of the first volumetric medical scanners available. Both resolution and acquisition time of images has improved since first commercialisation in the late 1970's (http://www.imaginis.com/ct-scan/history.asp, 1st August 2001).
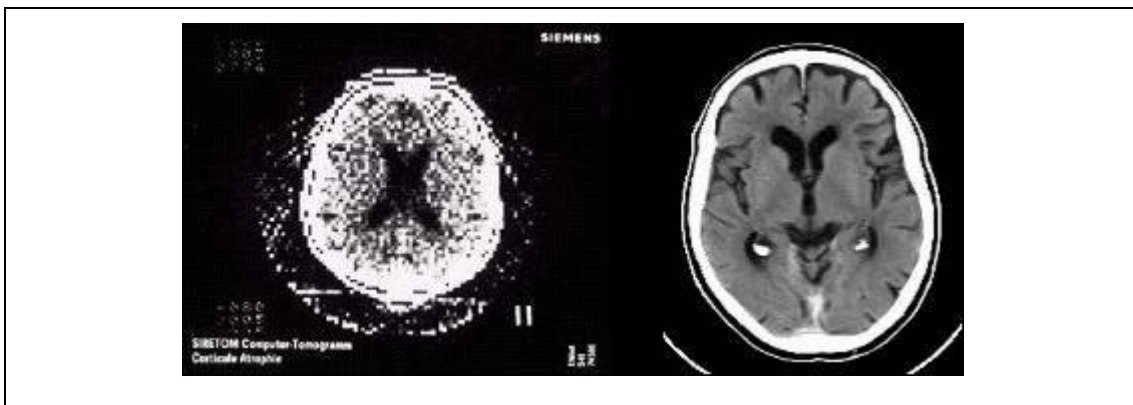
Figure 2-8: Comparison of old and new CT scanner images
(http://www.siemens.com , 28th August 2001)

Figure 2-8 shows a comparison of an older CT image on the left, which is in a 128 x 128 pixel matrix using a Siemens Siretom CT scanner, circa 1975. The image on the right is obtained from a modern day CT scanner, where the tissue of the brain is seen. Older generation scanners were designed for the head only and it would take days for image reconstruction (http://www.imaginis.com , 1st August 2001).

---

[1] Also known as computed axial tomography (CAT) scanning
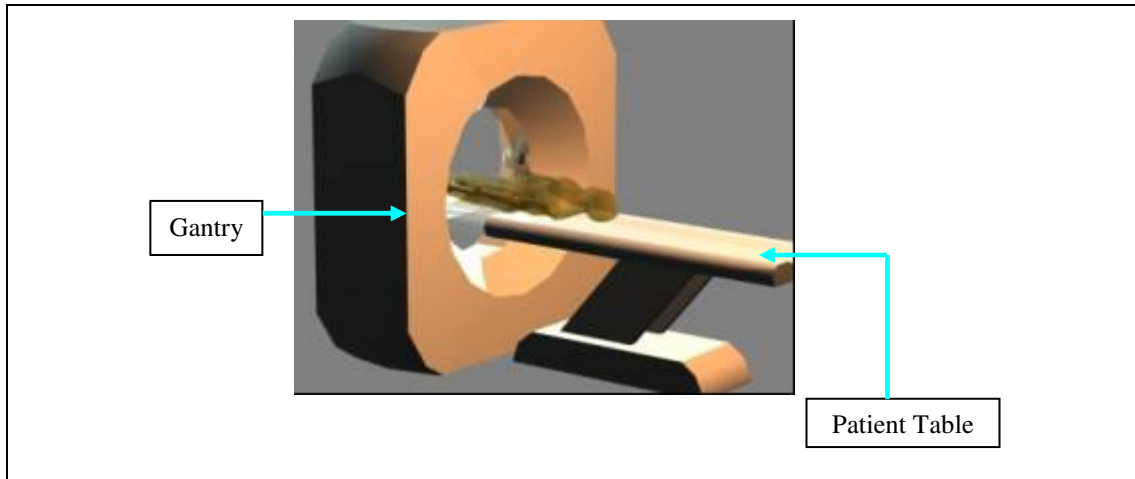
Figure 2-9: Major components of a CT scanner
(http://www.mcw.edu, 28 August 2001)

Figure 2-9 shows a rendered image of the major components of a CT scanner, the gantry and the patient table. The gantry houses the image acquisition equipment and a motorised patient table that moves the patient into the gantry. MRI scanners have a similar external structure to Figure 2-9.

CT operates using x-rays emitted from the gantry. As x-rays pass through the body they are absorbed or attenuated (weakened) at differing levels creating a matrix or profile of x-ray beams of different strengths. X-rays have a defined spectrum and the grey values of resulting images are standardised as Hounsfield units (HU). A value of 0 HU is the density of water, bone is typically greater than 400 HU and metallic implants are greater than 1000HU, (http://en2.wikipedia.org/wiki/CAT_scan, 5 December 2003).

Figure 2-10 shows an application of the HU scale, and how one would apply this to the limitations of a 256 greyscale display of a CT scanner to improve resolution. "Range" 1 shows HU values from air at -1000HU to cortical bone at 1000HU. "Range 2" illustrates a CT study where the radiologist was interested in the HU range of fat (-100HU) to congealed blood (<100HU). The 256 greyscale colours of the CT scanner are standardised to this range (-100HU → 100HU) and a higher resolution is obtained in the CT scan. Selection of the HU range before scanning is important and improves both the resolution and definition of the images.
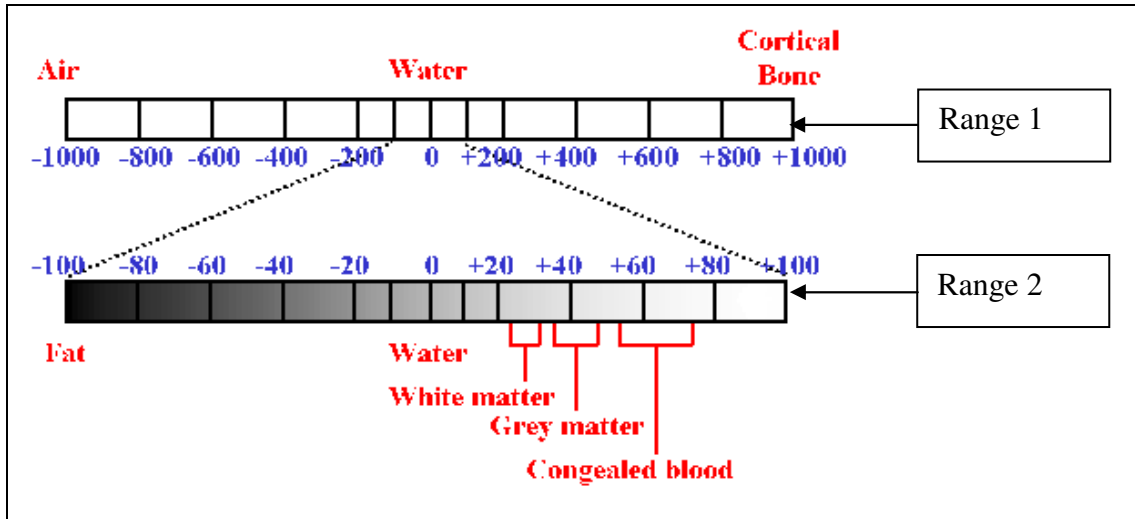
Figure 2-10: The Hounsfield scale

(http://cal.man.ac.uk/student_projects/2000/mmmr7gjw/technique8.htm, 5 December 2003)

a   b
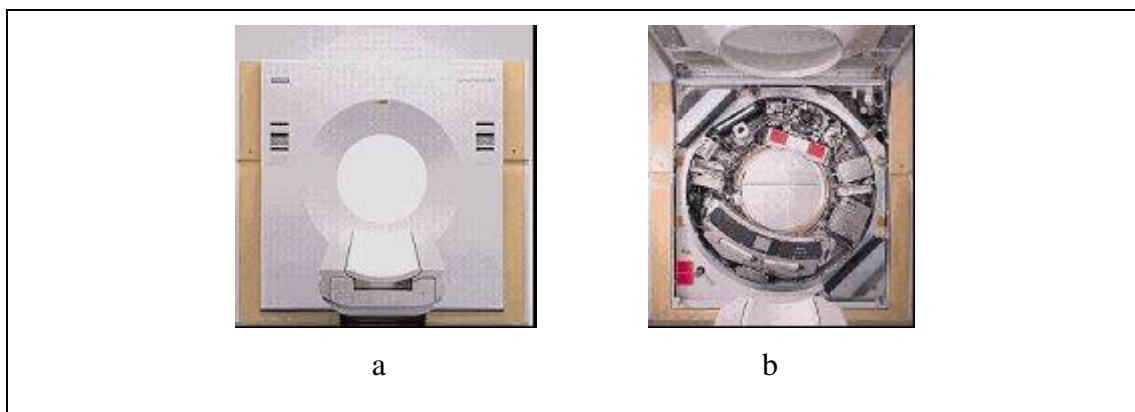
Figure 2-11: Siemens Somatom gantry

(http://www.siemens.com , 28th August 2001)

Figure 2-11a shows the housing of a modern day CT scanning gantry, and Figure 2-11b the x-ray tube and the sensor array. This scanner has a fan beam array of sensors that rotate in conjunction with the x-ray tube 360° around the patient. Every 360° a "slice" or image is acquired, and is collimated (focused) to a thickness between 1mm and 10mm using lead shutters in front of the x-ray tube and x-ray detector array. Typically, in one revolution, 1000 profiles are sampled, which are backwards reconstructed to a dedicated computer to create a 2 dimensional image (http://www.imaginis.com/ct-scan/how_ct.asp, 1st August 2001).
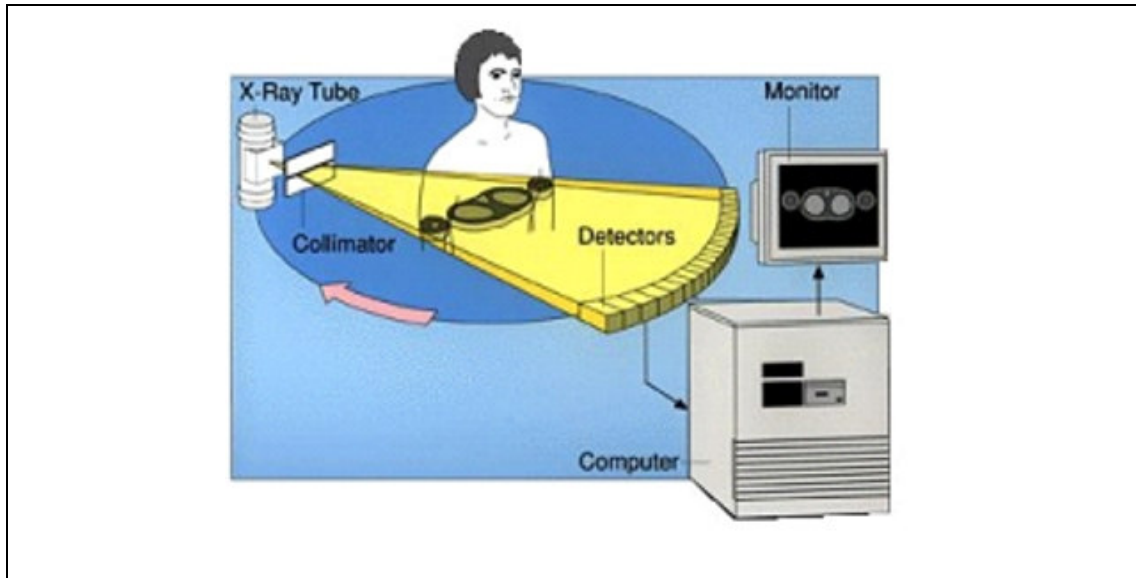
Figure 2-12: The CT scanning process
(http://www.imaginis.com/ct-scan/how_ct.asp, 1st August 2001)

Figure 2-12 shows the CT scanning process, using a fan beam detector array. The CT slices are processed in the computer and viewed on the monitor.

Spiral scanning is a new CT scanning method. An advantage of spiral or helical scanning is the ability for continuous scanning. Single detector row spiral CT scanners (SDCT) have a detector array similar to that illustrated in Figure 2-12 with between 500 and 900 detectors. Multi detector row CT (MDCT) still emits a single radiation beam but has multiple rows of detectors, typically between 8 and 32 rows. An advantage of MDCT is that up to 4 images are obtained from 1 revolution of the scanner (Horton *et al,* 2002, p. 144, Lawler and Fishman, 2002, p. 78).
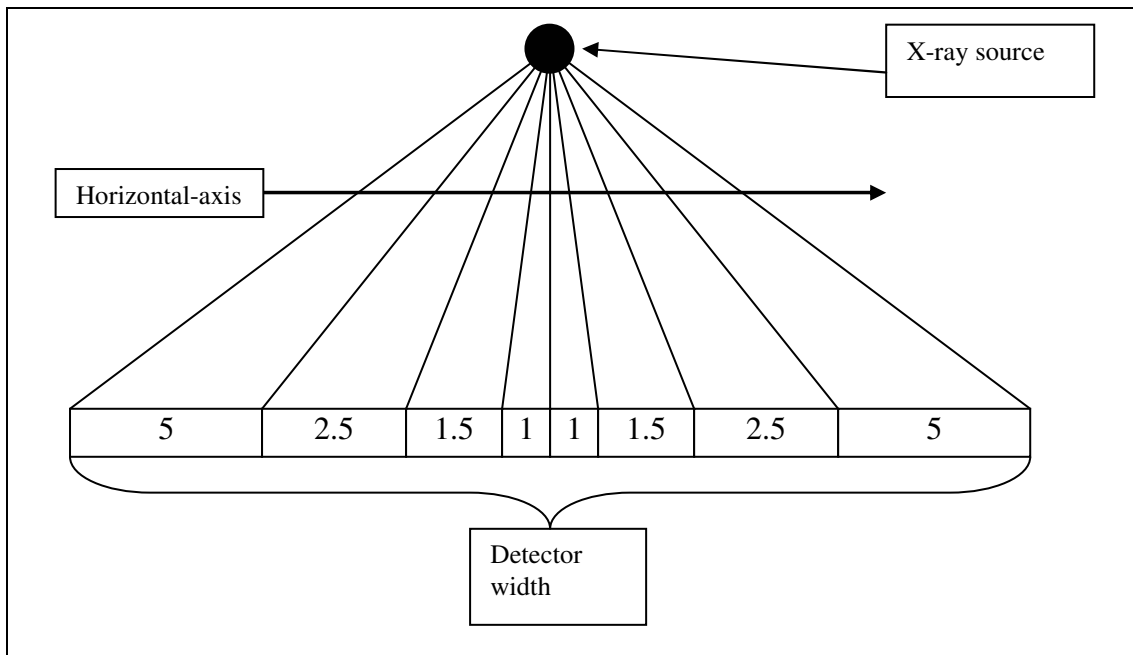
Figure 2-13: The MDCT detector array

(Adapted from Horton *et al,* 2002, p. 147)

Figure 2-13 illustrates an MDCT detector array of varying width with the horizontal-axis which passes through the centre of the gantry. Each detector array is set at a certain thickness, in the figure: 1, 1.5, 2.5, and 5mm scan thickness are obtained simultaneously. More than one array can be used during a rotation and the processed slice can have combinations of slice thickness (Lawler and Fishman, 2002, p. 80). An example is given by Horton *et al* (2002, p. 147) and both the 5mm and 1mm array can be selected and the 5mm slice distance is printed onto film in 2D and the 1mm slices are used for digital 3D reconstruction.

2.3.3 Imaging summary

The industrial and medical imaging techniques discussed in sub-sections 2.3.1 and 2.3.2 are summarised in this section. Table 2-1 summarises and compares the imaging techniques discussed, excluding the dynamic medical scanners of PET and SPECT. The industrial techniques are scalable, which affects the scanners' specifications. It is assumed the scanners are set up for an object with overall dimensions of 100mm in all directions.

The categories in Table 2-1 include values from literature for resolution and uncertainty. A rating from 1 to 4 is given for cost where 1 is less than R1000, 2 is less than R500 000, 3 is less than R1 million, and 4 is greater than R1 million. A comparative rating of low (L), medium (M) and high (H) is given for speed, and a "yes" or "no" for colour ability.

Table 2-1: Imaging summary

Method	Resolution	Uncertainty	Cost	Speed	Colour ability
Manual	>1mm	≈100µm	1	L	No
CMM	7µm	<25µm	2	L	No
Time/Light in flight	1mm	<0.5mm	2	M	No
Moiré and structured light	100µm	30µm	2	H	Yes
Photogrammetry	100µm	>30µm	2	H	Yes
CT scanning	0.5-1mm	1mm	4	H	N/A[1]
MRI scanning	0.5-1mm	1mm	4	H	N/A[1]

[1]Colours using CT/MRI are based on density and not object colour

In Table 2-1, the resolution, is the minimum spacing of data points one can obtain, with the uncertainty an indication of how close each point is to its correct position. Both resolution and uncertainty have values associated with them obtained from literature. A comparative approximation is made on cost, which is assumed to be only the capital cost in this case of a system utilising the method indicated. The speed category indicates how quickly data points are collected. The colour ability category indicates whether colour scanning can be performed using this method.

Manual measurement is the worst performing in both resolution and uncertainty, compared to the contact measurement system (CMM), which is the best performing in these categories. The downside to the CMM is the low digitising speed as only one point is digitised at a time, when compared to the non-contact methods using a CCD, in which millions of data points are captured in a few seconds. Both CT and MRI scanning are fast at digitising, as multiple models may be scanned at once. Medical scanners cost the most, followed by the automated systems of both contact and non-contact measurement systems. This investigation uses a combination of industrial and medical scanning systems including CMM, Optical and CT methods to achieve the objectives in section 1.5.

2.4 Image Processing

Scan data whether from an industrial or medical scanner, consists of a number of points that require manipulation and processing before they can be used in traditional design software. Image processing tasks for reverse engineering include 3D data conversion, merging a series of scans and filling holes in the data.

2.4.1 Industrial image processing

The file output from industrial scanners is usually a point cloud, which is all of the digitised points that are represented by x, y and z coordinates in the file. Additional information is also stored including the scanner name and type and the use of colour. Non-contact measurement systems usually take a number of scans to digitise an object from different angles. Each file requires joining together when multiple scans are taken. The joining together of scans is termed registration. The registration process can be related to taking a series of panoramic or aerial 2D photographs and aligning them.
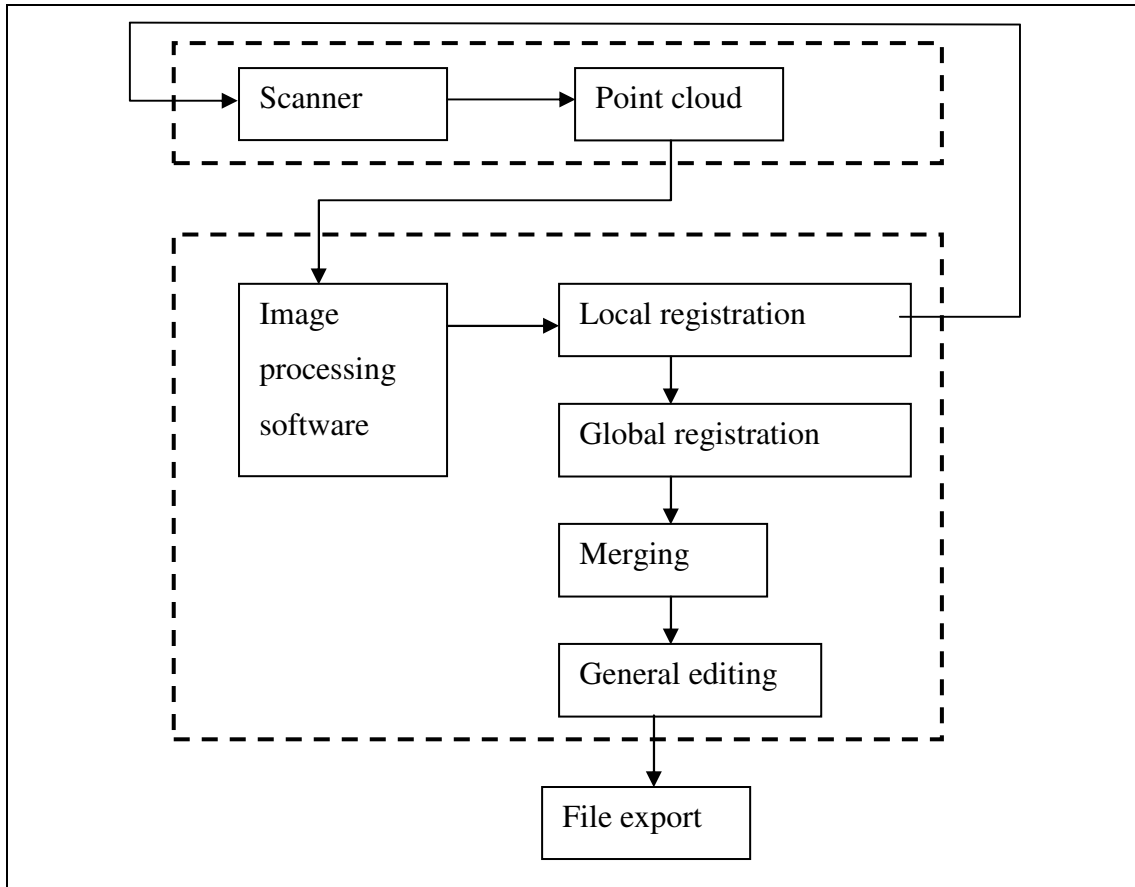
Figure 2-14: Image processing activities

Figure 2-14 shows the process of taking multiple scans and registering them to create the digital object. As each scan is taken, it can be locally registered, or alternatively, local registration can be performed when all scans are obtained. An automated global registration procedure is used to fine tune the registration. Merging of the registered data creates a single surface model. General model editing is performed including file repair and hole filling. File export is used when alternative file types are required.

The local registration of data uses mathematical algorithms, or in the case of indexed CMM data, can be registered directly from the known coordinates. Local registration using mathematical algorithms consists of setting a fixed scan and a floating scan. The fixed scan is an immovable reference object and the floating scan is moved to specified coordinates. Coordinates are specified by selecting a pre-determined number of corresponding points on both the fixed and floating scan. The local registration process continues until all scans have been registered. It is standard in the

commercially available software packages to offer 2 or 3 of the following local registration options: 1-point, 3-point and n-point registration.
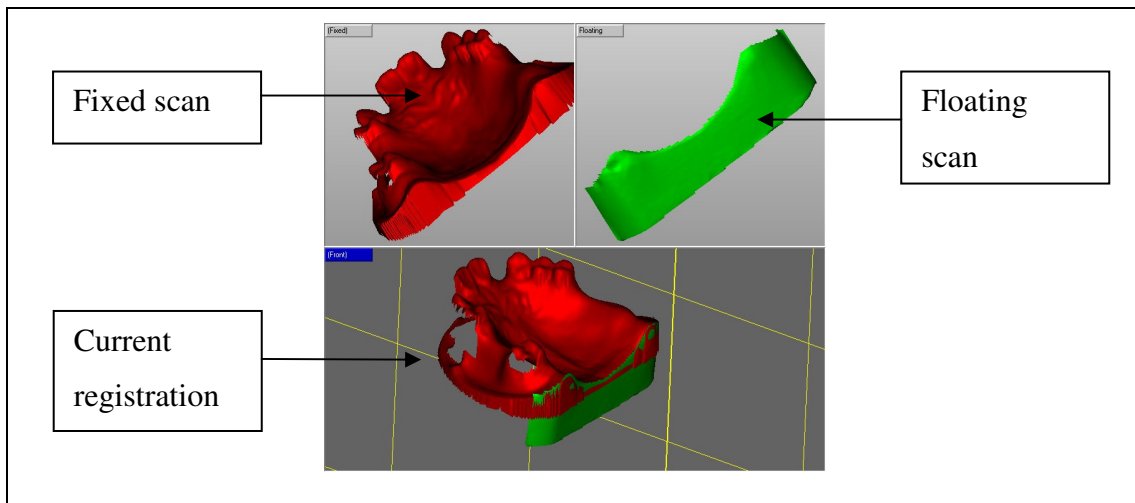
Figure 2-15: Manual image registration

Figure 2-15 shows the local registration of two scans. The current registration shows how the two scans are positioned in space. The two scans are not 100% registered, but close enough to use the automated global registration algorithm.

The global registration algorithm is used after local registration to "fine tune" the manually registered scans. The global registration algorithms are similar to those discussed by Zhang (1994, pp. 119-152) and Xu, Ye and Fan (2002, p. 498), and based on the iterative closest point matching (ICPM) algorithm. Xu, Ye and Fan describe the global registration process as mathematically intensive and faster if the local registration is accurate.
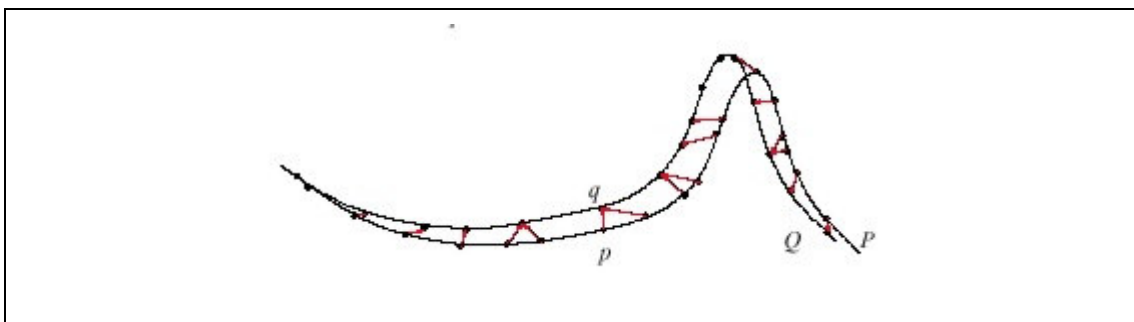
Figure 2-16: The ICPM algorithm

(Bernardini and Rushmeier, 2002, p. 152)

Figure 2-16 illustrates the global registration of two surfaces, surface P and surface Q using point p and point q. The ICPM algorithm takes two steps. The first step identifies pairs of candidate corresponding points in an area of overlap such as p and q. The second step is an optimisation procedure that computes a rigid transformation of the points using a least squares technique. This process is iterated until some convergence criterion is satisfied. The distance between scans are reduced after each iteration, until a true matching pair of points can be identified.

This algorithm converges to a local, but not necessarily global, minimum, depending on the initial configuration (the local registration discussed previously). A potential problem is illustrated with two manually registered cylindrical surfaces. These two surfaces can slide freely over each other with a local minimum being achieved. This is why it is important to ensure scans have as many features as possible for registration (Bernardini and Rushmeier, 2002, pp. 149-172). If necessary, additional features are added to the physical part to aid the registration process.

The final step in creating a solid model is termed merging; it is this process that removes all of the overlapping data, usually selecting the best data. This process also creates a tessellated surface across the entire model. Surface tessellation involves using flat polygons to cover and approximate the model. Tessellation approximates curved surfaces using many polygons, compared to a flat surface where few polygons are required for representation. The surface polygons can be triangles such as those used in the STL file format.

Merging scanned data creates a digital model with no geometric features and is called an organic model in this investigation. Organic models require editing such as hole filling to create a watertight model. The holes are generally created where the scanner cannot digitise or errors occurred during merging and tessellation (Fadel and Kirschman, 1996, pp. 9-10). Curless and Levoy (1996, pp. 304-310) use the marching cubes algorithm for hole filling in triangulated data, this algorithm is also used for the surfacing of point cloud data. Schroeder, Zarge and Lorensen (1992, p. 65) describe the marching cubes algorithm as a "…brute force surface construction algorithm that creates iso-density surfaces from the data". Other methods for triangulation of point cloud data for surfacing and hole filling include Delaunay triangulation algorithms,

triangulation based on signed distance function and triangulation based on α-shapes (Liu *et al,* 2002, pp. 634-635). Delaunay triangulation is performed by placing a circumscribed circle through three arbitrary points and making sure no other points exist in that circle (Lee *et al,* 2001, pp. 691-704).

2.4.2 Medical image processing

Medical images are diagnostic in nature, and not originally intended for manufacturing purposes. Medical file formats are generally incompatible with standard CAD formats. When using CT or other volumetric medical scanning systems, there is an additional process involved of converting the data from the medical format, usually digital imaging and communication in medicine (DICOM) format, (Lee *et al,* 2001, p.114), (Brown, Britton and Plummer, 1998, p. 236) to an industrial imaging format such as ASCII point cloud, stereolithography (STL), or NURBS curves and surfaces.
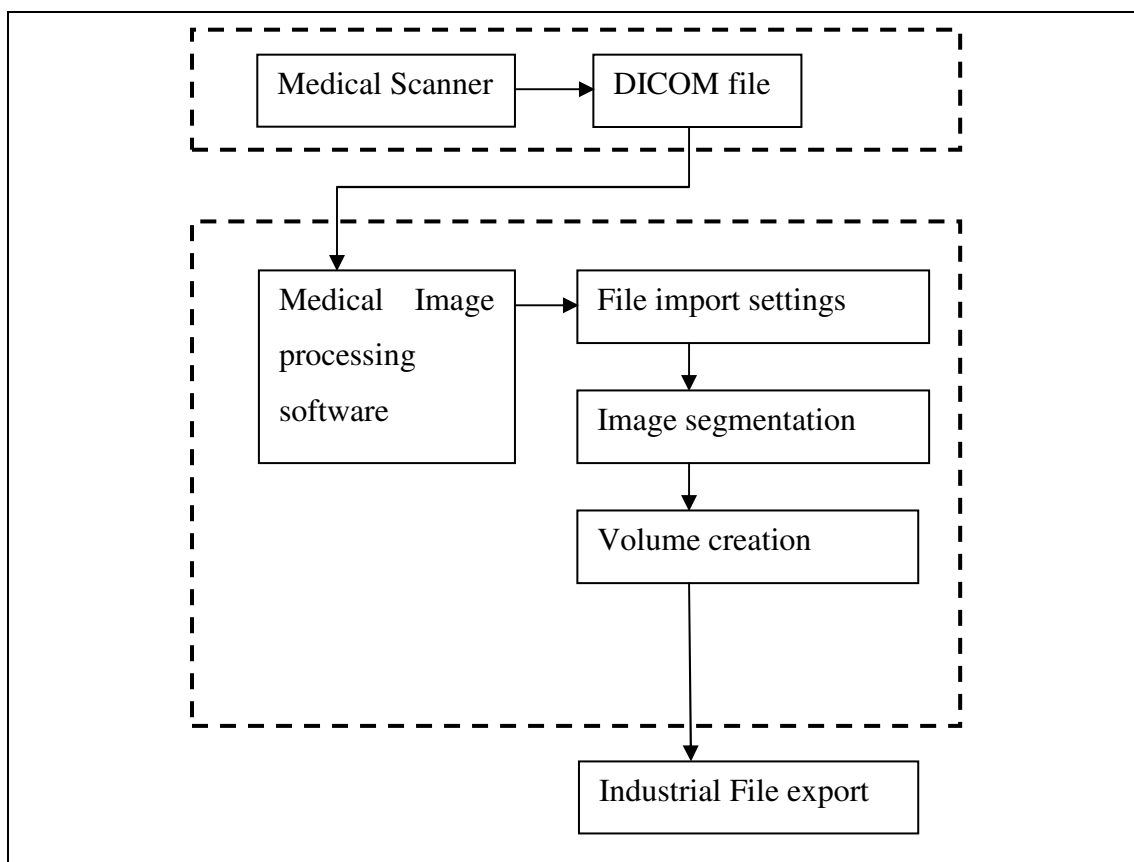
Figure 2-17: Medical image processing

Figure 2-17 illustrates the process used for medical image conversion and processing. The process starts with the DICOM file being exported from the medical scanner. The DICOM file is imported into the medical image processing software, sometimes requiring additional import settings. The image object is selected in the medical image (segmented) and the selection is propagated through the volume. The 3D object is now a single surface organic object and is exported into an industrial file format. Unlike industrial scan files, there are no holes in the medical volumes.

Commercially available medical image processing software packages include Anatomics Biobuild, Materialise Mimics and Tomovision Slice-o-matic. These packages offer both medical image processing and file format conversion.

The separation of the anatomical structures including bone and tissue structures is termed image segmentation. Image segmentation is performed by selecting certain greyscale pixel values and applying a threshold to select several HU values which fall into the required category (Lopponen *et al*, 1997, pp. 47-49). Chang, Wysk and Wang (1991, pp. 460-462), describe the function of image segmentation as selecting which elements of are to be considered edge candidates. Edges are found by applying Roberts' cross operator to each intensity value and comparing the gradient approximation.
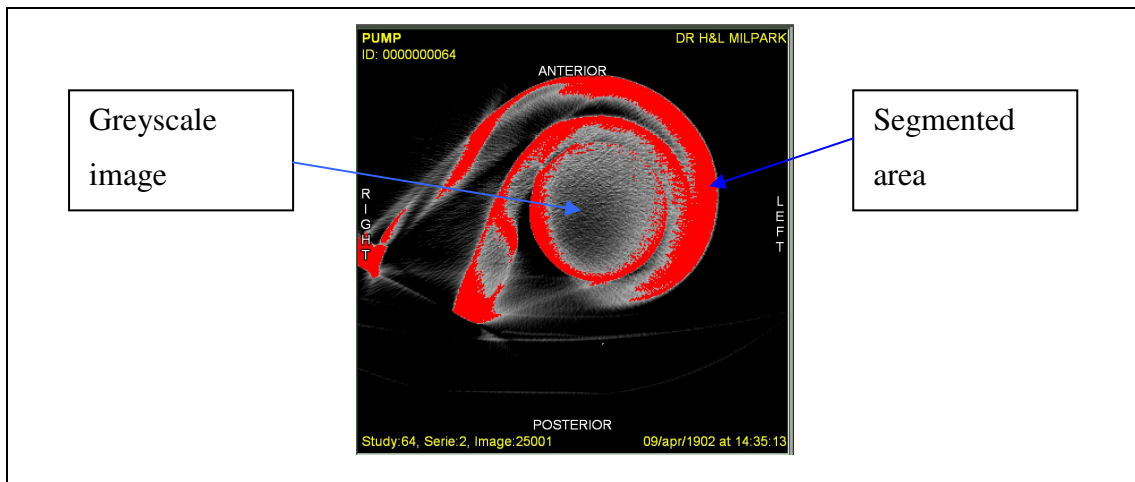
Figure 2-18: Image segmentation of a CT scan

Figure 2-18 shows a segmented CT scan of a pump. In this particular example, a lower and upper range of greyscale values are selected and applied to the image. This

area can be separated from the other parts of the image. Image segmentation can be applied to a single scan or to a volumetric solid by propagating the values through all of the stacked images. Commercially available 2D imaging packages, such as Corel Draw and Adobe Photoshop also possess image segmentation ability on a colour scale. These 2D packages are unsuitable for 3D medical image segmentation in this investigation as they cannot reconstruct 3D information.

2.5 Design

Design using organic data is different to design using data originally created in a traditional CAD system. This investigation focuses on organic based design, which Mullineux (2002, p. 871) describes as improving the aesthetics of a product. Product aesthetics are difficult to quantify mathematically and requires a less precise definition. Organic design involves the manipulation of data obtained from scanning systems where a surface is represented by a series of points rather than a continuous mathematical function. Specialised software is available that assists in organic design and makes manufacturing of organic data easier. To understand the complexity of organic design one needs to compare it to traditional CAD design and get an overview of how a CAD system operates and the various objects one can encounter in a CAD system.

2.5.1 CAD systems

There are two types of design methods on a modern CAD system. The first method designs using object primitives (primitives such as cylinders and blocks) and sketches. The second method designs mathematically with object parameters, such as dimensions (Werner *et al*, 2000, pp. 181-184). The second method of design in a CAD system is termed parametric design. Parametric design is better when dimensions and constraints are available and reduces design time especially for industrial objects. An example where time savings occur is in the case of a stepped shaft.
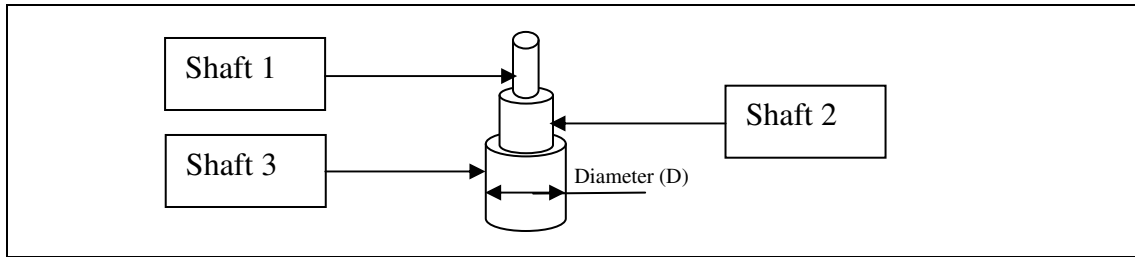
Figure 2-19: Stepped shaft

All three shafts in Figure 2-19 can be designed as a function of the dimension "D". The second and third shafts may be 0.5*D and 0.25*D respectively. A single modification to the dimension "D" at any stage of the design process updates all dimensions.

Modelling human anatomy poses significant problems especially when a 3D image of the existing anatomy is required. Fadel and Kirschman (1996, p. 5) explain how human anatomy is complex in form and used is in a CAD system as a series of curve approximations from several measurements. The number of curves required to increase accuracy makes this approach as tedious.

Apart from basic primitives, CAD systems can design in curves, and generate complex surfaces from the curves. This approach is more feasible when approximating human anatomy. CAD systems use mathematical techniques to represent organic data including splines, bezier curves and B-splines. These curve types enable a designer to represent an organic curve using a parametric representation in each coordinate (x, y and z). The non-uniform rational B-spline (NURBS) curve allows localised modification of the curve itself. Working with spline models such as NURBS in a traditional CAD environment is according to Dachille, Qin and Kaufman (2001, p. 403) "associated with the tedious and indirect manipulation via a large number of (often irregular) control vertices." This still remains one of the best methods to approximate organic data. Surfaces can be represented by combining two or more curves using equation 2-1.

$$r(t,s) = \sum_i \sum_j B_i(t)B_j(s)p_{ij} \quad 0 \leq t,s \leq 1 \qquad \textbf{(2-1)}$$

Where s and t are unit vectors

i and j are indices for each corner

p is the location of a corner

B is a function of the B-spline curve
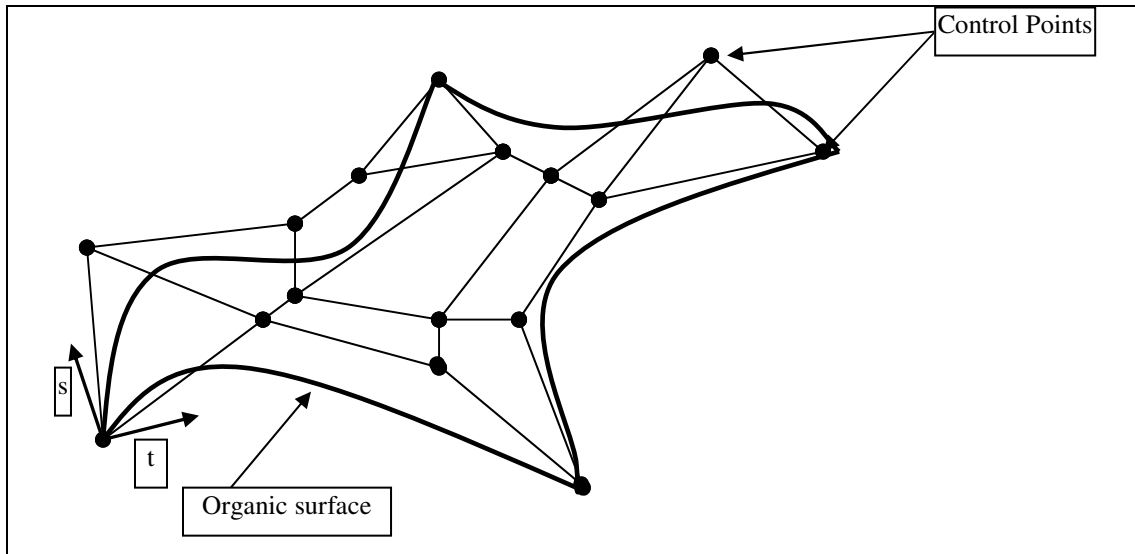
Figure 2-20: A single NURBS surface

(Adapted from Chang, Wysk, and Wang, 1998, p. 105)

Figure 2-20 shows a typical NURBS surface with the control points one needs to manipulate to change the structure of the surface. A digital model typically consists of hundreds of these four cornered patches (Chang, Wysk, and Wang, 1998, pp. 104-105). Mullineux (2002, pp. 871-879) introduces an algorithm to work with surfaces and provide the ability to model aesthetically by automatically moving a large number of control points to achieve aesthetic curvature between patches, the algorithm still requires work. Systems that can make use of these surfaces and curves could speed up the design of organic structures like human anatomy, especially if they could be based on the sense of touch, i.e. be haptic.
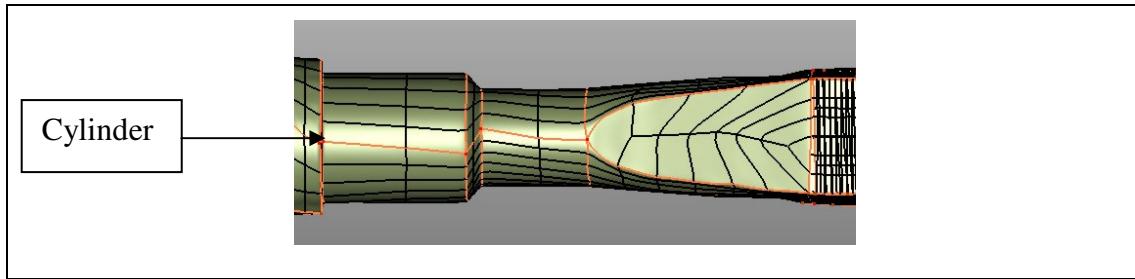
Figure 2-21: A NURBS surface model

Figure 2-21 illustrates a typical industrial object represented by hundreds of NURBS surfaces. The processing includes placing a curve network over the organic surface and creating NURBS surfaces. This data may now be imported and edited in a CAD system.

CAD systems may become unstable and very slow when working with complex data such as that illustrated in Figure 2-21. A cylinder which can be described simply in a CAD system requires many four sided surfaces, this number increases with complex human anatomy. Modifications to the cylinder illustrated in Figure 2-21 require redefining every spline that make up the NURBS surfaces. For human anatomy it is infeasible to modify and edit geometry using a traditional CAD system.

2.5.2 Organic design systems

Unlike traditional CAD systems, organic design systems can offer both parametric modelling and better data handling with organic data. Organic design software packages include Deskartes, Freeform and 3D Max. This software is used to design organic shapes and edit them with relative ease. One still manipulates control points when editing surfaces, but system instability is less likely.

The following functions are usually available in organic design software:

1. Importing, editing and exporting STL data
2. Repairing of STL data
3. Exporting in IGES file format (For export to CAD)
4. Basic primitive construction
5. Offsetting of complex surfaces and volumes

6. Hollowing of complex volumes

7. Boolean operations

Although all of these functions, excluding STL import, are available in CAD systems, organic design software can manipulate and edit organic data easier. NURBS curve approximations are not necessary and one can edit the STL file directly in organic design software. The STL file format is also the standard file format with almost all RP systems in use today (Dolenc and Makela, 1996, p. 20).

STL models

The registration and merging of data, using image processing software, generates an object with a single layered surface. The object has no mathematical definition and is represented by either by an ASCII point cloud (x, y and z coordinates) or the STL file formats.

An ASCII point cloud is a model that is represented by points on the digitised model, and STL is a faceted format whereby the model is tessellated and represented by triangles. Faceted STL models are often easier to edit and visualise due to a less dense structure.

Tessellation algorithms often create large polygonal models with over 100 000 triangles, a problem compounded by high resolution scanning systems. Several reduction techniques are used to retain accuracy whilst reducing the triangle count; this process is termed decimation (Schroeder, Zarge and Lorensen, 1992, p. 65). The algorithm makes multiple passes of the surface and identifies candidate triangles, the triangles are removed and replaced with a single triangle whilst meeting surface tolerance criteria. A problem with decimation algorithms is known to exist at sharp corners, where these are rounded to some degree.

Fadel and Kirschman (1996, p. 7) discuss the format of the STL file. There are two representations of STL: binary and ASCII, both of these formats describe the coordinates of three points that form a triangle in space and it's out pointing normal. The binary format results in much smaller file sizes, typically a ratio of 6:1, but the

ASCII STL format is readable for visual analysis. The structure of the binary format is as follows:

A header of 84 bytes, the first 80 of which are used for file information, such as the author's name, the last four bytes represent the number of triangular facets.

Next, for each facet, 50 bytes are used to represent the x, y and z components of the normal to the facet, then the x, y and z coordinates of each vertex of the triangle. Four bytes are used for each coordinate; the last two bytes are not used. Taking into account that optical scanners can output an STL file with more than 500 000 triangles per scan, An STL file can easily be a size of 100MB or more. Further information on the STL file format is available in Appendix D.

During a conversion to STL, from either imaged data or a CAD package, there are several errors that occur in an STL file, that need to be repaired before any form of manufacturing takes place. Fadel and Kirschman (1996, p. 9), describe some of the typical errors:

- More than two triangles per edge (mid-line node)
- Truncation errors
- Flipped triangle normals
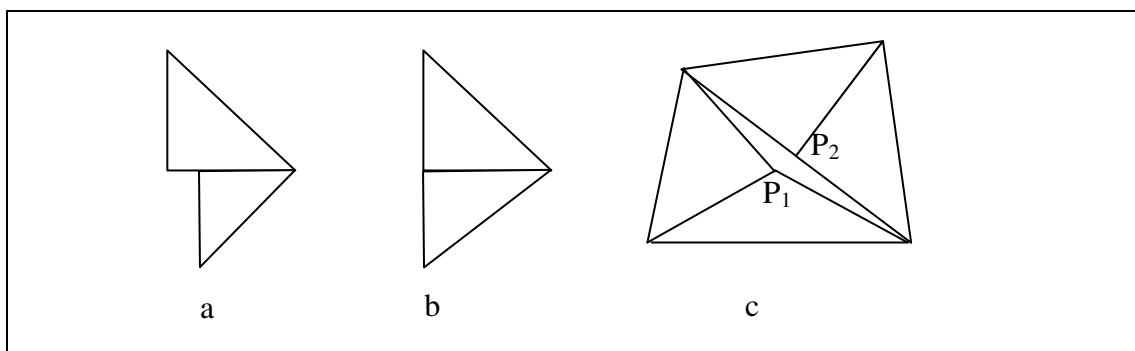
Figure 2-22: STL file errors
(Adapted from Fadel and Kirschman, 1996, p. 10)

Figure 2-22 shows a graphical description of the errors described by Fadel and Kirschman. Figure 2-22(a) shows how more than one triangle can share a common edge (mid-line node), Figure 2-22(b) shows a correct edge condition and Figure 2-22(c) shows a small hole that is formed from truncation errors, causing one point

(P_1 and P_2) to be defined at multiple locations. Hole filling algorithms, (see section 2.4.1) are not used to fill these holes, and the triangles are generally replaced. A flipped normal on a triangle causes operations such as offsetting and hollowing to produce undesired results. These errors are repaired in organic design software and can cause undesirable results such as stepped surfaces where holes exist.

Haptic design

A problem associated with traditional CAD and organic design packages, is that one relies on a 2D mouse interface to interact with a 3D object (Dachille, Qin and Kaufman, 2001, pp. 403-404). A new commercially available method is that of haptic (touch sensitive) interaction.

Haptics is defined by Bholat *et al* (1999, p. 349) as "the science of applying tactile sensation and control to interaction with the environment." The origin of haptics is from mechanical devices that were designed to handle hazardous materials (Thurfjell *et al*, 2002, p. 210). There are two distinct classes of haptic devices: impedance controlled and admittance-controlled (Thurfjell *et al,* 2002, p. 210).

The control of an impedance-controlled device is as follows: the user moves the haptic device, and the haptic device reacts with a (usually opposing) force if a virtual object is encountered. An example of an impedance controlled haptics device is the Phantom. In admittance control the opposite is true; the haptics device measures the force in and reacts with a displacement output. An example of an admittance control device is the FCS Haptic Master used in trucking gearbox simulators.

A typical haptic device provides between 2 and 6 degrees of freedom, and varies physically from a simple joystick (Thomas *et al*, 2001, pp. 53-54) to a complex robotic arm (Dachille, Qin and Kaufman, 2001, p. 404). In design applications, one can use both a 3D interaction device and the sense of touch to aid positioning on the digital model surface. A commercially available system for haptic design is the Phantom. The Phantom is a 3-degree of freedom impedance controlled haptic device that allows the user to virtually "feel" digital models.

The human skin is sensitive to vibrations greater than 500Hz, and haptic devices require an update rate greater than 1kHz for realistic feedback (Gregory *et al*, 2000, p. 70, Dachille, Qin and Kaufman, 2001, p. 409, Thurfjell *et al,* 2002, p. 212). Vibrations experienced with haptic systems are a symptom of low update rates. The Phantom exerts up to eighteen Newtons of force in a virtual environment with update rates greater than 1 kHz (Thomas *et al,* 2001, pp. 53-55).

Freeform, (Sensable Technologies) is organic design software, with an exception that the Phantom adds haptic interaction to the software. Freeform imports and exports a variety of file formats including STL. Freeform converts imported files into a voxel (3D pixel) format for use with the Phantom. Figure 2-23 illustrates the difference between a pixel, which can be rendered in 3D and a voxel which is a true 3D representation with depth, height and width. A voxel can have a density associated with it for touch applications, which gives a digital model a realistic "feel" to it when using the Phantom device.
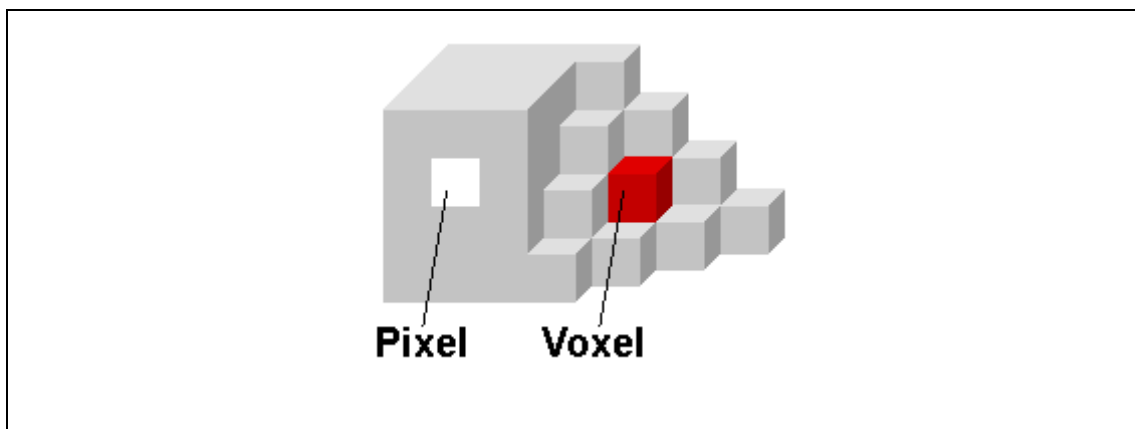
Figure 2-23: Voxel and pixel representation
(http://cal.man.ac.uk/student_projects/2000/mmmr7gjw/technique8.htm, 5 December 2003)

The Freeform system combines organic design principles with CAD functions. The Freeform system may be suited for medical design applications as one can apply traditional CAD procedures to organic shapes using the sense of touch, combining artistic skills with digital functions.

2.5.3 Design conclusions

Design software and hardware must be selected based on the design requirements and types of models one encounters. Difficulties are encountered when one tries to combine organic data, obtained from scanning systems with CAD software.

Haptic design systems may speed up design work with organic data offering and both create and edit organic shapes with reduced effort. Visual changes are made to digital models without tedious mathematical manipulation of individual surfaces and curves. Haptic design may assist in achieving increased aesthetics and accuracy for prosthetics required in the objectives in section 1.5. This research employs haptic design technology in its methods.

2.6 Rapid Prototyping

Rapid prototyping (RP) refers to the group of emerging technologies for the direct fabrication of objects from computer based designs (Jee and Sachs, 2000, p. 97) and allows shorter turn around times in manufacturing (Webb, 2000, p. 149). 3D Systems (Valencia, CA, USA), introduced the first commercially available system in the late 1980's, the stereolithography apparatus (SLA) (Kai and Fai, 1997a, p. 116, Webb, 2000, p. 150). There are now several RP systems available worldwide that cater for a variety of prototyping applications.

Commercially available RP systems use different materials and technologies, but are similar in that they manufacture in a traditionally additive method. RP is the layer-by-layer fabrication of a physical object from computer data of a virtual object that is sliced into cross sections (Choi and Samavedam, 2001, pp. 99-100, Young, Yu and Kwong, 2001, pp. 1035-1049).

In an early medical application, Mankovich *et al* (1994, pp. 875-889) traces the outline of CT scans, inverts them and manufactures a layered model of an inverted ear by milling the contours out of plastic. Mankovich *et al* encounters problems with the registration of the milled plastic layers, the misalignment of the layers, and thickness

of the plastic (2mm) creates inaccuracies. Beumer *et al* (1996, p. 467) and McGurk *et al* (1997, p. 170) use a milling machine and Styrofoam sheets to create a manually layered model of the cranium. The resulting model from Beumer *et* al is illustrated in Figure 2-24, where one can see the inaccuracies generated by the layer thickness. Petzold, Zeilhofer and Kalender (1999, p. 278) state the geometric accuracy of these milled models as ±1.5mm.

Figure 2-24: A milled cranial model
(Beumer *et al*, 1996, p. 467)

Not all medical applications use a layered construction technique, and attempts have been made at milling solid models. Penkner *et al* (1999, pp. 482-484) mills an inverted ear out of a solid block of polyurethane and Webb (2000, p. 150) mills a cranial model of a patients defect, similar to that illustrated in Figure 2-24. Problems experienced when milling these models includes the tool flexing whilst milling and the need for a multi axis milling machine for complex geometry.

The use of milling for medical applications described by Mankovich *et al* (1994), Beumer *et al* (1996), Penkner *et al* (1999) and Webb (2000) illustrates the need for a direct method of fabrication that requires minimal human intervention. RP can provide this method and improve on accuracy through automated registration of layers and reduced layer thickness.

RP methods fall into three basic types: liquid, solid and powder based systems (Webb, 2000, p. 149). Selected technologies from each of the three types of systems are next discussed.

Stereolithography (SLA), (3D Systems, Valencia, CA), is a liquid based RP system which finds substantial use in the medical industry (Webb, 2000 p. 150). SLA creates models out of acrylate photopolymer or epoxy resin, tracing a low powered ultraviolet laser across a vat filled with resin (McGurk *et al*, 1997, p. 170).
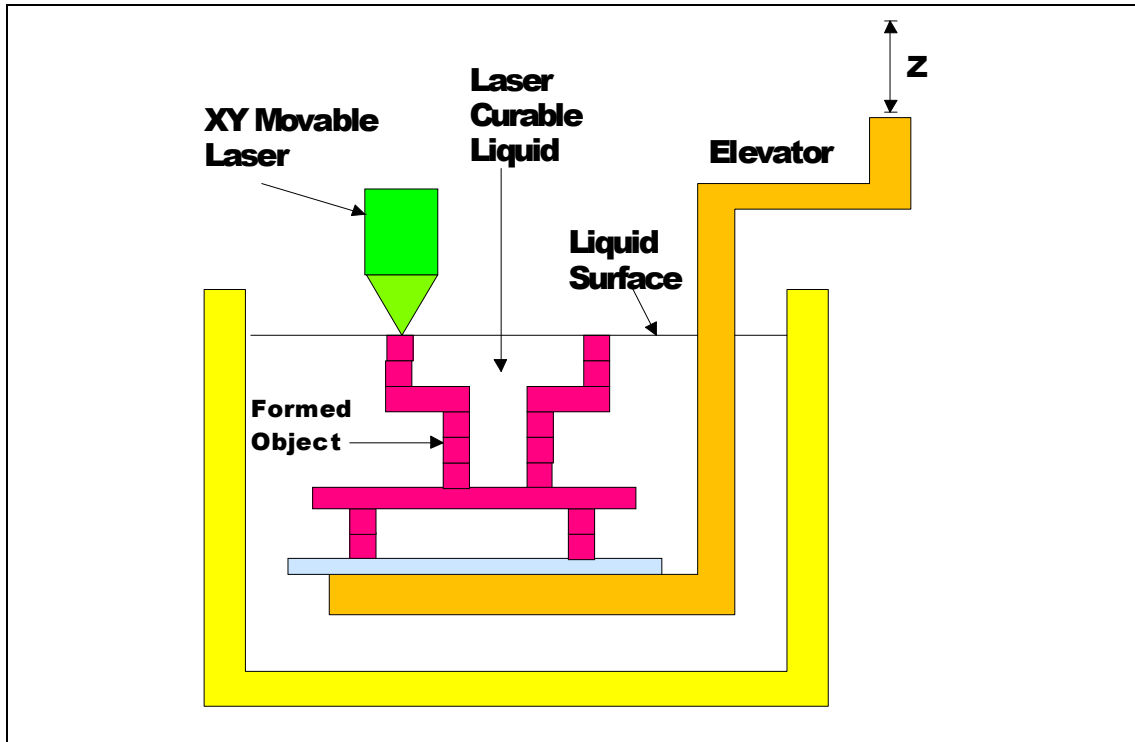
Figure 2-25: The SLA process
(Adapted from Wright, (2001), p. 134)

Figure 2-25 shows the main components of an SLA system. Note that the elevator starts near the liquid surface and moves downwards during building with the liquid level covering the previous layer. The typical layer thickness achieved is 0.1-0.5mm, with a geometric accuracy of ±0.1mm (Petzold, Zeilhofer and Kalender, 1999, pp. 279-280).

Fused deposition modelling (FDM), was developed by Stratasys incorporated, (Minneapolis, Minnesota, USA). FDM is a solid based RP system that creates 3D models out of heated thermoplastic material extruded through a nozzle (Figure 2-26a). The nozzle is moved around the x-y table until a layer is formed and the table then lowers (Potamianos *et al*, 1998, pp. 385-386). The FDM system uses a variety of

materials including: polycarbonate, polypropylene, clinical grade ABS and various polyesters (Potamianos *et al*, 1998, p. 385, Sanghera *et al*, 2001, p. 279).
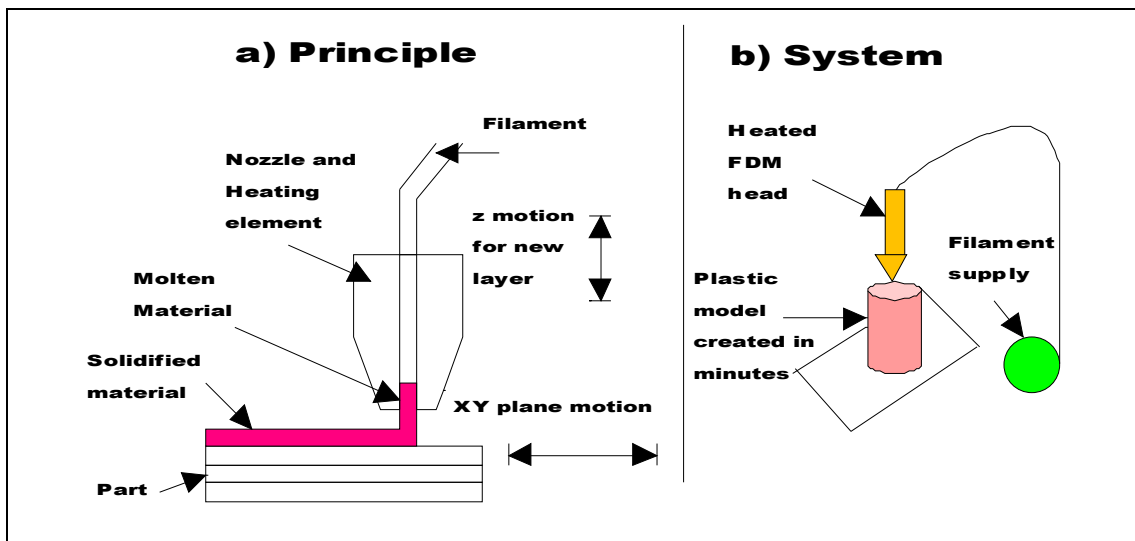
Figure 2-26: The FDM process
(Wright, 2001, p. 145)

Figure 2-26a shows the moveable nozzle of the FDM system extruding a thin stream of material onto the platform to form a layer. The material solidifies after leaving the nozzle and heating element, and acts as the base for the following layer. Figure 2-26b shows the overall system and material supply for a typical FDM system.

Selective laser sintering (SLS) is a technology commercialised by DTM[1] Corporation, (Austin, TX, USA). SLS is a powder-based system that creates models out of a heat fusible powder such as polycarbonate, or powdered metals. A modulated laser beam is traced over a layer of the powder and selectively fuses particles together. Once a solid thin slice is created, the next layer is started (McGurk *et al,* 1997, p 171). Figure 2-27 illustrates the SLS process. The metal powders create a porous part; a dense part is created by infiltrating the porous part with a metal of lower melting temperature, such as copper (Katz and Smith, 2001, p. 1497).

---

[1] DTM was purchased by 3D systems during the course of this investigtation
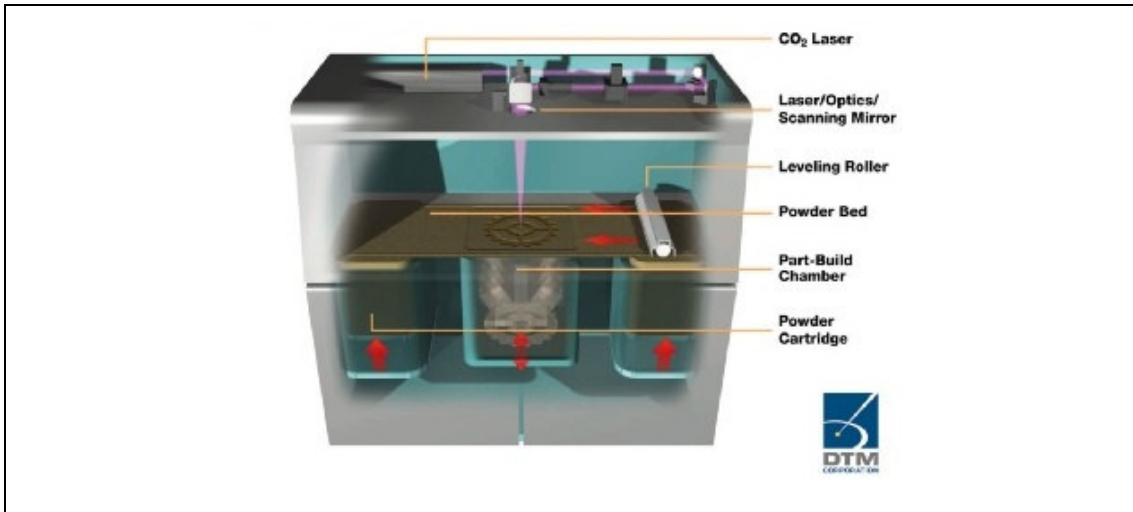
Figure 2-27: SLS process

(http://rpdrc.ic.polyu.edu.hk/content/rp_for_arch_short_guide_4.htm; 5 May 2004)

Multi-jet modelling (MJM), commercialised by 3D Systems, creates prototypes using wax as a build material and is a liquid based process.

Figure 2-28: MJM process
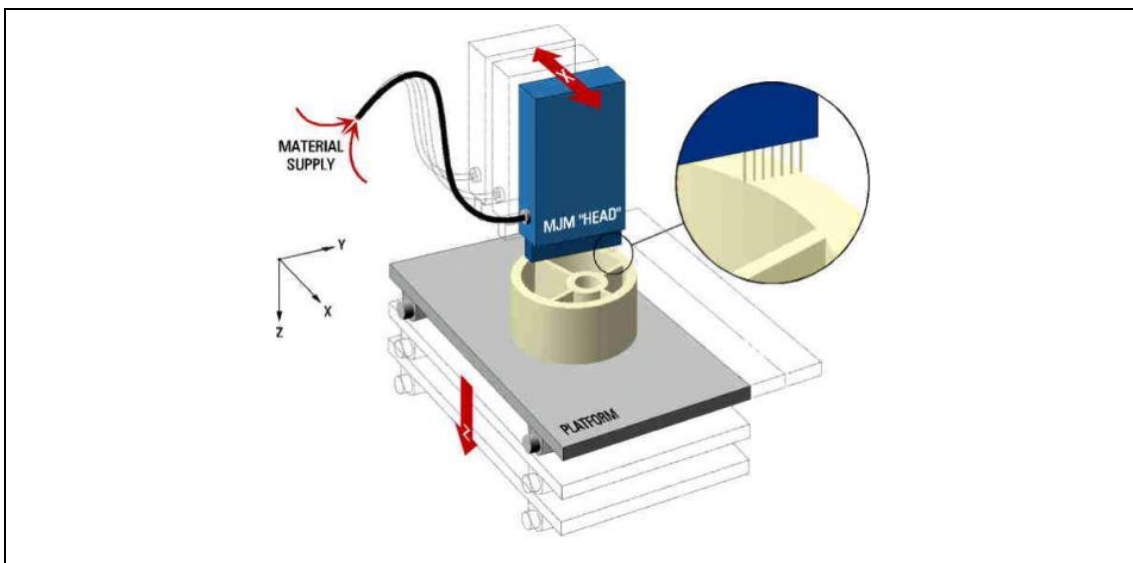
(http://www.turkcadcam.net/rapor/otoinsa/images/ ; 5 May 2004)

Figure 2-28 illustrates the MJM process. A multi-jet (MJM) head passes in the X-direction and deposits thin layers of molten wax as the head reaches the end; it steps in the Y-direction to create a uniform surface of molten wax. The Thermojet system, which uses MJM technology, has over 3000 jets dispersing molten wax over the build area. The jets are individually turned on and off to place the wax in the correct position. The Thermojet system has a layer thickness between 0.03mm to 0.1mm.

MJM systems use wax supports on the underside of models. The supports are thin vertical walls of wax that are easily broken off the model by hand. This results in a rough under surface and a smooth and glossy surface for the up facing portions of the wax prototype. A feature of the Thermojet system is that it is designed for office environments and works as a network printer (Cooper, 2001, pp. 44-48 and Petzold, Zeilhofer and Kalender, 1999, p. 278).

Table 2-2: Selected RP machines, vendors and specifications
(Adapted from Cooper, 2001, p. 214)

Process	System	Vendor	Max part size(mm)	Speed	General Material
SLA	SLA 3500	3D Systems	356 x 356 x 407	Fast	Epoxy
	SLA 7000	3D Systems	508 x 508 x 585	Very fast	Epoxy
FDM	Genisys	Stratasys	204 x 254 x 204	Fast	Polyester
	FDM 3000	Stratasys	254 x 254 x 407	Moderate	ABS
	Quantum	Stratasys	610 x 508 x 610	Fast	ABS
SLS	Sinterstation 2500+	DTM Corp.	381 x 331 x 432	Fast	Polymer
	LENS 750	OPtomec	305 x 305 x 305	Fast	Metal
	LENS 850	Optomec	458 x 458 x 1067	Fast	Metal
	Pro Metal	Extrude Hone	305 x 305 x 305	Fast	Metal
MJM	Model Maker II	Sanders Prototype	153 x 305 x 204	Slow	Wax
	Thermojet	3D Systems	178 x 254 x 204	Very fast	Wax
	Z402[1]	Z corporation	204 x 254 x 204	Very fast	Plaster

Table 2-2 shows an adaptation of Cooper's (2001, p. 214) comparison of commercially available RP machines. The table is ordered by process used, (SLA, FDM, SLS and MJM). Cooper (2001, p. 214) selects several of the commercially available prototyping systems and illustrates: the maximum prototype size, speed and build material used by each system. The speeds are listed in a general and comparative sense, but no basis is provided. The speed of prototyping systems is highly dependent on part geometry and human input. The general material column shows the material used to build prototypes by each type of machine. The materials cover a broad range of applications, but build size and tolerances vary.

Objective 1 requires the development of a digital process for implant and prosthesis design and manufacture. RP can provide the manufacturing interface for organic design data. This data is not parametrically controlled, and originates from a scanning

---

[1] The Z402 can build prototypes in colour

source. The data obtained from imaging systems, discussed in section 2.3 and modelled using techniques discussed in section 2.5 can be manufactured directly from edited STL data, thus eliminating the need to use a traditional CAD system. Combining RP with the artistic ability to sculpt digitally (using Freeform), a physical pattern for an implant or prosthesis can be designed and fabricated.

Surgical planning in medicine tries to minimise the duration of surgery to prevent the risk of complications. Full anatomical models can be viewed as virtual prototypes in organic design software and manufactured before surgery using RP. D'Urso *et al* (2000, p. 200), describe the ideal prosthesis as customised to restore the original anatomy and be prefabricated to minimise operating time and inherent risks. Although external facial prosthetics are used in this investigation, RP may achieve both increased aesthetics and accuracy for these applications. The Thermojet system, rated as very fast in Table 2-2 using wax as a build material, may fabricate anatomy that can be cast into another material. This research uses an MJM system for RP requirements and casting which is next discussed.

2.7 Casting

The Egyptians and Koreans developed casting in about 5000BC. Wright (2001, pp. 160-167), lists the popular casting methods as lost wax investment casting; Ceramic mould investment casting; shell moulding; conventional sand moulding and die casting.

Casting tolerances can vary from 75 microns for the lost wax process to 375 microns for the sand casting processes. Lost wax investment casting is used for items such as turbine blades which require a high degree of accuracy (Wright, 2001, pp. 160-167). Lost wax investment casting requires a wax model to start with, which the Thermojet printer can provide. This research requires high accuracy and uses a modified version of the industrial lost wax investment casting. Modifications to the process include lower temperatures and the use of silicone and acrylic instead of metals.

2.8 Medical Applications

Section 2.8 introduces the medical topics investigated in this dissertation. Sub-section 2.8.1 discusses the traditional medical procedures for cranioplasty. Sub-section 2.8.2 describes the anatomy of the auricle (ear) and sub-section 2.8.3 discusses facial prosthetics, and in particular the auricular prosthesis. Sub-sections 2.8.4 and 2.8.5 discuss firstly the effect computers are having on modern medicine and secondly examine existing research on customised human anatomy fabrication and includes cases using both RP and traditional CNC manufacturing techniques.

2.8.1 Cranioplasty

Craniofacial surgery aims at improving both the patient's physical condition and his or her appearance (Mankovich *et al*, 1994, pp. 875-876). The traditional method of planning craniofacial surgical procedures uses photographs, models clinical examinations and normative standards (Cutting *et al*, 1986, p. 877). With the introduction of 3D CT scanning techniques, many advances have been made including craniofacial simulation software based on virtual 3D CT reconstructions, for patients requiring surgical reconstruction of the cranium, (Girod *et al,* 2001, p. 157), and physical construction of the skull or portions thereof using RP to produce a physical model for custom implants and preoperative planning (D'Urso *et al,* 2000, pp. 200-201), (Petzold, Zeilhofer and Kalender, 1999, pp. 277-284), (Winder *et al*, 1999, pp. 26-27), (Sailer *et al,* 1998, pp. 327-333) and (Mankovich *et al*, 1994, pp. 875-889).

Winder *et al* (1999, pp. 26-28) describe the traditional method for the manufacture of a custom titanium implant in craniofacial surgery. An impression of the defect is taken through the shaved overlying skin. A dental stone mould is obtained from the impression. A thin titanium sheet is formed to approximate the contours required using the dental stone mould. Winder *et al* report that in a particular hospital where a review was carried out, 23 percent of the titanium implants were ill fitting and 41 percent of frontal plates have a poor aesthetic quality.

There is significant use of non-metallic implants in cranioplasty applications. An acrylic material used is Poly-methyl-methacrylate, (PMMA). Advantages of PMMA include: low cost, easy casting and demonstration of long-term biocompatibility. Disadvantages of PMMA when conducted *in situ* are the exothermic and potentially toxic nature of polymerisation (D'Urso *et al,* 2000, pp. 200-201). The polymerisation can cause damage to sensitive dural and sub-dural structures and release monomer into the patient's circulation. Use of PMMA *in situ* is the standard approach.

Kai and Fai (1997b, pp. 221-224) discuss two cranioplasty cases using RP, one case in which a cancerous brain tumour is removed and another for reconstruction of the skull. In both cases, an SLA model is made of the skull for operation planning and moulding of an implant respectively. These two cases highlight the expensive trend of using large RP models for operation planning and implant design. This dissertation uses an implant case in cranioplasty to satisfy the objectives in section 1.5.

2.8.2 The anatomy of the auricle (Ear)

The auricle (ear) is an irregular and complex surface. According to Lumley (1990, p. 16) the external auricle (ear or pinna) is formed from a number of irregularly shaped pieces of fibrocartilage covered by firmly adherent skin.

Figure 2-29: Auricular anatomy

(Lumley, 1990, p. 16)

The anatomy of the external auricle, illustrated in Figure 2-29, is divided into the following areas:

1 Helix
2 Antihelix
3 Triangular Fossa
4 Tragus
5 Antitragus
6 Lobule
7 External Acoustic Meatus

The seven areas of anatomy form discussion points when comparing a traditional and digitally manufactured ear prosthesis.

The ear has a dependant lobule and an anterior tragus overlapping the opening of the external acoustic meatus. The external acoustic meatus is mainly cartilaginous laterally and bony medially. The ear, with the triangular fossa being sunk into the ear and yet other parts laterally raised such as the tragus has considerable geometric

detail. Areas of concern for a digitised ear are the undercuts, dips and raised parts of the surface of the ear. An industrial imaging system requires several angles to view this geometry and obtain a full geometric description.

2.8.3 Facial prosthetics

A facial prosthesis is designed when a patient has either a disfigured region or is missing some portion of the facial anatomy. The facial anatomy includes a number of features such as the nose, mouth or ear. Unlike an implant, a prosthesis can be removed by the patient and can include an oral prosthesis which duplicates anatomy inside the mouth. One of the more difficult regions to manufacture is the auricle (ear) due to the complex geometry and undercuts described in sub-section 2.8.2. The manufacture of an auricular prosthesis is discussed in this section in detail.

Wang (1999b, p. 634), describes the loss of an auricle as the result of trauma, congenital disease, or surgical ablation of benign or malignant tumours. A congenital condition, hemifacial microsomnia (HFM) refers to patients with unilateral microtia, macrostomnia, and failure of formation of the mandibular ramus and condoyle, it is also the second most common craniofacial malformation after cleft lip and palate (Wang, 1999a, p. 492). Auricular deformities are often a result of HFM and it is reported that 1 in 3500 births are affected (Wang and Andres, 1999, p. 197).

There are two methods for rectification of an auricular defect: surgical reconstruction or the use of a silicone prosthesis. The surgical reconstruction method consists of reconstruction of the ear using a cartilage framework, draped by skin, whilst a silicone prosthesis is modelled by a prosthodontist.

Park (2000, p. 1473-1487) uses an improved surgical method for microtia reconstruction, where there are often ear remnants remaining on the affected side. The method includes an incision of the skin made in the affected area, and tissue expanders are inserted. The expander is injected with a saline solution for a period of five months to create loose skin with which to work. An ear framework, created from autogenous rib cartilage, is inserted into the flaps. The loose skin is formed around

this framework to create a new ear surgically. Park (2000, p. 1473-1487) describes the aesthetics of the reconstructed ear as favourable with minimal complications.
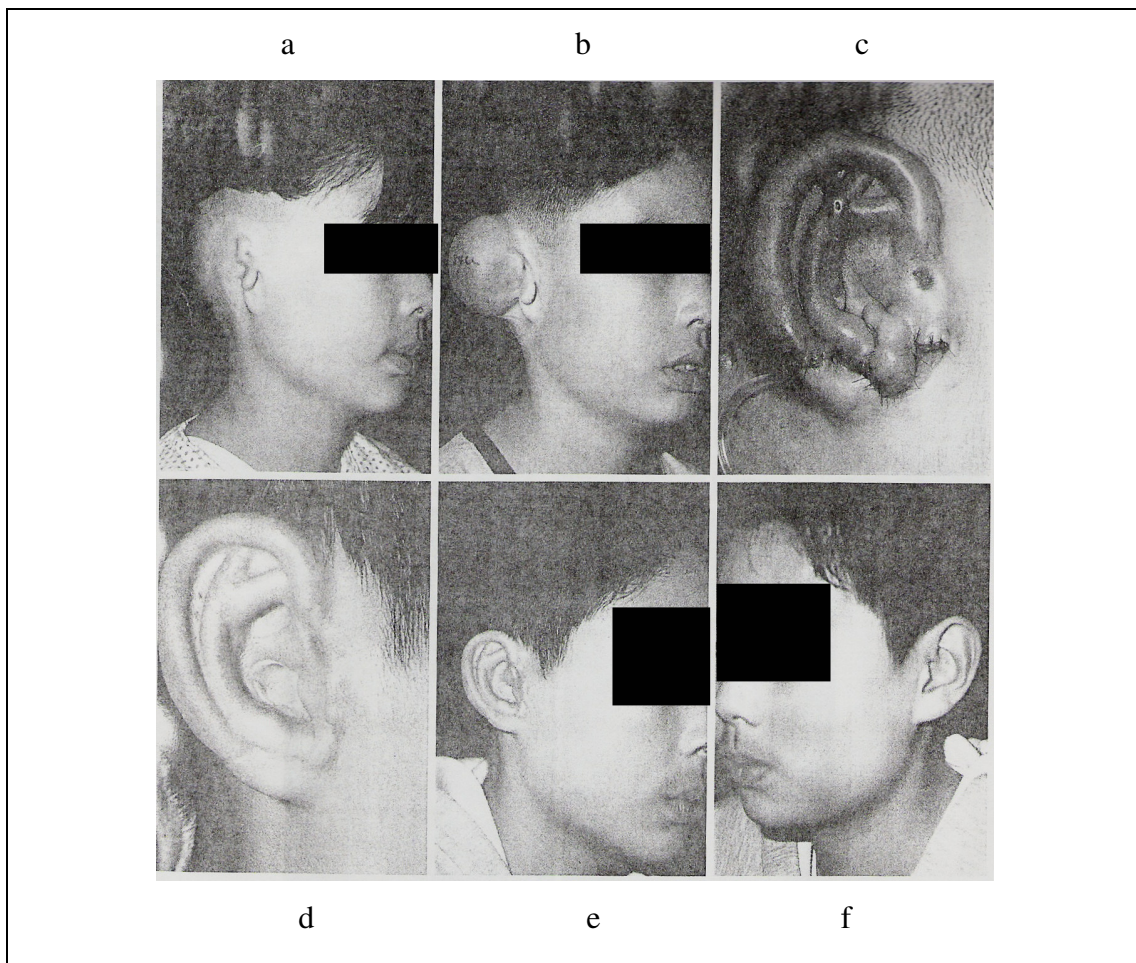
Figure 2-30: Surgical ear reconstruction
(Park, 2000, p. 1483)

Figure 2-30 shows the results Park obtains from one of his case studies using a patient with microtia. Figure 2-30(a-f) shows the following steps and results in surgical ear reconstruction:

a) Patient with microtia and the ear remnants
b) Final stage of tissue expansion
c) The immediate postoperative results
d) A close-up of the surgically reconstructed ear
e) The reconstructed ear
f) The normal remaining ear

Figure 2-30d shows the results of surgical reconstruction. The reconstruction seems to have all of the anatomical points illustrated in Figure 2-29, but is consists of highly accentuated contours compared to the normal ear illustrated in Figure 2-30f. Wang and Andres (1999, p. 200) state "Reconstructive ear surgery is one of the most demanding challenges for the plastic surgeon because of the ears complex structure." This statement is evident from the results obtained by Park (2000).

Modern ear prostheses are retained with adhesive, which include: interfacing pastes, liquids, sprays or double sided tape (Parel, 1980, p. 552). The other option prospective patients have, is that of bone integrated implants (Asher *et al,* 1999, pp. 228-233). When bone integrated implants are used, the ear prosthesis is fitted with a metal bar that interfaces with implants placed in the postauriculotemporal region (Parel *et al,* 1986, pp. 600-601). Methods of attachment include: clips or magnets (Allen *et al,* 2000, p. 99). Allen *et al* reports that difficulties and limitations associated with adhesives include: adverse skin reactions, loss of adhesion and extensive tissue coverage to increase retention. An advantage of using an implant-retained prosthesis is the patients' confidence in placement (Asher *et al*, 1999, p. 228). This type of prosthesis is fitted and removed with ease, compared to the adhesive options where placement must take place in front of a mirror. Given the surgery involved with bone integrated implants, adhesives are still used (Parel *et al,* 1986, p. 606).
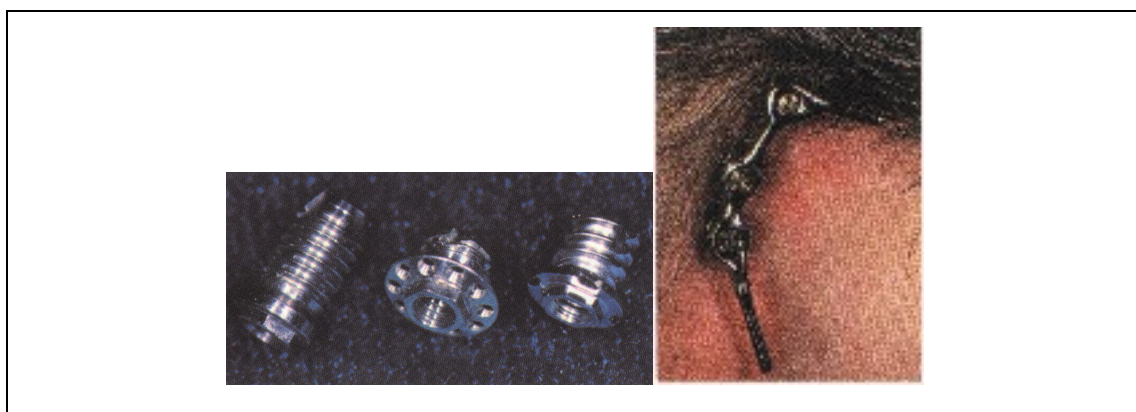
Figure 2-31: Ear implants and a metal retaining bar
(Beumer *et al*, 1996, p. 438)

Figure 2-31 shows the mechanical retention mechanism for an implant retained prosthesis and the standard titanium implants used for prosthesis retention.
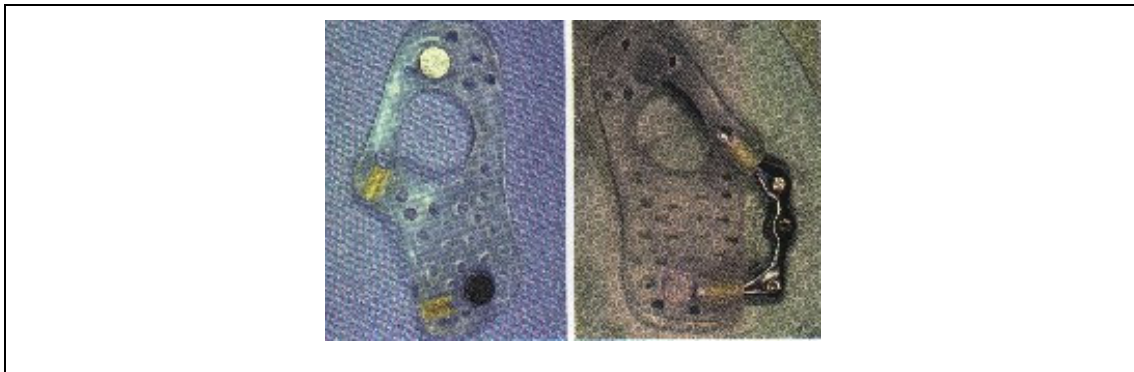
Figure 2-32: Acrylic substructure
(Beumer *et al*, 1996, p 443)

Figure 2-32 shows an acrylic substructure used to mount the fittings on an implant-retained prosthesis. The sub-structure still requires a prosthesis to be designed and moulded over the substructure.

The design of the silicone prosthesis, uses similar techniques independent of the method of attachment chosen. The general practice is to sculpt the ear prosthesis by hand out of either clay or wax (Lemon *et al,* 1996, p. 292-293, Asher *et al*, 1999, p. 229, Wang, 1999b, p. 634). Kai *et al* (2000, pp. 43-44) describe how this widely adopted process requires experience skill and time. Lemon *et al* (1996, pp. 292-293), describe how several methods have been devised to aid the sculpting process. The methods include the use of the reverse ear from a family member, individual with compatible ear morphology and the photocopying a model of the existing ear onto a transparency flipping and using the image as an aid whilst sculpting and the use of a mirror whilst sculpting. Older attempts include those by Nusinov and Gay (1980, pp. 68-71) using an indelible pencil to trace the general outline of the ear from the cast model and superimposing the measurements onto a sculpted ear.

The cast model of the existing ear can be obtained using a process described by Kubon, Kurtz and Piro (2000, pp. 648-651). The steps are as follows:

1. The patient is placed in a dental chair and the inner ear is blocked with lubricated cotton and any facial hair in the region of the ear is lubricated.
2. Medium body polyether is syringed under the helix and lobe of the remaining ear.
3. Light body polyvinyl siloxane is syringed over the remaining portions of the ear.
4. The chemical dissimilarity of the two materials won't allow them to bond, thus creating a two-piece mould when set.
5. The impression is removed from the patient when set.
6. Plaster-of-paris is poured in and around the impression and allowed to set.

Kubon, Kurtz and Piro (2000, p. 649) use medium body polyether for its high rigidity as it forms a support structure, and light body polyvinyl siloxane because of its high resistance to deformation, ease of flow and high tear strength on setting.

Parrott and Machet (2001, pp. 66-72) use CT scanning to obtain a digital model of an ear for the creation of an auricular prosthesis. Although the slice distance of 1mm is unsatisfactory, use of the Freeform system from Sensable technologies allows for additional smoothing and processing to be conducted on the digital model. Kai *et al* (2000, p. 43), says that most facial implants do not serve a functional purpose but rather to enhance appearance. Using this philosophy for a digital design process, one can understand that internal medical scanners, such as the CT scanner used by Parrott and Machet (2001, p. 66-72) are not necessary for prosthetics, as it is the external, non-functional anatomy that contributes to the aesthetics of the final prosthesis.

Kai *et al* (2000, pp. 42-53) uses a laser digitiser for obtaining digital data of a patients healthy ear. A CAD system is used for designing a mould from which an ear prosthesis is produced. Four RP methods are investigated including: SLA, SLS and

FDM to prototype the ear moulds. The investigation concludes that a laser digitiser reduces time and minimise patients involvement in the prosthesis creation process.

The traditional process of creating an ear prosthesis, even using the aids described by Lemon *et al,* is a process that requires both artistic and technical skill. The digital and RP models Kai *et al* produce assist in speeding up the process, but lack a design and manipulation option in the process.

A digital process using imaging, design and manufacture may remove some of the artistic ability currently required and speed up the process.

2.8.4 Selected Trends in Modern Medicine

Computers are often used as a support tool for the diagnosis, operation planning and treatment in both medicine and dentistry (Hassfield and Mühling, 2001, p. 2). One explanation is the increase in computing power that is now available relative to the cost of computing systems and software. While there has been work undertaken in selected medical applications, the use of advanced technologies in section 2.8.1 and 2.8.3 may encounter acceptance problems. This section considers the acceptance of two similar technologies. This section considers the experimental use of real-time imaging and haptics with a specific focus on the medical applications.

Real time medical imaging

Abovitz (2001, p. 401), and Wickham (1994, pp. 193-195) describe how surgery is performed an open invasive manner, with a reliance on the art and skill of a surgeon. There is a movement to change this either to less invasive procedures, or improve procedures, by incorporating computing technology to the operating room. For example, Wickham describes how adequate vision as the utmost importance in the development of minimally invasive operations. Laparoscopy, (minimally invasive surgery, using fibre optics for visualising), offers patients a shorter hospital stay, better cosmesis, and less postoperative pain in a variety of applications (Corvera and Kirkwood, 1997, p. 587). Laparascopy is one example where technology is being

harnessed in the operating room, and in this case, the doctor requires a small incision to view what previously would require a large incision.

Intraoperative navigational systems, using real time imaging, are being developed globally to aid surgery. Several systems have been developed, for applications including, bimaxillary orthagnic surgery using a mechanical navigation system and positional sensors, (Santler, 2000, pp. 287-293), general surgery using the whole arm manipulator (WAM) which combines both haptics and robotics for navigation purposes, (Abovitz, 2001, pp. 401-405), neurosurgery through the use of a system called the wand whereby previously acquired MRI scans are registered on the patient spatially using a mechanical arm, this allows the surgeon to know precisely where he is by looking at the 3D reconstruction of the MRI image, (Buckingham and Buckingham, 1995, pp. 1479-1482). Robotic systems allow a surgeon to perform the operation off site (Telemedicine applications), and use small incisions, whilst relaying real time images on the progress of the operation.

Virtual reality (VR) and haptics

The term "virtual reality" (VR) was introduced by Lanier in 1989 (Meier, Rawn and Krummel, 2001, p. 372) and the technology now available is proving to be a viable method for preoperative planning. VR is defined by McGovern (1994, p. 1054) as "…human interaction in an environment that is simulated by a computer." Medical areas that are being influenced by VR include: education and training, preoperative diagnostics, preoperative planning, intraoperative applications, postoperative applications and telemedicine (Meier, Rawn and Krummel, 2001, pp. 377-379).

Humans interface in the real world with five senses, namely: sight, sound, touch, smell and taste. Current computer interfaces such as a mouse, keyboard and monitor are not well suited to VR applications as they do not establish an immediate connection with our senses (Meier, Rawn and Krummel, 2001, pp. 374-376). Meier Rawn and Krummel have presented the following percentages of our sensory input, sight: 70%, sound: 20%, touch/haptics: ~5%, smell and taste are both in the early experimental phase, and still need to be quantified. Although haptics is only 5% of

our sensory input, it plays a crucial role in digital surgical applications (Meier, Rawn and Krummel, 2001, p. 375).

A variety of haptic systems are used for surgical planning and training, Gibson *et al* (1998, p. 121-132) use a Phantom haptic system for surgical simulation of arthroscopic knee surgery. Using a series of MRI scans, a 3D volumetric construction of the knee is generated and the tissue and bone stiffness properties are entered. Although the model is still primitive as a training simulator, deformation of the volumetric model is possible, the next stage of the project is to incorporate tissue deformation, cutting and suturing, allowing surgeons to practise digitally. Bholat *et al* (1999, 349-355) conduct an experiment determining the use of haptics during minimal invasive surgery. The study concludes that laparoscopic instruments do in fact provide surgeons with haptic feedback. This result is being used in the development of laparoscopic simulators that include force feedback results.

The incorporation of haptic technology into medicine for simulation purposes is not only limited to surgery and Thomas *et al* (2000, p. 53-64) use a dental simulator to train dental students in the haptic skills of dentistry. The haptic forces of traditional instruments are used on digital teeth models. A haptic joystick, offering two degrees of freedom, compared to the Phantom with six degrees of freedom is used to manipulate the virtual tools. Thomas *et al* conclude that the test subjects expressed a strong desire for the system to have six degrees of freedom to accurately portray a dental tool in free space. The reason for using a 2-degree of freedom haptic device is that the graphics are a 2D representation. The system demonstrates a degree of success with dentists detecting carious lesions in enamel and dentin through touch.

With similar imaging and haptic technologies, this research should not have a problem in implementation.

2.8.5 Customised anatomy design and fabrication

RP is primarily used in the medical field as a visual aid for surgical preparation, using models prepared from medical imaging modalities such as CT. D'Urso *et al* (1999,

pp. 490-500), use SLA for creating cerebrovascular models for patients with aneurysms. The models provide a physical tactile method for surgical planning. Sanghera *et al* (2001, pp. 280-281) investigate the effectiveness of prototypes in the improvement of patient treatment. Nine projects are undertaken and prototypes are grown for the nine anatomical sites. The prototypes include: shoulder, hip, knee, mandibular, and spine section models. The prototyping system used for the survey was an FDM 1560 from Stratasys incorporated. The results from the survey include that prototype models should be available routinely for complex orthopaedic surgery. Consultants from maxillofacial/craniofacial surgery showed the most interest in the study. Sanghera *et al* (2001) concludes that the superior treatment plans resulting from use of the prototypes can potentially reduce the number of follow up procedures to correct irregularities.

Not all custom implant projects use RP. Werner *et al* (2000, pp. 181-186) use a milling machine for fabricating a custom human hip joint. CT scans of the joint area are segmented using medical modelling software to isolate cortical bone from other soft tissue. A uniform point cloud is generated of the isolated bone structure through each CT slice. A geometric curve is passed through each of the data sets, and smoothed using additional mathematical algorithms. The resulting non-uniform rational B-spline (NURBS) curves are exported to a traditional CAD system for further design and editing . A 2½-axis CNC milling machine, is used to cut the tooling paths designed by the computer aided manufacturing (CAM) software. The role of CAM software is to virtually machine the part from stock and generate the tool cutting paths for physical manufacture using a CNC manufacturing process.
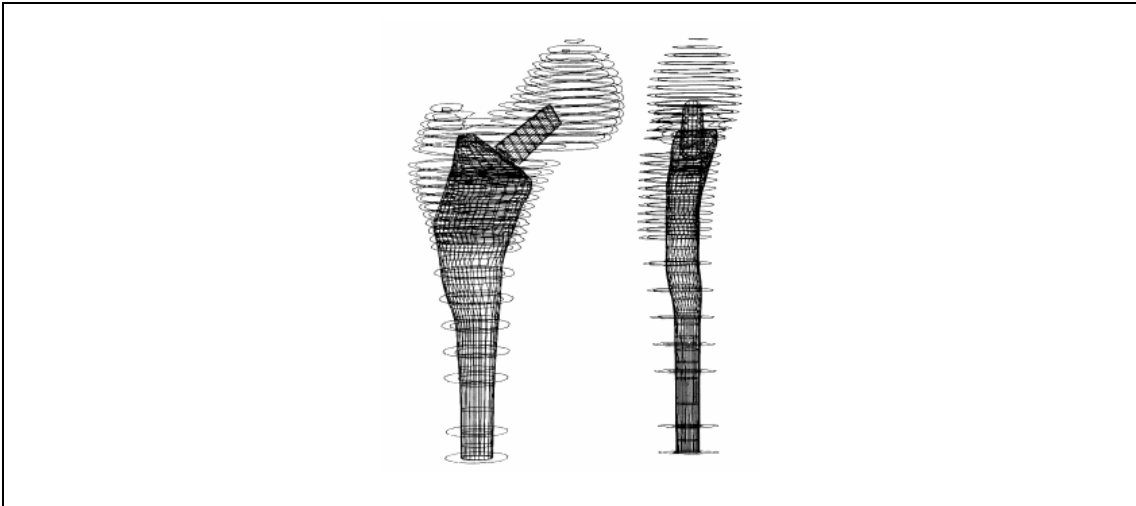
Figure 2-33: Curve approximation of the femur

(Werner *et al*, 2000, p. 183)

Werner *et al* experiences a problem with the large data set required to prevent discrete steps from appearing in the machined model and this is illustrated in Figure 2-33. This case study illustrates a need for organic design software, discussed in sub-section 2.5.2 to prevent the need of using a traditional CAD system for editing data. The NURBS curves used by Werner *et al*, are generally exported using the international graphics exchange standard (IGES). The IGES file format is supported by most international CAD vendors but is unfortunately interpreted differently by competing CAD vendors, (Fadel and Kirschman, 1996, p. 7). The different interpretations make IGES files difficult to edit, as experienced by Werner *et al*.

Using organic design systems and bypassing the need for traditional CAD software, allows the same freedom of design, but without the time associated with curve and surface manipulation.

2.9 Evaluation Criteria

The evaluation or assessment of quality of the products manufactured and processes used in this research provides a measure to compare the traditional and digital processes.

Product quality is a complex multidimensional factor for which no single definition exists (Sebastianelli and Tamimi, 2002, p. 451). Differences in product quality reflect the differences in product attributes. The assessment of product attributes is highly subjective and can differ considerably among individuals (Zhang, 2001, p. 710). Garvin (1988, pp.49-50) presents eight dimensions or categories of quality that allow quality to be analysed and quantified. The eight dimensions of quality and each definition is displayed in Table 2-3.

Table 2-3: The eight quality dimensions
Garvin, (1988), pp. 49-50

Dimension	Definition
Performance	The primary operating characteristics of a product
Features	The secondary characteristics of a product that supplement its functioning
Reliability	The products probability of failure free performance over a specified period of time
Conformance	The degree to which a products physical and performance characteristics meet specifications
Durability	A measure of useful product life
Serviceability	The ease, speed, courtesy and competency of repair
Aesthetics	How the product looks feels sounds tastes or smells, and is based on personal preference
Perceived quality	Quality based on image, brand name or advertising rather than product attributes and is subjective

Several of the dimensions presented in Table 2-3 involve directly measurable product attributes, but others require subjective individualised analysis. Not all of the dimensions in Table 2-3 apply to a particular product or process, and when measuring quality, one selects the dimensions relevant to the study and trade these off against other factors (Garvin, 1988, pp. 61-62 and Bicheno, 2002, pp. 16-17). Priest and Sanchez (1988, p. 17) provide a definition of product quality as "…a measure of how well the design meets all requirements of the customer and other groups that interact with the product." This definition globally encompasses design quality, and Garvin's eight dimensions provide the factors for measuring customers' requirements for design quality.

This research develops a digital process for custom implants and prostheses, and compares the process to the traditional methods on selected factors. Both implants and prostheses are custom products, and as such cannot be easily compared to a global

specification. Both processes produce different products, one made digitally where repeatability may be achieved, and the other by hand with artistic talent and low repeatability. The customer for both products is a patient who requires an implant or prosthesis either for health or aesthetic reasons. This process of comparison that is required can be considered as benchmarking, which Prasad (1998, p. 272) defines as increasing a products functional worth and used to measure performance and determine the products best features.

The important dimensions, for an implant and prosthesis are displayed in Table 2-4 and consist of dimensions extracted from Garvin's work:

Table 2-4: Quality factors

Quality Dimensions	Factor	Definition
Conformance	Accuracy	The closeness of match between the manufactured prosthesis or implant to the digital model
Aesthetics, Perceived quality	Aesthetics	The appearance and styling of a prosthesis or implant based on subjective measurments
Performance	Cost	the cost of the process or method
Performance	Speed	the speed of the process or method

Table 2-4 consists of three columns, "Quality dimensions" is the selected dimension from Garvin's work, "Factor" is the reworded name of the dimension in this research to simplify it and "Definition" defines each factor with relation to this research.

Accuracy is an objective measurement that can be measured using several methods. The accuracy of digital models may be measured by comparing the models to one another and taking measurements. Some of the industrial image processing software, discussed in sub-section 2.4.1, have digital metrology tools including linear and angular measurements. The digital tools require a base measurement or specification in order to provide meaningful results. Organic data won't have an easily obtainable specification. Methods of comparing organic data include digital comparisons, where one digital model is aligned to another using an ICPM algorithm and evaluating the minium distance between the models. The information can be displayed using colour error maps. The colour error maps use a scale of colours to indicate the intervals that errors fall into. Figure 2-34 shows an example of a colour error map with the deviations in the model.
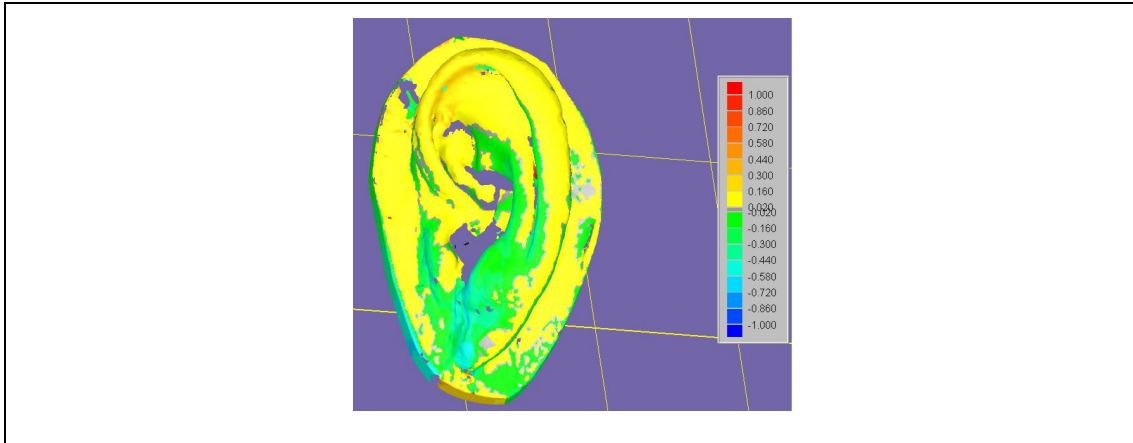
Figure 2-34: A colour error map

There may be difficulty in comparing a hand made and digitally generated product objectively, but digital imaging can provide comparison data at several steps in a digital process.

Aesthetic appeal is a subjective term and based on customers' perceptions and personal preferences. One method of measuring such attributes for is that of a customer survey. This survey is similar to that used by Sebastianelli and Tamimi (2002, pp. 442-447) who survey quality managers on how they asses their companies focus on each of Garvin's quality dimensions.

Excluding open ended questions, assessment of a survey is through the use of scales such as a question with one or more answers that a respondent can choose. The type of scale chosen is dependant on the existence or non-existence of the following properties (Bless and Higson-Smith, 1995, p. 100):

1. *Magnitude,* the possibility of comparing different amounts or intensities of a variable.
2. *Equal intervals,* allows magnitude to be expresses by a certain number of units of a scale with equal intervals.
3. *Absolute zero,* is a value indicating that the measurement of a variable is meaningless if it is non-existent.

Aesthetics can be measured using an ordinal scale (Sebastianelli and Tamimi, 2002, pp. 442-447). An ordinal scale possesses magnitude, but allows for both comparison and the establishment of rank order between different values of a variable (Bless and Higson-Smith, 1995, p. 100-101), (Cooper and Weekes, 1983, p. 38). An example of an ordinal scale is the feelings of a respondent as very happy, happy, indifferent, unhappy and very unhappy. This measurement does provide some comparison of respondent's feelings, but does not mean that very happy is twice as happy as happy, and as such does not possess equal intervals.

Analysis of an ordinal scale can consist of determining whether there is a significant difference in opinion between categories i.e. does a respondent perceive very happy different to happy. In an ordinal scale, the normality of distribution cannot be assumed and Bless and Kathuria (1993, p. 185) recommend non-parametric or distribution free tests. Non-parametric tests can evaluate whether or not the two or more populations are not significantly different (H_0) or are in fact significantly different (H_1). The χ^2 test (chi-squared test) can be used to evaluate differences in aesthetic appeal (Bless and Kathuria, 1993, p. 186).

Cost savings are usually cited as justification for automating tasks using computers in many instances (Slack, 1991, p. 80). This research may offer cost savings by time and labour, but capital outlay for new technologies may prove inhibitive. Cost comparisons can be performed based on: labour, equipment capital and material costs. Both the traditional and digital processes are producing custom once-off products, and costs vary from product to product, but a general comparison may provide an indication of the magnitude for each process.

Speed, like cost can be measured directly from both the traditional and digital processes. The time for each step of a process can be measured, but varies from product to product, and again this measurement provides magnitudes for both the traditional and digital processes.

The evaluation criteria of accuracy, aesthetics, cost and speed form a quality review for both a traditional and proposed digital process for prosthetics and implants.

Accuracy, cost and speed can be measured directly from each process and method, but measuring and comparing aesthetics requires people's opinions.

2.10 Literature Review Conclusions

The literature review has explored the various aspects of using new technology in medical applications with a focus on the reverse engineering process, including: imaging, image processing, design and the use of RP for medical applications. The literature has explored techniques that can assist in achieving the objectives stated in section 1.5.

Section 2.3 describes both industrial and medical scanning techniques. Industrial imaging techniques can be used for the acquisition of external human anatomical geometry, but requires the advanced image processing software described in section 2.4 to register the images taken from different angles. Both contact and non-contact measurement systems may digitise external anatomy using image processing software. A CMM (contact measurement) is more accurate than non-contact measuring systems, but slower. CT scanning provides a method for the digitisation of internal human geometry for the creation of custom cranial implants. It is also routine take CT images for diagnosis, this same data can be used for reverse engineering purposes. The slice distance is expected to be the largest error with CT images and must be minimised.

Image processing software provides an interface to design software and processes the industrial scans from point clouds to a tessellated model without holes. Analysis of the STL files can be performed in the image processing software to prevent the STL errors discussed by Fadel and Kirschman (1996, p. 9). The geometric complexity of the human ear prevents all of it from being digitised with the industrial scanners and curvature based hole filling algorithms extrapolate missing surface information.

Haptic technology can digitally duplicate the traditional hand made approach of implants and prostheses often used by doctors, discussed in sections 2.8.1 and 2.8.3. Whilst still allowing the traditional carving methods, surgeons may perform a tactile

analysis on models, and assist in preoperative planning. Digital scanning and haptic modelling may create digital benefits, such as the storage of anatomy for future reference. Haptic design may prevent the tedious design pace experienced by Fadel and Kirschman (1996, p. 5) and Dachille, Qin and Kaufman (2001, p. 403). If enough of the anatomy for a prosthesis or implant is scanned, editing of the digital model, even with haptic technology, may be minimal. Haptic design systems may prevent the need to convert to NURBS surfaces for CAD systems and work directly on STL files. Haptic design may increase the working speed when compared to the traditional hand methods, with increased accuracy and repeatability.

RP has seen extensive use in the medical industry (section 2.8.1), but little has been pursued in using RP with digital design. The lack of design is based partly on the inability of CAD systems to deal with the data, which is addressed in this research. This additional step of digital design may lower the cost of RP models, as only the required part is being prototyped.

A selected case study of both an auricular prosthesis and cranial implant highlights both design capability and functionality of a digital process. New RP systems that prototype in wax means that materials can be cast directly, without intermediate tooling development. Time may be saved with use of the STL file format throughout the reverse engineering process from scanning to fabrication.

The evaluation criteria in section 2.9 assist in quantifying the results of a quality survey and review of the process. These results may be used to quantify and establish the advantages or disadvantages of a digital process in custom anatomical fabrication. This evaluation shows how the proposed digital process compares to the traditional methods of medical practitioners using some of the dimensions of quality proposed by Garvin (1988, pp. 49-50).

3   Apparatus

Chapter 3 describes the apparatus used in the investigation. The apparatus includes all of the software and hardware requirements for a digital reverse engineering and manufacturing investigation.

3.1 Process Overview

The apparatus used in the research is displayed in the order it is used in the generic reverse engineering process discussed in section 2.1.
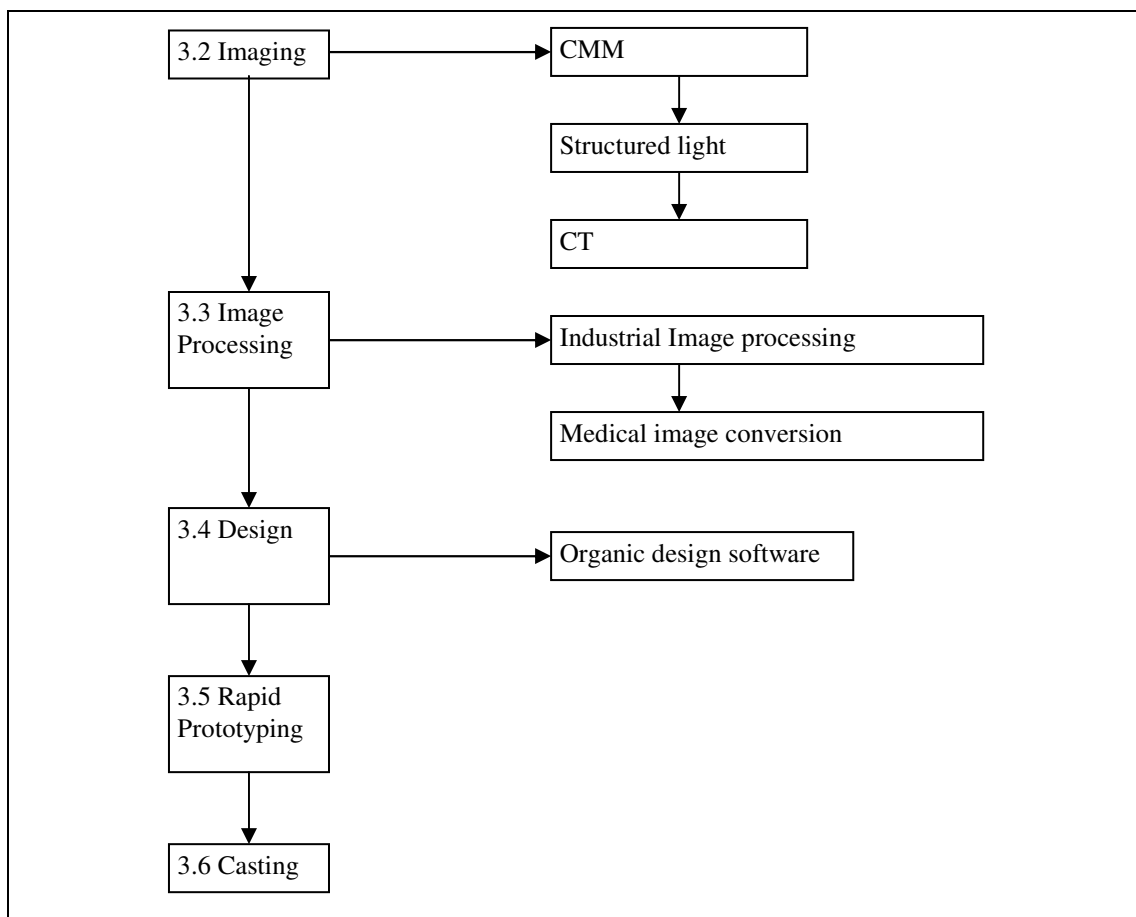
Figure 3-1: Process and chapter layout overview

Figure 3-1 shows the reader a flowchart of the digital process and the section where the apparatus appears. The reader can refer back to Figure 2-1, with the generic process of reverse engineering. The first step in the process is the acquisition of a digital model using both industrial and medical scanning systems. This is followed by both industrial and medical image processing, coupled with an organic design system for editing of the models. Manufacture consists of prototyping into wax and direct casting of the prototype.

The industrial scanning systems include a CMM (Renishaw Cyclone) and a structured light system (Breuckmann Optotop). A Phillips CT scanner is used for medical imaging. The image processing software for the industrial scanners is Raindrop Geomagic studio and Innovmetric Polyworks. The medical images are processed and converted using Tomovision slice-o-matic. Organic design of human anatomy and in particular an implant or prosthesis is done using the Freeform system from Sensable technologies. The prototyping of a wax prosthesis or implant is accomplished using a Thermojet RP system and cast into the desired material using traditional medical casting techniques.

A personal computer (PC) is used throughout the research and has the following specifications:

1. Intel Pentium IV 1.4Ghz processor speed
2. 1 GB RAM
3. Windows 2000 SP2
4. ATI Rage pro graphics card with 128MB video memory
5. 21" computer screen

3.2 Imaging

The apparatus used for imaging includes categories of: CMM, structured light and CT. Sub-sections 3.2.1 to 3.2.3 discuss the technical details of the three imaging systems.

3.2.1 Renishaw Cyclone

The Renishaw cyclone is a CMM digitising system, using the principles discussed in section 2.3.1, and uses a probe or laser for digitising. The particular system used in this research is a first generation cyclone and uses a mechanical probe. Second generation systems are capable of using a laser for scanning. Technical specifications for the first generation Renishaw Cyclone can be viewed in Appendix A.
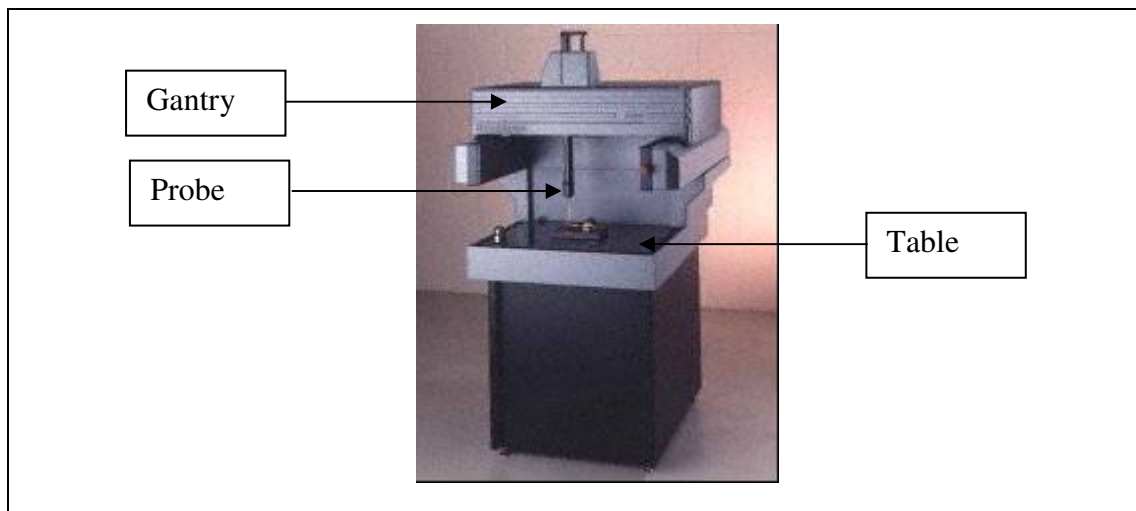
Figure 3-2: First generation Renishaw Cyclone
(http://www.renishaw.com , 19 December 2002)

Figure 3-2 shows the major components of the first generation Renishaw Cyclone used in this research. The first generation Renishaw Cyclone is referred to as a Renishaw Cyclone for the remainder of this research. The major components include an overhead gantry that uses a pneumatic system to control x and y motion (horizontal motion). The Renishaw Cyclone requires a dedicated air supply to control this motion. A motor controls the vertical or z-direction of the probe. A granite table ensures stability of an object whilst scanning. The Renishaw Cyclone is not portable and requires fixing to a solid floor.

The Renishaw Cyclone operates by monitoring the probe for resistance in the vertical z-direction or deflection in the horizontal plane. When the probe comes into contact with an object, the probe either resists or deflects, causing the system to respond and

move the probe over the object. The resistance is set at approximately 50 grams, but the probe deflection is variable.

The Renishaw Cyclone is fitted with probes of different geometries and sizes. The probe size is based on the required resolution, a smaller probe can measure finer detail, and probe geometry determines the types of features that can be measured. Accuracy of the system is 7µm, and reportedly offers high repeatability. The probe geometries include the ball, disk and needle shapes. The ball shaped probe is ideal for scanning objects with no sharp curvatures and no significant undercuts. The disk shaped probe is used for applications where the object has undercuts that need to be digitised. The needle probe is thinner than the other geometries and used for finer scanning and in areas exhibiting high internal curvature and can't be reached by a larger ball-shaped probe.
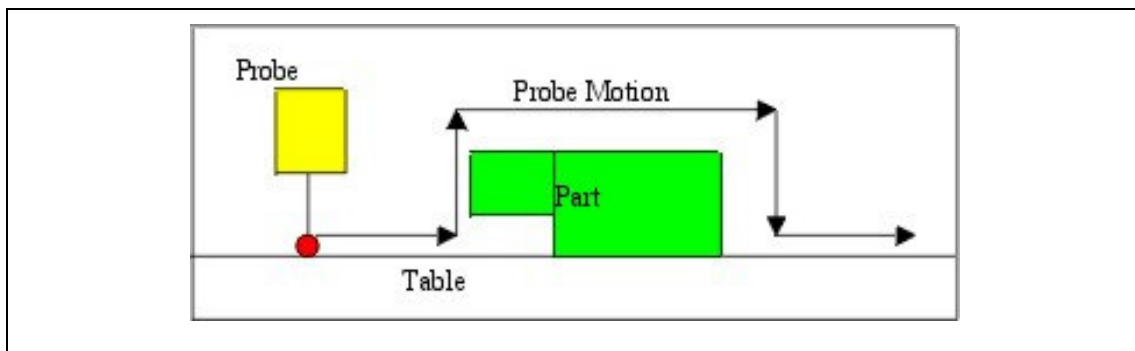
Figure 3-3: Ball-shaped probe
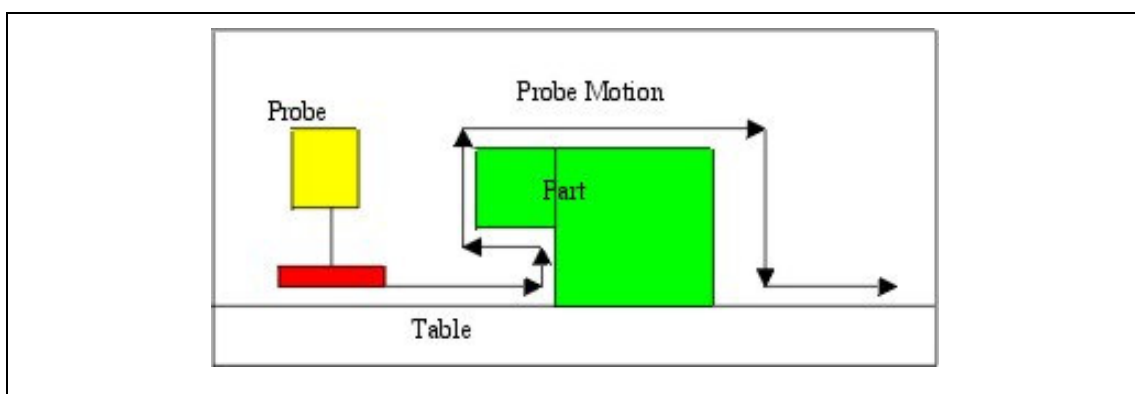
Figure 3-4: Disk-shaped probe

Figure 3-3 and Figure 3-4 show the paths followed by a ball and disk shaped probe respectively. The ball shaped probe cannot scan undercuts as the extension column that mounts the probe is in the way. A description of the probe components is

provided in Figure 2-2. The disk-shaped probe can scan undercuts, but there is difficulty in scanning horizontal convex and concave curvatures because of the disk diameter.

The probe type selected affects the results and one must ensure the correct probe type is selected to prevent scanning errors. Compensations for probe dimensions, that are discussed in section 2.3.1, are made on tessellated surface formats such as STL, by the Trace cut software that accompanies the Renishaw Cyclone. The compensation includes the offsetting of the tessellated surface, using a surface normal to the centre of the probe at each required position.

The Trace cut software is the proprietary controller software for the Renishaw Cyclone. The software controls the calibration and settings of the Renishaw Cyclone. Calibration of the Renishaw cyclone consists of measuring the diameter of a steel ball mounted on the granite table and comparing the results to the theoretical ones on file. Calibration is required every time a different probe is used, but is performed by the operator.

3.2.2 Breuckmann Optotop

The Breuckmann Optotop is a high end digitising system offered by Breuckmann GmbH, (Torenstr. 14, 88709 Meersburg, Germany). Technical specifications can be viewed in Appendix A.

The system uses the miniature projection technique (MPT) and employs the structured light method discussed in sub-section 2.3.1. The hardware components of the system consist of a projector and a CCD camera.
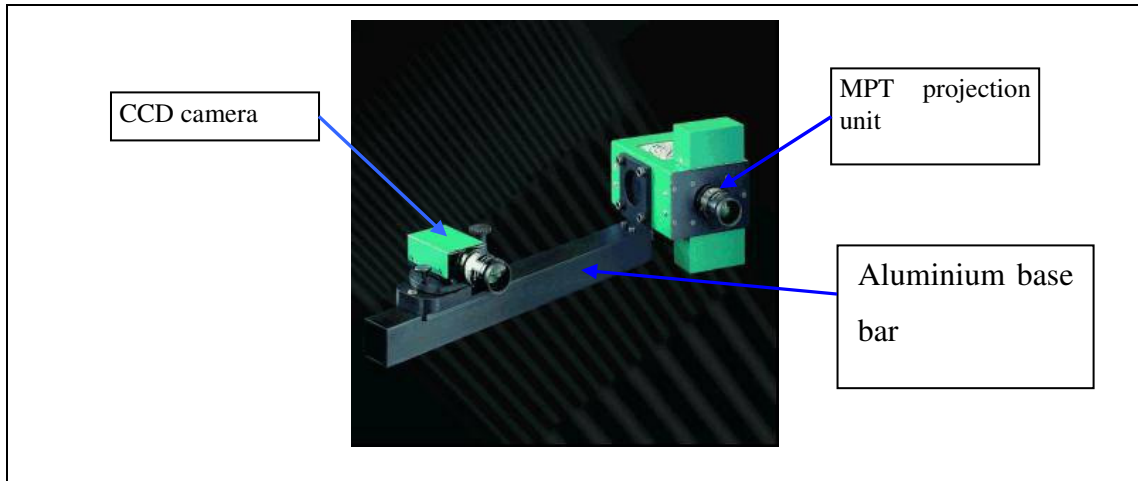
Figure 3-5: Breuckmann Optotop system
(http://www.breuckmann.com ; 22 January 2002)

Figure 3-5 shows the main components of the Breuckmann Optotop system. A rigid aluminium bar mounts the CCD and projector. The scanning volume and angle between the CCD and projector that are discussed in sub-section 2.3.1 are controlled by the length of the bar. Fixed mounting holes are on the bar that control angle and the longer the bar the bigger the scanning volume.
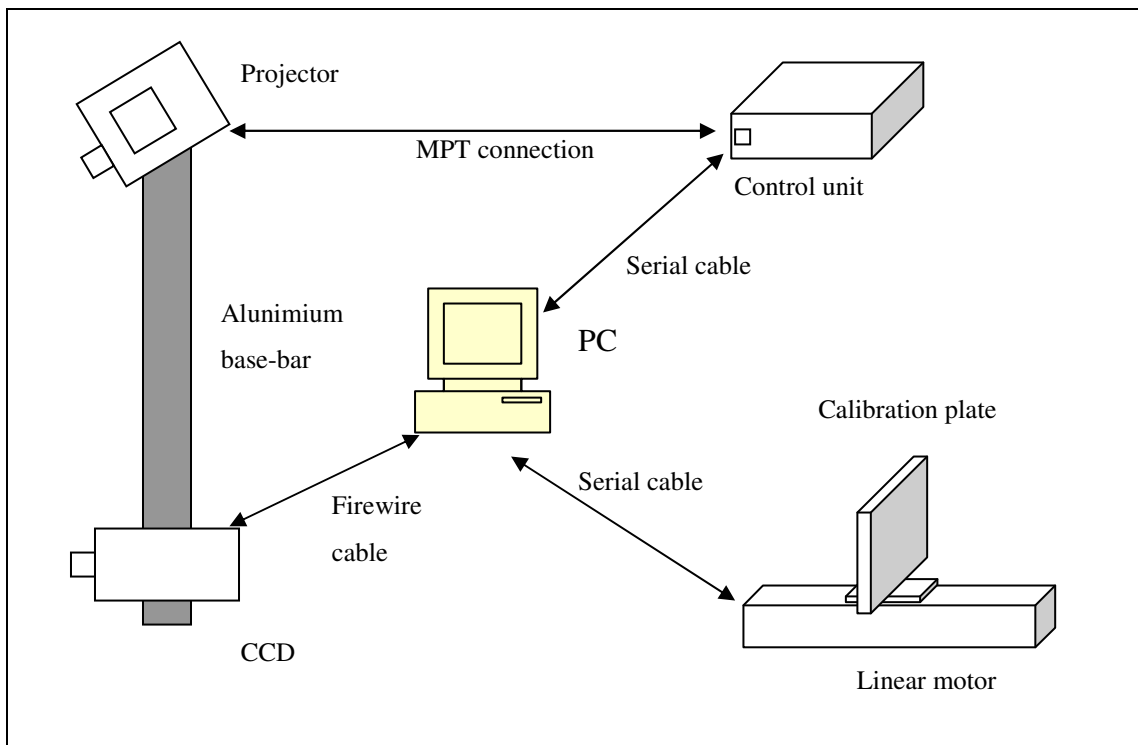
Figure 3-6: Breuckmann Optotop layout

Figure 3-6 shows the layout and connection of the Breuckmann Optotop system. The CCD is attached directly to a fire wire port on a PC using a standard fire wire cable. The projector uses a special cable and connects to the control unit. The control unit uses an independent power supply and a cable linking it to the serial port of a PC. Breuckmann system calibration uses a linear motor, connected to a serial port of a PC. A calibration plate mounts onto the linear motor. The base bar mounts onto a camera tripod making the system portable.

The Breuckmann Optotop uses the proprietary Optocat software for calibration and scanning. One can use several methods of scanning including index mark matching (photogrammetry) and contour matching. Index mark matching uses several circular stickers of known dimensions that are placed on an object for image registration. The local and global registration of index marks is performed in the Optocat software. Contour matching uses the features of an object for registration using the ICPM algorithm discussed in sub-section 2.4.1. An external image processing program is required for contour matching.

The digital greyscale CCD has a resolution of 1280 x 1024 pixels. The MPT projection unit consists of a 100W halogen bulb which projects light onto an object. Structured light is generated by means of gratings, which are written onto a common wafer. Figure 3-7a shows how the structured light is projected and Figure 3-7b shows the composition of a typical wafer. The different gratings are addressed in real time video by moving the wafer up and down within the projection unit. The projected structured light is measured by triangulation using the known angle and distance between the projector and CCD.
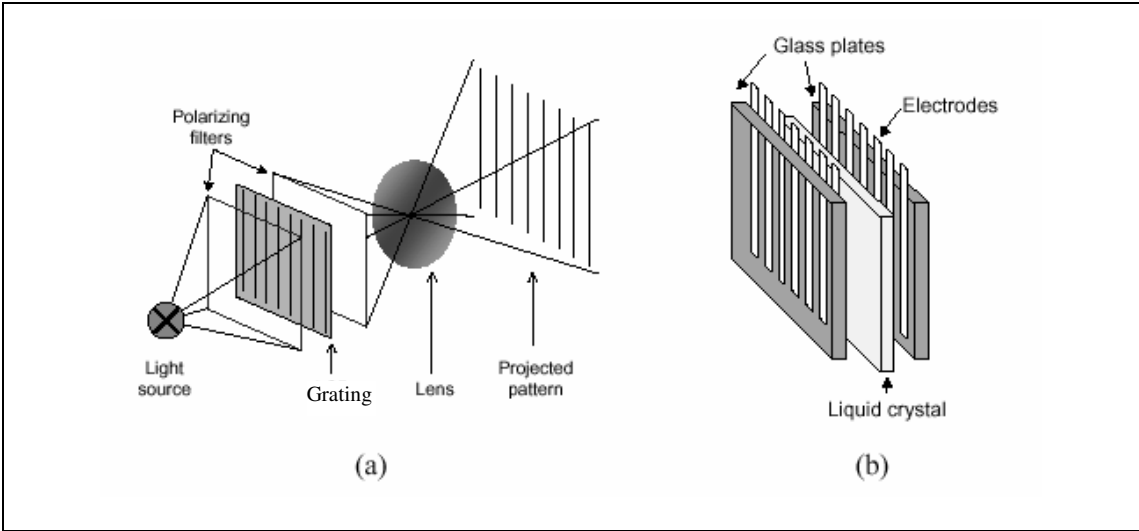
Figure 3-7: An LCD grating

(Guhring *et al*, 2000, p. 3)

The base bar size selected and distance between the camera and projector determines the scanning volume. The distance and angle between the CCD and projector are established during the calibration procedure of the unit. Calibration consists of placing an aluminium plate onto a linear motor. The aluminium plate contains a number of evenly spaced circles of known dimensions in a grid fashion around the plate. The aluminium plate is moved to 20 predefined locations, and is scanned at each location. The circle diameters increase relative to the Breuckmann Optotop as the aluminium plate moves closer to the aluminium base-bar, and these diameters are compared to theoretical values at known distances.
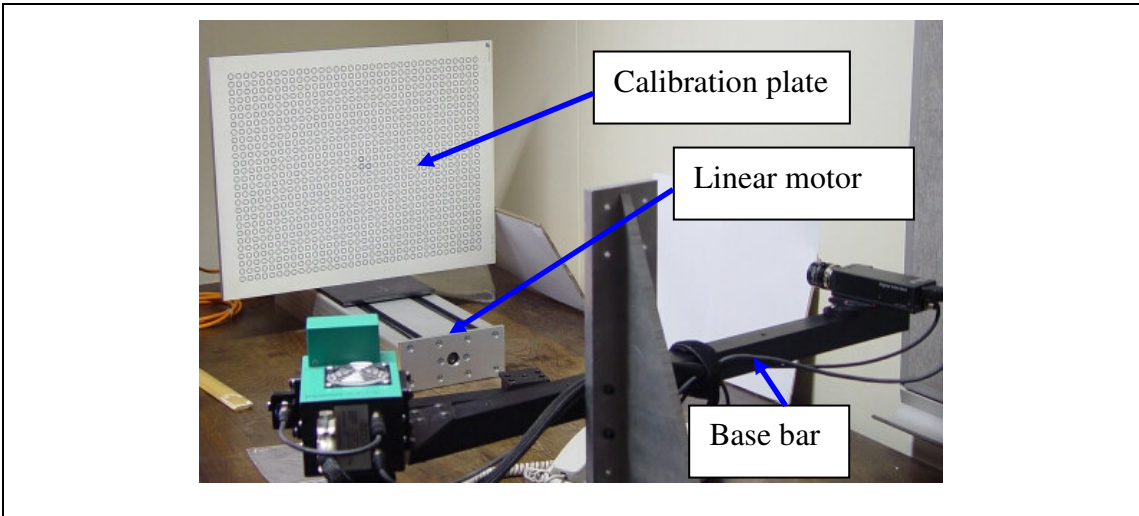
Figure 3-8: A calibration plate

Figure 3-8 shows both the calibration plate (HF-360) and linear motor with the aluminium base-bar in the foreground. The variable scanning volume of the Breuckmann Optotop is illustrated in Table 3-1. Increasing the scanning volume affects resolution and accuracy, but does not affect speed.

Table 3-1: Scanning volumes for the Breuckmann Optotop

Scale	Scanning volume (x * y *z) (mm)	Minimum resolution (mm)	Feature accuracy (µm)
Small (HF-80)	61 x 45 * 30	0.075	10
Medium (HF-160)	153 x 113 * 100	0.200	20
Large (HF-360)	345 x 255 * 220	0.400	40

The calibration plates are sensitive and care must be taken not to touch the surface of the plate, as the oil from fingers creates an area of glare on the plate. The system is calibrated frequently (e.g. every ten scans) or when a different scanning volume is required. When several viewing angles are required, one has the option of moving either the object being scanned or the tripod that mounts the aluminium base-bar. Vibration is a source of error, caused by loose mountings on the unit.

3.2.3 Phillips CT

A Phillips CT scanner is used for medical image acquisition. The Phillips CT scanner operates on the principles discussed in sub-section 2.3.2 and is a SDCT (Single detector row CT) scanner capable of spiral or helical scanning. The CT scanner provides a maximum resolution of 512 x 512 pixels, and has a slice distance capability of between 1mm and 10mm. The scanner uses a fan beam with the x-ray source rotating around the patient. The detector array remains stationary during scanning and this concept is illustrated in Figure 3-9.
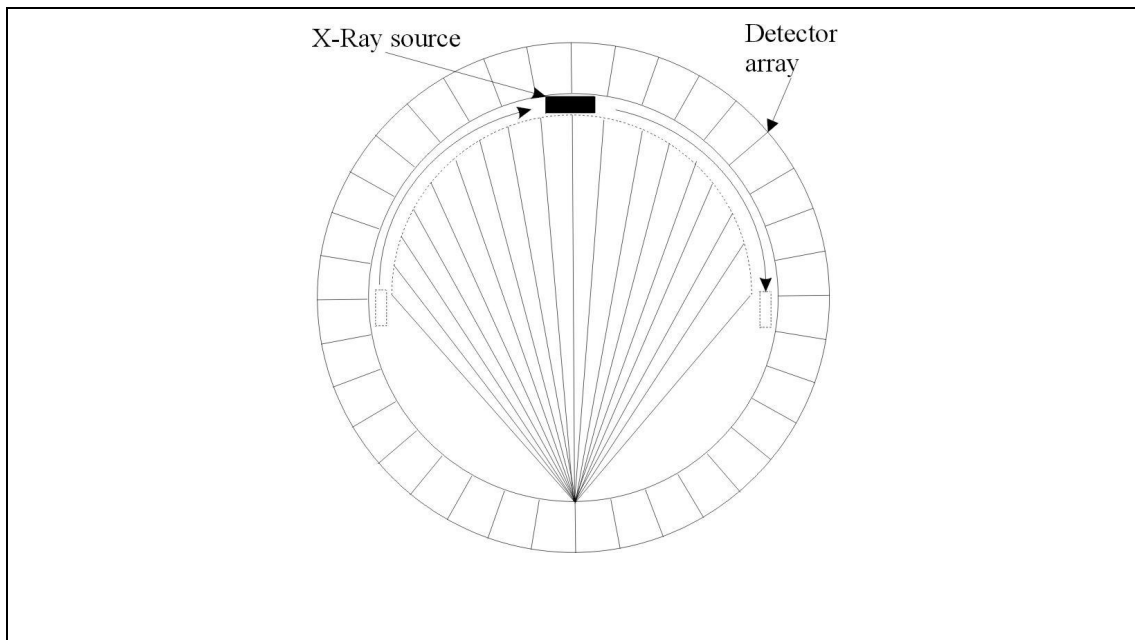
Figure 3-9: Fourth generation CT scanner

(Adapted from Bronzino *et al,* 2000, p. 62-4)

CT scanners achieve helical or spiral scanning using self lubricating slip ring technology to make electrical connections with rotating components. This prevents the need for both electrical and signal cables that would otherwise require unwinding between scans (Bronzino *et al,* 2000, p. 62-4). The Phillips CT scanner uses a bremsstrahlung x-ray tube for the radiation source. The tubes produce x-rays by accelerating a beam of electrons onto a target anode. The power requirements of the tubes are typically 120kV at 200mA to 500mA, producing x-rays with an energy spectrum ranging between 30 and 120 kV (Bronzino *et al,* 2000, p. 62-5).

The maximum uncertainty in the system is the slice distance, between 1mm and 10mm. The slice distance is selected depending on the application, a small slice distances reduces the lifespan of the x-ray tubes and a patient is in the scanner for a longer period. Use of the Phillips CT scanner requires a trained radiologist.

3.3 Image processing

Industrial image processing software includes: Raindrop Geomagic Studio and Innovmetric Polyworks. Scan registration and basic model editing, discussed in sub-

section 2.4.1, makes use of industrial image processing software. Conversion of DICOM data to STL data uses the medical processing and conversion software, Tomovision slice-o-matic. Tomovision performs image segmentation, discussed in sub-section 2.4.2, with DICOM data.

3.3.1 Raindrop Geomagic

Raindrop Geomagic consists of two programs namely, Geomagic studio and Geomagic qualify. Geomagic studio is image processing software and is used for the image processing tasks discussed in sub-section 2.4.1 and conversion to NURBS surfaces. Geomagic Qualify is an inspection and analysis package used for 3D metrology and 3D comparisons. Raindrop Geomagic requires a minimum of 512MB Ram and a Pentium 4 processor. The PC used in this research exceeds these specifications.

Geomagic Studio imports unprocessed data from many scanning systems including the Breuckmann Optotop discussed in sub-section 3.2.2. Geomagic Studio has three curve sampling algorithms including; ordered (matrix of points), linear (samples at a set distance), curvature (samples less in curved areas). This reduces the number of points in raw scan data to speed up processing time and is useful for complex geometry such as the ear where many scans are required. Geomagic studio offers 1 and 3 point local registration options for scanned images and can import and register STL files. The STL import is useful when multiple scans are made using a Renishaw Cyclone scanner.

Geomagic Studio's editing functions include:

1. analysis of errors in STL files,
2. analysis of whether or not a model is watertight,
3. curvature and flat based hole filling,
4. And model translation and scaling.

The analysis of STL errors with Geomagic Studio includes checking for common STL errors illustrated in Figure 2-22, and discussed by Fadel and Kirschman (1996, p. 9). The error checking function is important to ensure file compatibility with downstream STL editing applications, and in particular, design applications. A watertight model is solid and has no holes. Most image processing and STL editing packages offer flat hole filling, but few posses curvature based which extrapolates surface information. This function is important when working with organic shapes, especially complex geometry such as the ear. Model translation and scaling is available in most STL editing packages, but is important for reorienting a model in world coordinates (Absolute coordinates) and also for applying a scaling factor when casting.

Geomagic Studio offers little control and very few parameters are available for change when using a function. This approach makes the system easy to use as most functions operate using a point and click approach. Hole filling can be done quickly by selecting the hole to be filled.

Geomagic Qualify is an extension of Geomagic studio provides digital comparisons based on model dimensions. Models are aligned with each other using either the ICPM algorithm or datum based registration using model features. The registration minimises the error between two model surfaces. The registration employing the ICPM algorithm is known as best fit alignment and registration using datum's is known as datum based alignment. The best-fit alignment is used for comparison of two sets of data with no distinct datum points, such as human anatomy. Datum based alignment uses known datum's on both objects, these datum's are features on both models and are easily identifiable. Datum based alignment uses datums and then the ICPM algorithm for any remaining degrees of freedom.

A comparison consists either of comparing a CAD models to a scanned model or comparing two scanned models. Geomagic Qualify compares a variety of file formats including IGES, STL and point cloud. This research uses Geomagic qualify for comparing two scanned models, as CAD data is unavailable for human anatomy.

3.3.2 Innovmetric Polyworks

Innovmetric Polyworks, like Raindrop Geomagic is image processing software and used for the tasks discussed in sub-section 2.4.1. Innovmetric Polyworks consists of a number of separate modules. The available modules in this research are IMAlign, IMCompress and IMEdit. IMAlign is used for image processing including local and global registration and merging. IMCompress is used for decimation of large STL files (>6MB) to a smaller more usable size, using decimation algorithms discussed in subsection 2.4.1 by Schroeder, Zarge and Lorensen (1992, p. 65). IMEdit is an STL editing package, with the typical editing functions discussed in sub-section 2.5.2.

There are differences in data handling for local and global registration when compared to Raindrop Geomagic. Some differences include visual data sampling, to reduce the number of points displayed on the PC screen, and an N-point local registration option. IMAlign does not import STL files directly so additional processing is required for local registration of CMM data. Innovmetric Polyworks offers the user control of every aspect of the program with respect to the processed model. This makes the program complex initially, but more powerful when mastered.

Hole filling is a complex operation in IMAlign, and requires that the user describe several features of a surface, including several control points, and can be related to the manipulation of IGES curves via control points discussed in sub-section 2.5.1. IMAlign does not have the ability for direct STL import, and data from an offset Renishaw Cyclone STL file requires conversion to a point cloud first.

3.3.3 Tomovision Slice-o-matic

Tomovision Slice-o-matic is medical imaging software designed for both visualisation and conversion of CT and MRI scans. There are three modules to Slice-o-matic including Basic, Tag and 3D. The basic module contains functions to measure and visualise 2D images from CT and MRI scanners. The Tag module is used for image segmentation, discussed in sub-section 2.4.2, and used for volumetric computation.

Image segmentation is performed on a 2D scan and propagated through multiple scans. The 3D module is used for exporting to different formats including IGES curves and STL files.

This investigation uses Tomovision Slice-o-matic for the conversion of CT images to a volumetric model and exporting to STL. Slice-o-matic contains many additional features including editing functions and advanced analysis tools for medical scans, but these are unused in this research.

3.4 Organic design hardware and software

Design using organic data from scanning systems, discussed in sub-section 2.5.2, and in particular the editing and modification of implants and prostheses is performed using the Freeform system and a haptic device. The haptic device used with the Freeform software is the Phantom haptic device (Sensable Technologies, Boston, MA). The Phantom is a 6-degree of freedom input device and 3-degree of freedom force output device based on impedance control theory, discussed in sub-section 2.5.2.
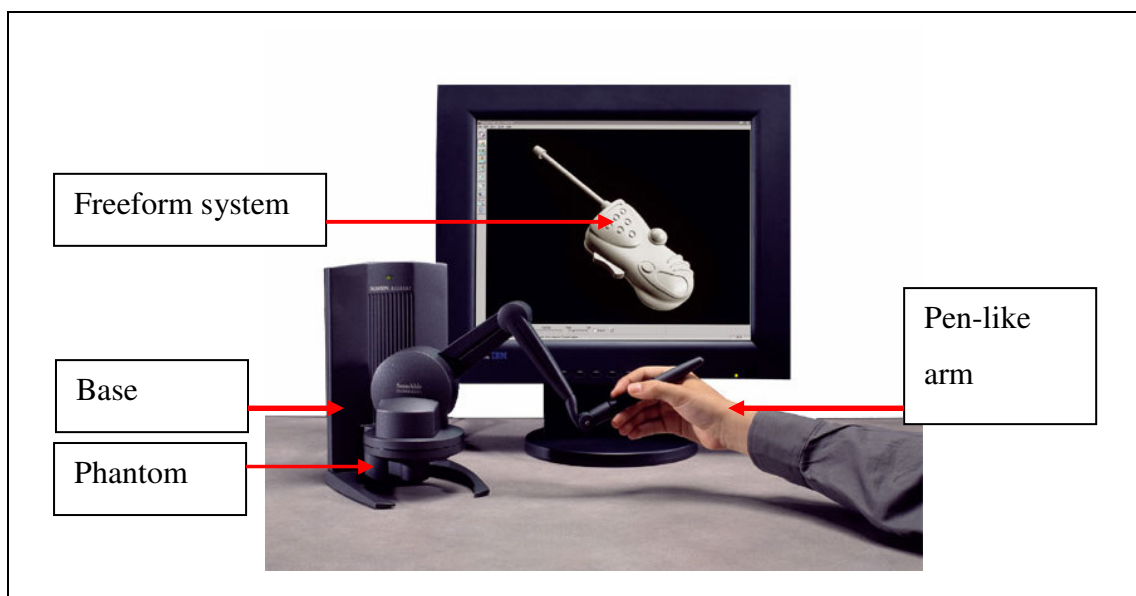
Figure 3-10: The Phantom device
(http://www.sensable.com, 29 August 2001)

The Phantom, illustrated in Figure 3-10, consists of a pen-like arm that the user grasps for haptic manipulation of data. The Phantom is supported by a solid base weighing 5 kilograms to create a stable working environment, to counter the output forces in touch applications. The computer screen in the background is displaying an image from the Freeform system.

The Freeform system is organic design software, using both a traditional keyboard and mouse for input and a Phantom haptic device to provide the sense of touch. The Freeform system includes a file import and export option for STL files. The imported STL surface files are converted to a voxel format (3D pixel).

Sculptors traditionally have access to a variety of clays with different hardness properties. This means that if carving is performed with a lot of force, more material is removed. The Freeform system provides a digital equivalent in density manipulation, to control the effect a tool has on material removal. Model density is manipulated using different material properties, which exert different forces on the Phantom device. The Freeform system currently supports two densities at a time, a variable one, running from "soft" to "hard" and a fixed density which prevents any material removal.

The accuracy of a model in the Freeform system is dependent on the voxel size chosen, which is limited by the amount of RAM and CPU power a PC has available. The voxel size selection is known as clay coarseness in the Freeform system. A high clay coarseness value (large voxels) requires less system resources, but fine changes cannot be made to a model. A low clay coarseness value (small voxels) requires more system resources, and the user risks getting the vibrations associated with a low update rate, discussed by Gregory *et al* (2000, p. 70), Dachille, Qin and Kaufman (2001, p. 409) and Thurfjell *et al* (2002, 212) in sub-section 2.5.2.

The Freeform systems haptic design and editing functionality includes:

1. carving
2. smoothing
3. tugging

The haptic design functionality makes full use of a three dimensional workspace and the sense of touch. The carving functions include several different shaped tools. The smoothing function performs both local smoothing by brushing a tool over the surface and global smoothing by selecting an entire area. The tugging function edits a model by tugging clay over a large area. Mullineux (2002, pp. 871-879) proposes a similar method for working with IGES in sub-section 2.5.1, except that the data is "tugged" using the sense of touch.

The Freeform systems standard design functions include typical CAD functionality such as: extruding a sketch, embossing, boolean operations, smoothing and various clay manipulation tools. An advantage of the Freeform system over traditional CAD system's are the smooth transitions obtained from boolean and extrusion operations. Smooth transitions may be a requirement when creating custom anatomy with a focus on increased aesthetic appeal.

3.5 Rapid Prototyping (RP)

For the fabrication of wax models, an RP system is selected due to the complex anatomical geometry and the ability to use STL files.

3.5.1 Thermojet printing

The Thermojet printer by 3D Systems, (Valencia CA, USA), is an RP system that uses wax as its build material. The system is based on the multi-jet-modelling (MJM) technology.

Figure 3-11: 3D systems Thermojet printer
(http://www.3dsystems.com; 19 December 2002)

The system has a build capacity of 250 x 190 x 200mm. The wax used by the printer is designed for investment casting and comes in three colours each indicating different ash contents. The Thermojet Printer is designed to work as a network printer, which instead of using ink, uses a wax build material. The system places layers of wax down, with a height typically between 0.03mm to 0.1mm. Once the build process is completed, the supports for overhanging areas are removed either by a brush or blade. Further technical specifications of the Thermojet can be viewed in Appendix A.

3.6 Casting techniques

The casting techniques used during the investigation are a modified version of the industrial lost wax process discussed in section 2.7. The casting is performed at the department of prosthetic dentistry, University of the Witwatersrand. There are several pieces of apparatus used for casting and are described in this section. The apparatus includes: a dental flask, dental vice and a heated water bath

Dental flasks are brass containers used in dentistry for casting prostheses. Dental flasks come in two halves with detachable bases. There are several standard sized flasks available, selected based on the size of casting required.
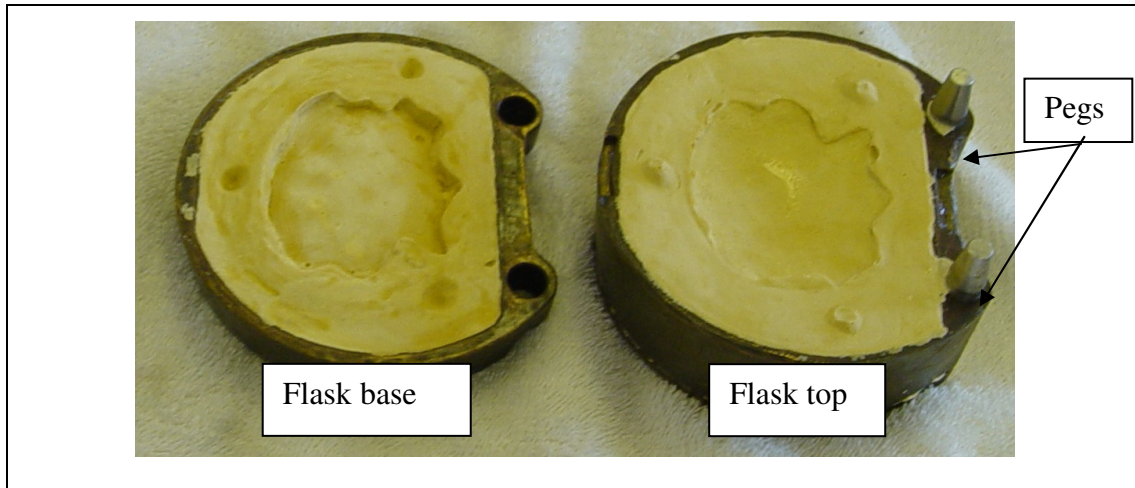
Figure 3-12: Dental flask components

Figure 3-12 shows the base and top of a typical dental flask with plaster mixture in it. The flask has two pegs for alignment when the flask is closed, illustrated in the figure. The flask top has a removable end-cap to assist in pouring in plaster mixture. Dental flasks are used during the research as containers for all investment casting activities.

A dental vice is used to apply pressure to the dental flasks to ensure both a smooth surface finish and reduce the time the plaster takes to set. Figure 3-13 shows a typical dental vice used during the investigation with a dental flask in place. Features of the dental vice include a handle to manually increase the pressure, and a pressure gauge to indicate the pressure exerted on the dental flask.
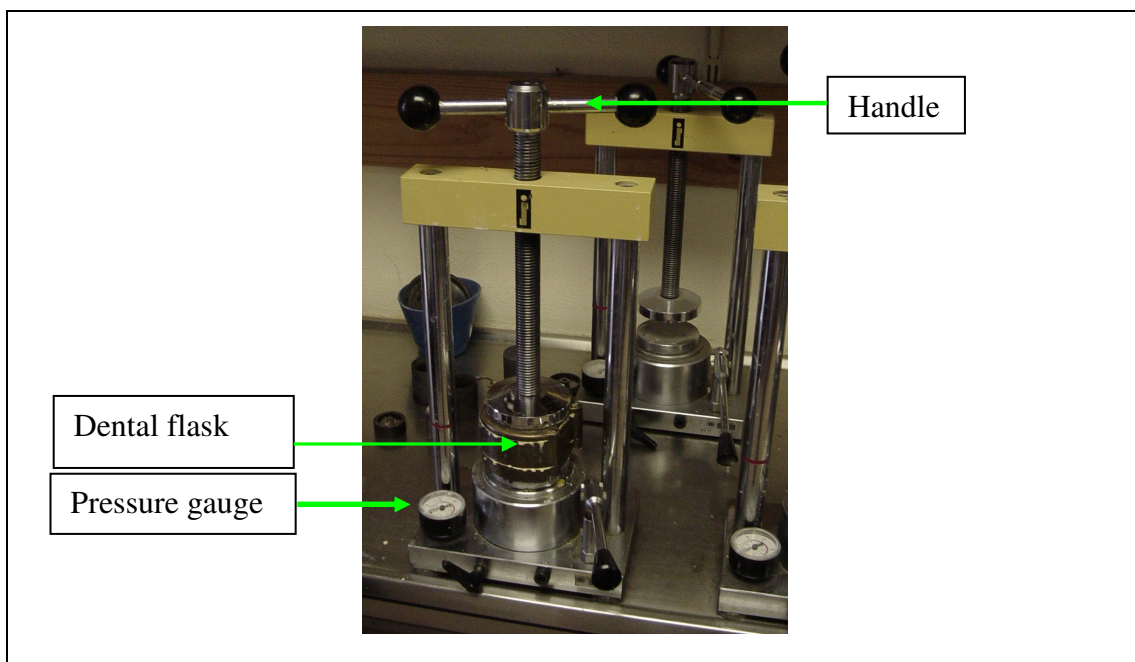
Figure 3-13: Dental vice

A heated water bath is used to remove the wax from the plaster model for the purposes of investment casting as described in section 2.7. Figure 3-14 shows a heated water bath used during the research.
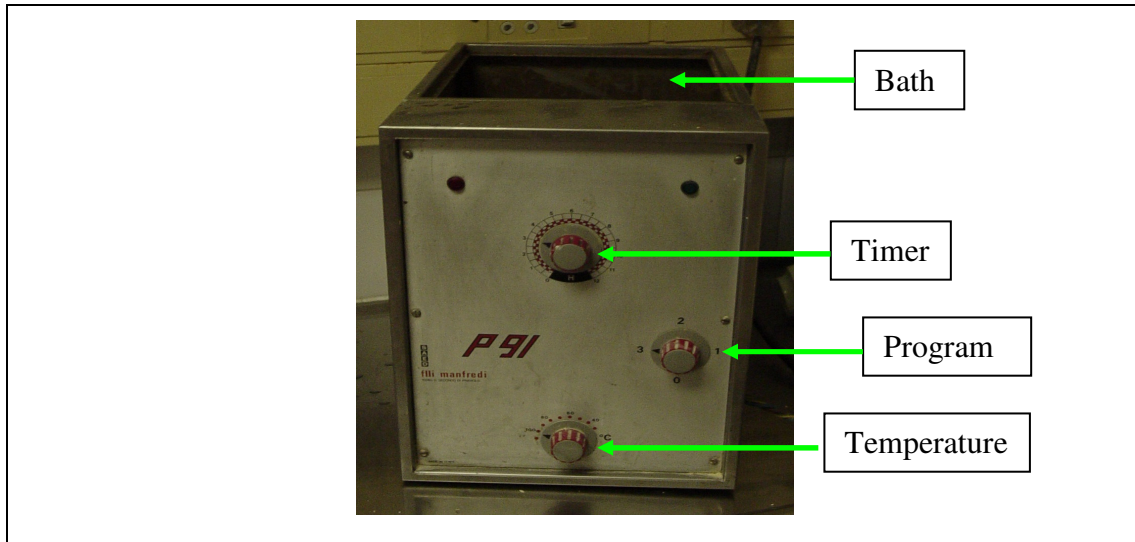
Figure 3-14: Heated water bath

The heated water bath has a bath where the both the water and dental flasks are placed and a timer that automatically switches off the device after a specified duration. A program button is available for items that require several temperatures at predefined durations. The temperature knob located on the bottom of the device has settings from 40ºC to 100ºC. This concludes the apparatus used in the investigation for the digital process described in section 3.1. The exact steps used in the investigation are next described in chapter 4.

Method

4.1 Introduction

The methods used during the investigation are described in this chapter. Chapter 4 starts with the general methods required for a digital reverse engineering process in sections 4.2 to 4.6. This includes general procedures for imaging, image processing, design, rapid prototyping and casting. Section 4.7 presents the specific method for the four case studies.
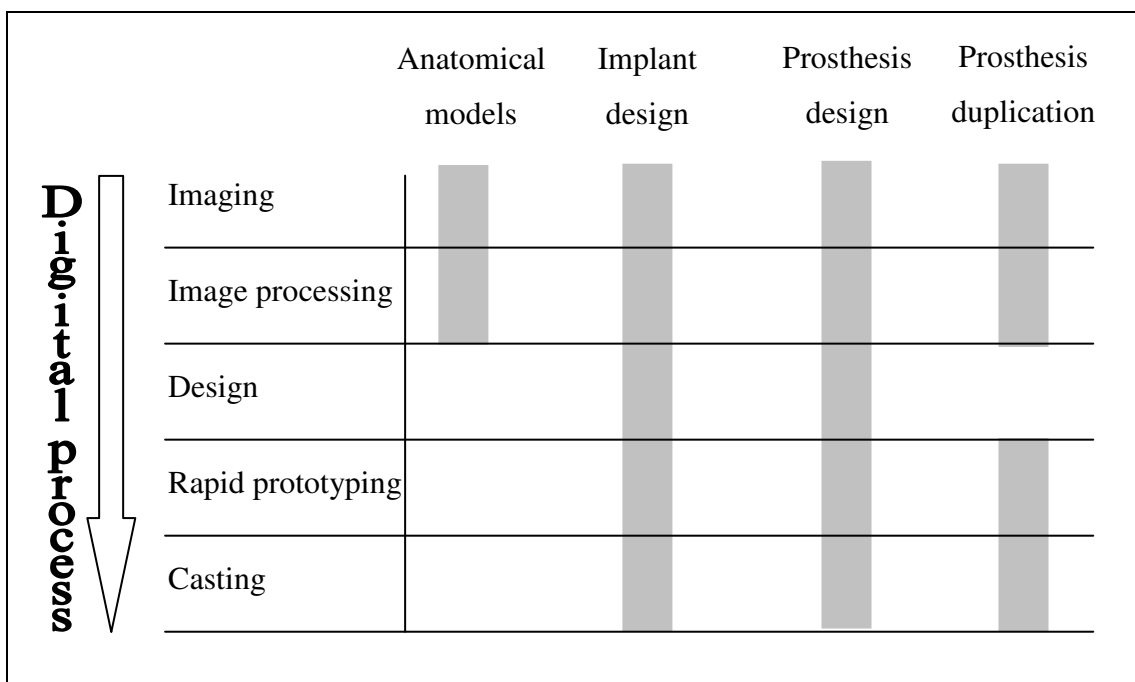
Figure 4-1: Case study flow

Figure 4-1 shows the process flow for the four case studies with respect to the digital process. The first case study uses a set of four anatomical models, which are scanned using three types of imaging, and image processed using two types of image processing software. This case study uses two steps in the generic reverse engineering process, but provides a comparison between the different scanning and image

processing systems. The second case study uses a dry human skull to test implant design using the digital process. The third case study presents the method of prosthesis design using both the traditional and digital process. The fourth case study uses an oral prosthesis as a duplication case study and requires no design modifications.

4.2 Imaging

This section outlines the general methods employed when using any of the following three imaging apparatus:

1. Renishaw Cyclone,
2. Breuckmann Optotop,
3. Phillips CT scanner.

4.2.1 Renishaw Cyclone

The investigation uses a series 1 Renishaw Cyclone system, located at Technikon Northern Gauteng as a contact measurement system option. The following steps outline the procedure when using the Renishaw Cyclone.

1. Place a probe into the sensor mount.
2. Start the Tracecut 22 software and use the initialisation sequence for the Renishaw Cyclone.
3. Place a part on the granite scanning table, using a vice for clamping irregularly shaped part geometries as illustrated in Figure 4-2.
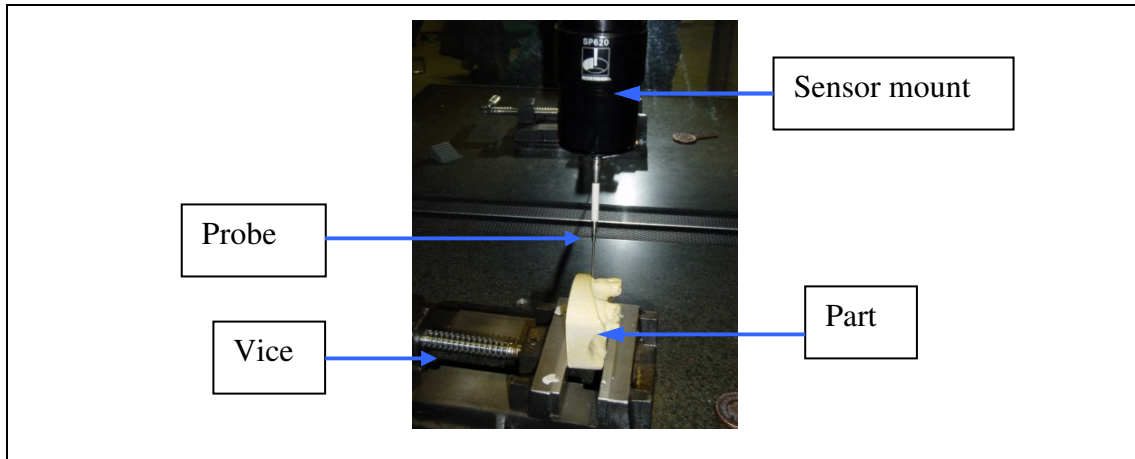
Figure 4-2: Renishaw Cyclone setup

4. Secure the vice so the part can withstand 0.5N force from the probe when scanning.

5. Select the default x and y axes, which are parallel to two sides of the granite table.

6. Disengage the servo motors and manually draw a rectangular profile around the extents of the part by grasping and moving the stylus. The sides of the rectangle are automatically aligned with the x and y axis.

7. Determine the minimum feature size of the part and set this as the step distance.

8. Select a scanning speed.

9. Set the Renishaw Cyclone to capture points and wait for scanning to complete.

10. Select the true surface command to offset the digital model by the radius of the probe to compensate for probe diameter discussed in sub-section 2.3.1.

11. Save the model as an STL file. A scan from the Renishaw Cyclone is illustrated in Figure 4-3
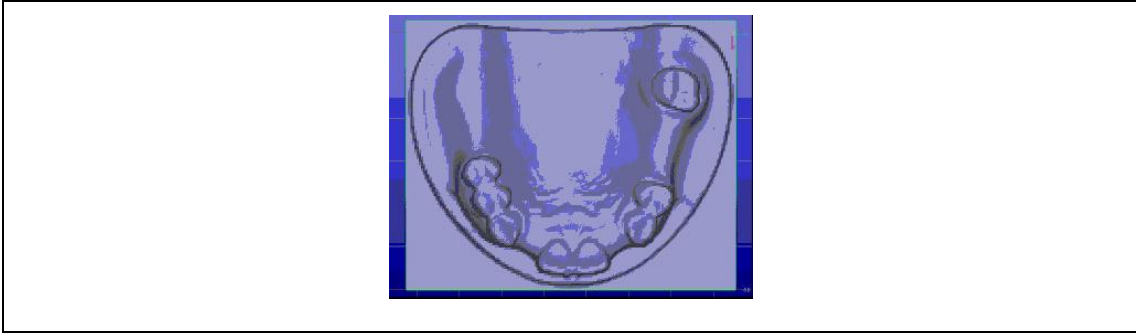
Figure 4-3: A Renishaw Cyclone scan

12. Move the part into a different orientation and repeat steps 4 to 11. Ensure that there is enough overlap on the scan for local registration purposes.

13. Repeat step 12 until the entire part is digitised.

4.2.2 Breuckmann Optotop

Use a Breuckmann Optotop system located at the University of the Witwatersrand for a non-contact measuring system option of 3D digitising. Calibration of the Breuckmann Optotop is required when the field of view is changed, or every ten scanning sessions. Calibration is required during the course of the research.

Calibration procedure

1. Plug the linear motor into the serial port of the PC.

2. Mount the calibration plate onto the linear motor using the supplied screws. Take care not to strip the threads of the plate as it is aluminium.

3. Mount the Breuckmann projector and camera onto a base-bar using the supplied screws.

4. Ensure that environmental vibrations are minimised during the calibration procedure.

5. Turn on the linear motor and Optotop control box.

6. Start version 2.61 of the Optocat software.

7. Initialise the Optocat software by selecting the correct field of view. The field of view is based on base bar and calibration plate size.

8. Use the Optocat software to move the calibration plate to the zero scanning position of the linear motor.

9. Use a tape measure to place the base bar the required distance from the linear motor.

10. Look at the calibration plate and adjust the focus of the projector by rotating the lens until the projected structured light is sharp and clear.
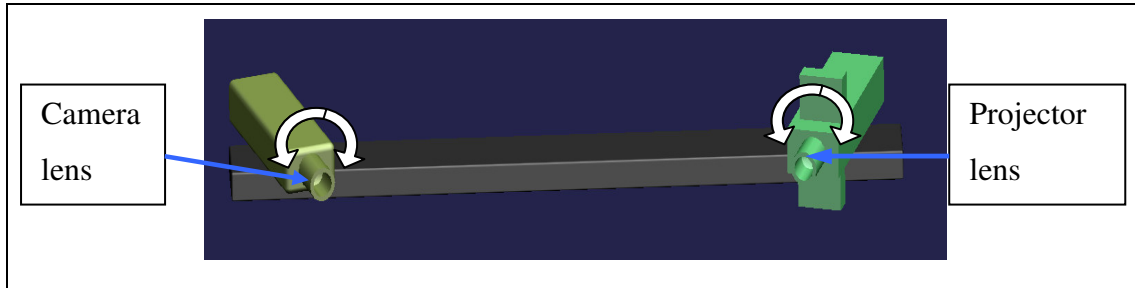
Figure 4-4: Focusing the camera and projector

11. Look at the PC screen and adjust the focus of the camera by rotating the lens until the image is clear.

12. Start the calibration sequence and the calibration plate automatically moves to twenty predefined positions.

13. The scanned calibration data is automatically compared to theoretical values.

14. Place a piece of flat white card (>2mm thick) over the calibration plate when calibration is complete and take a single scan. This scan of a flat surface is used to reduce phase banding error when scanning.

15. Switch the linear motor off and disconnect it from the PC serial port.

Scanning procedure

1. Switch the Optotop control unit on and start up version 2.61 of the Optocat software.

2. Select the correct field of view depending on the base-bar used.

3. Type in a file name for the project, making sure there are no spaces between the characters.

4. Select the fast measurement mode.

5. Select the required number of intensities, between 1 and 4, depending on environmental brightness.

6. Set the raster point size to the smallest feature size on the part.

7. Set the raster point distance the same as the raster point size. The raster point distance is the distance between the centres of the raster points.

8. Set the registration mode to contour matching.

9. Place the part on a dark, preferably matt black surface.

10. Use the two mounted laser pointers to determine the centre of the scanning volume and set the base-bar into the first scanning position.

11. Start the scanning sequence after which a series of vertical lines appears on the part, this is the structured light discussed in sub-sections 2.3.1 and 3.2.2. Figure 4-5 illustrates a structured light pattern on a part.

Figure 4-5: Structured light projection

12. Mask out a flat area of the scan to remove phase banding errors using an automated algorithm to compare the noise values to those obtained during calibration. Figure 4-6a illustrates the phase error in a scan and Figure 4-6b illustrates the phase error after removal, acceptable limits for the phase error lie between -2° and 2°.
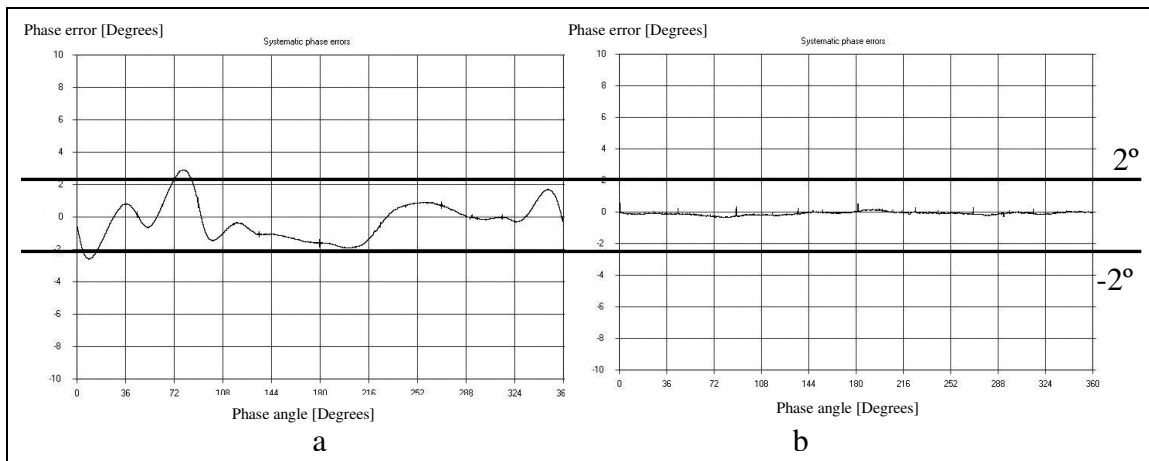
Figure 4-6: Phase error removal

13. Figure 4-7a illustrates phase banding error on a model and Figure 4-7b illustrates the same model with the phase error removed using the technique in step 12.
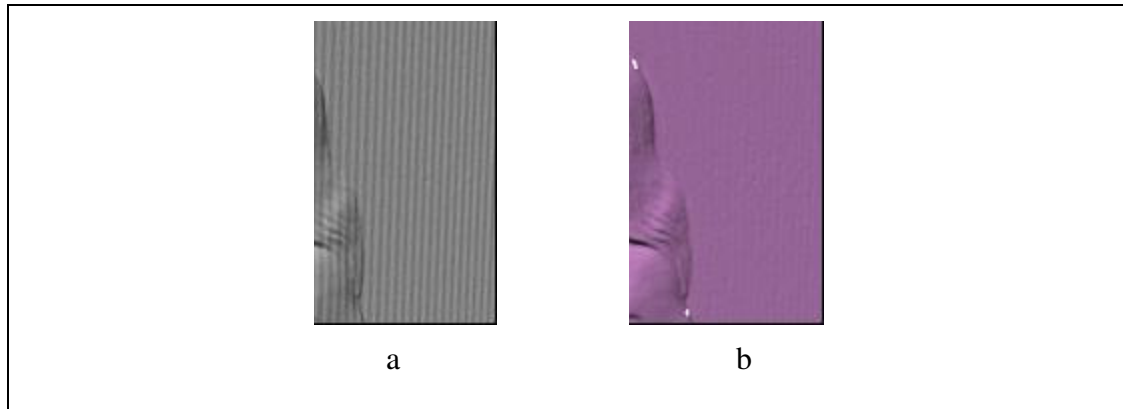
Figure 4-7: phase error ripples in the model

14. Mask out any unwanted data and select the save option which saves the required data.

15. Repeat steps 9 to 14 using different part orientations until the part is fully digitised.

4.2.3 Phillips CT scanner

The investigation uses a Phillips CT scanner, (Milpark hospital, Johannesburg, South Africa) as a medical scanning system. The procedure for CT scanning and writing the data to CD is presented here.

CT scanning procedure

1. Place one or more parts on the patient table.

2. Make a single test scan of the part and select a contrast that ensures the parts can be recognised and segmented within this HU range.

3. Select a slice distance of 1mm and start the scanning procedure. Figure 4-8 shows a typical slice from the Phillips CT scanner.
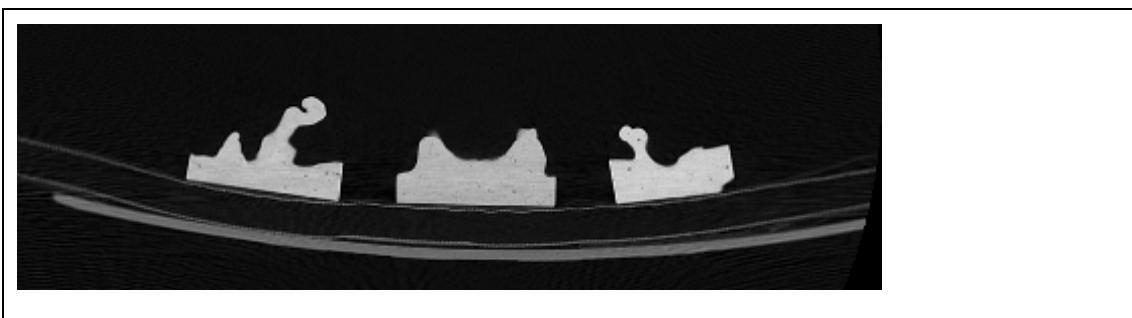
Figure 4-8: A CT slice image

4. Save the slice data to an optical disk and take it to Phillips medical division, Johannesburg, South Africa.

5. Use an Easyvision workstation to read the optical disk.

6. Use the DICOM standard and write the data to a standard CD-R for use in a PC.

4.3 Image processing

This section describes the method and procedures for processing image data from a Renishaw Cyclone, Breuckmann Optotop and Phillips CT scanner.

4.3.1 Renishaw Cyclone data

The data from the Renishaw Cyclone requires additional processing before registration and merging. Redundant data, called "flash" in this investigation, is removed. The flash removal can be done in any STL editing package, but Geomagic Studio is used during this investigation. Both local and global registration of data is performed once the flash data is removed.

<u>Removal of flash data and large triangles</u>
The method for removal of flash and other redundant data is described in this sub-section. The following steps are performed for using Geomagic Studio:

1. Start the Geomagic studio application and import the STL file.

2. Large undercuts in a part cannot be digitised and these leave large vertical triangles. This data is called "large triangles" in this research and they are also removed. Figure 4-9 illustrates the large triangles and flash data.
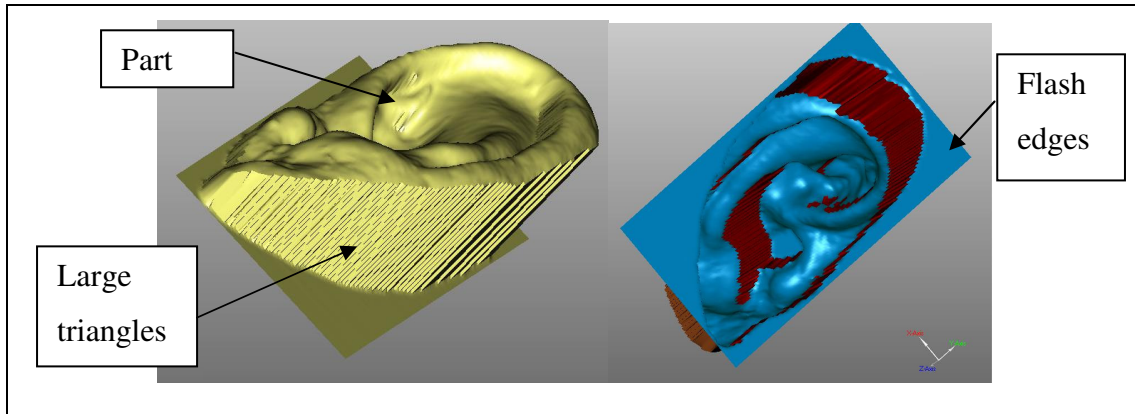
Figure 4-9: Large triangle removal

3. Use the measurement tool to determine the length of the large triangles.
4. Use the "select triangles of edge length" command with the measurement obtained from step 3.
5. Delete the selected long triangles.
6. Increase or decrease the edge length selection to alter triangle selection.
7. Select one triangle of the isolated flash data
8. Use the "select full components" command to select all of the flash triangles automatically and delete them.
9. Remove additional redundant triangles using manual selection and deletion.
10. Save the model as an STL file.
11. Repeat steps 1 to 10 for the remaining scan data.

Registration and merging

The method of registration and merging of Renishaw Cyclone data differs to optical scan data due to the import of a sparse point file, and in particular the STL file. The Tracecut limitation of offsetting surface files with normals, such as STL files generates additional import steps for Innovmetric Polyworks.

Geomagic Studio registration and merging of CMM data

1. Start the Geomagic studio application and import a particular parts scans.
2. Select all of the scans and group them.
3. Select the manual registration option and the screen, illustrated in Figure 4-10 appears showing three windows. Select the first two scans in the group.
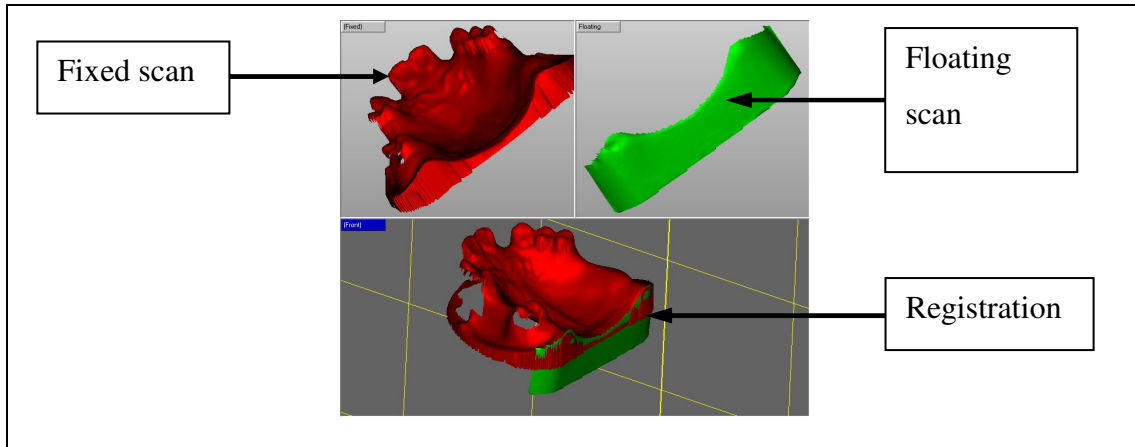
Figure 4-10: Manual registration in Geomagic Studio

4. Set one scan as a fixed scan and the other as floating. The fixed scan remains at its current coordinates and the floating scan is repositioned during local registration.

5. Select the three point local registration method.

6. Select a sampling rate for local registration to speed up the process. Sampling consists of selecting a percentage of points for the local registration algorithm. A lower sampling rate risks an incorrect local registration, but this can be resolved during the global registration algorithm.

7. Select the register command to apply a local ICPM algorithm.

8. Repeat the local registration process for all of the scans using the same fixed scan.

9. Start the global registration algorithm with a tolerance less than the step size of the Renishaw Cyclone.

10. Use the merge command and out put a single surfaced model.

11. Save the data as an STL file.

Innovmetric Polyworks registration and merging of CMM data

1. Start Innovmetric Polyworks and select the IMEdit option.

2. Open the STL file in IMEdit and select all of the triangle vertices. Figure 4-11 shows the selection of the triangle vertices.
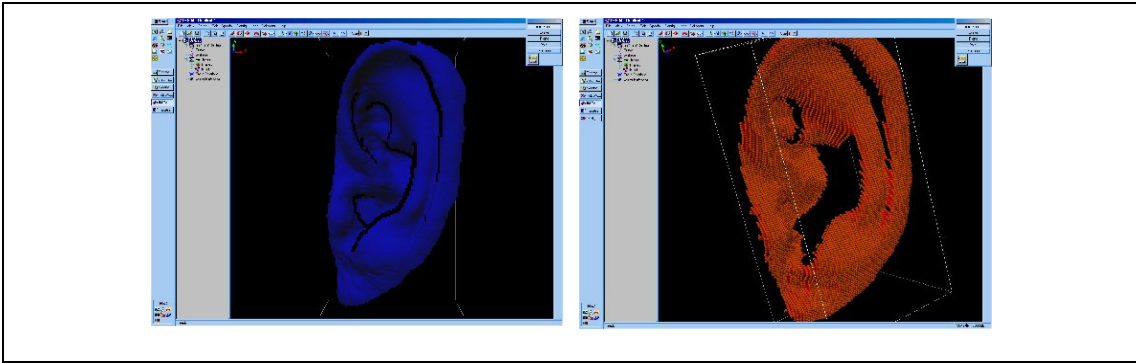
Figure 4-11: The Renishaw data opened in IMedit

3. Export the selected vertices using the "save vertices as point cloud" option in the edit menu. This selects the vertices in view, and thus some data won't be exported.

4. Repeat step 3 for the remaining scans.

5. Start the IMAlign application and open the point cloud files that are generated in step 3.

6. Select the maximum edge length as 2mm and the sample size to half of the Renishaw Cyclone's step distance.

7. Register all of the scans using N-point alignment, until all of the scans are locally registered.

8. Start the global registration algorithm.

9. Start the IMMerge application and merge the globally registered data to create a single surface STL file, use the Renishaw Cyclone step distance as IMMerge's step distance.

4.3.2 Breuckmann Optotop data

This section describes the registration and merging process of the Breuckmann Optotop data using either Geomagic Studio or Innovmetric Polyworks.

Raindrop Geomagic

1. Start the Raindrop Geomagic Studio application and import the Breuckmann data files.

2. Use the three point local registration algorithm to register the data.

3. Select a sampling rate for local registration to speed up the process. Sampling consists of selecting a percentage of points for the local registration algorithm. A lower sampling rate risks an incorrect registration, but this can be resolved during global registration.

4. Use the register command to apply a local ICPM algorithm using the selected points.

5. Repeat the local registration process for all of the scans, using the same fixed scan.

6. Start the global registration algorithm and use a tolerance less than the raster point size.

7. Figure 4-12 shows a globally registered point cloud from the Breuckmann Optotop. Note how dense the points are for the majority of the model, whilst areas that are difficult to scan have fewer points.
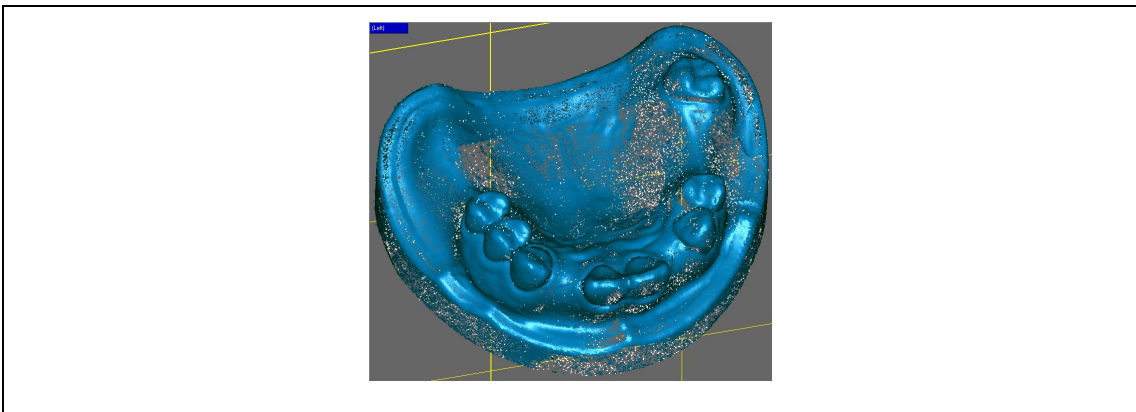
Figure 4-12: Globally registered Breuckmann Optotop data

8. Use the merge command to generate a single surfaced tessellated model.

9. Save the data as an STL file.

Innovmetric Polyworks

1. Start the IMAlign module of Innovmetric Polyworks and import the Breuckmann Optotop data files.

2. Select two scans and use the N-point registration option for local registration. Figure 4-13 shows two scans before registration.
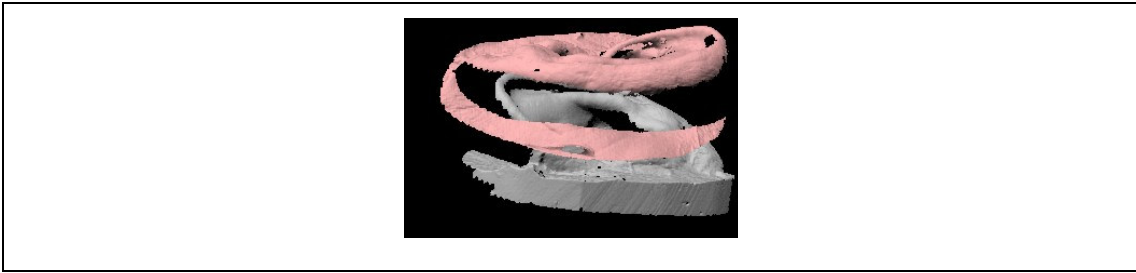
Figure 4-13: The Innovmetric Polyworks interface

3. Select a minimum of three corresponding points on each scan, more points make local registration faster. Figure 4-14 shows the point selection screen for local registration.
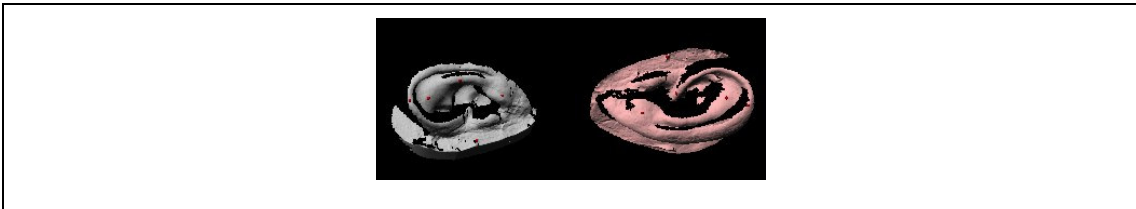
Figure 4-14: Local registration of two scans

4. Apply the local registration and visually inspect. Each scan remains a different colour during the registration process to assist in visualisation. A locally registered scan is illustrated in Figure 4-15.
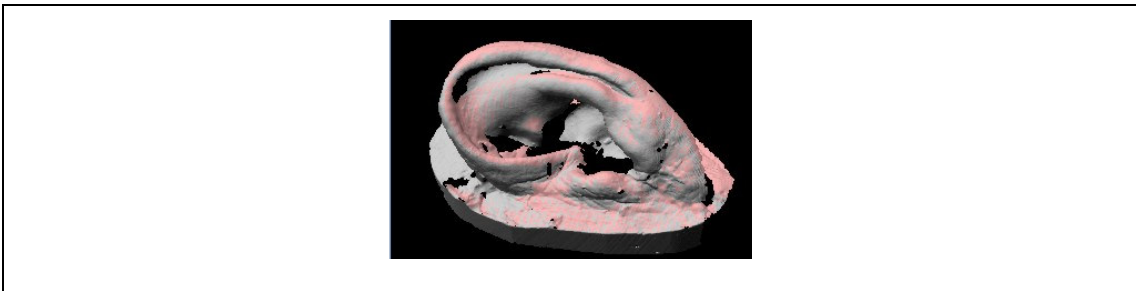
Figure 4-15: Local registration results

5. Repeat steps 2 to 4 until all of the scans have been locally registered.
6. Start the global registration algorithm.
7. Save the histograms of the registration.
8. Start the IMMerge application and merge the globally registered data to create a single surface STL file, use the Breuckmann's raster point distance as IMMerge's step distance

4.3.3 Phillips CT data

This section describes the processing of the Phillips CT data using Tomovision version 4.1. The processing consists of data segmentation, discussed in sub-section 2.4.2, and conversion to STL.

Tomovision

1. Start the Tomovision software and import the medical images.
2. Press the [space bar] to simultaneously show all of the images. Figure 4-16 illustrates six 2D CT images on the screen.
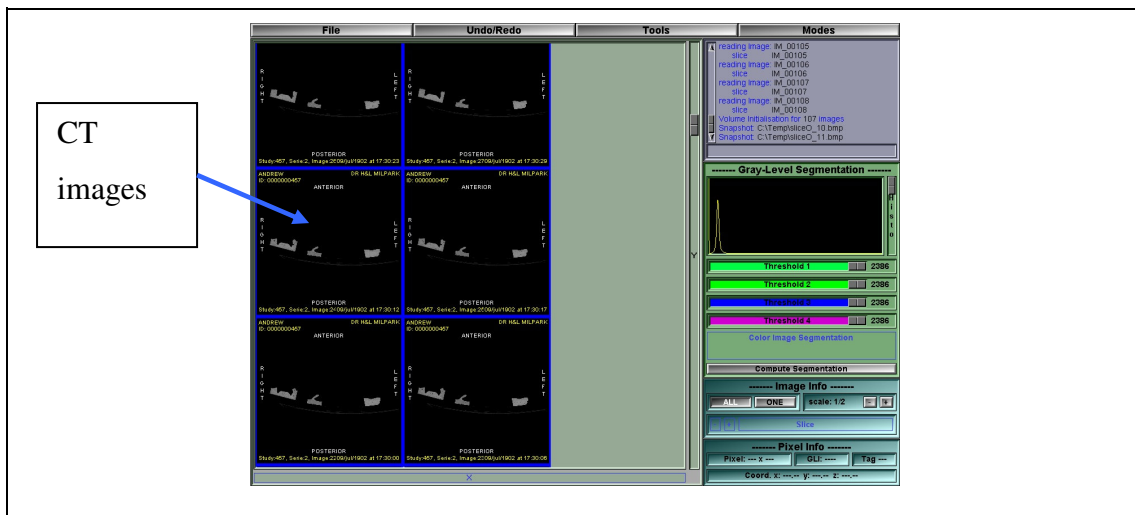
Figure 4-16: CT slice data

3. Press the [space bar] to show a single image.
4. Select the "Region growing" command from the menu.
5. Place the mouse cursor over a portion of the image displaying the required part. Note the threshold (HU) value that appears in the grey level segmentation graph illustrated in Figure 4-17. Move the cursor around the image and examine the extents of the grey level for the entire object.
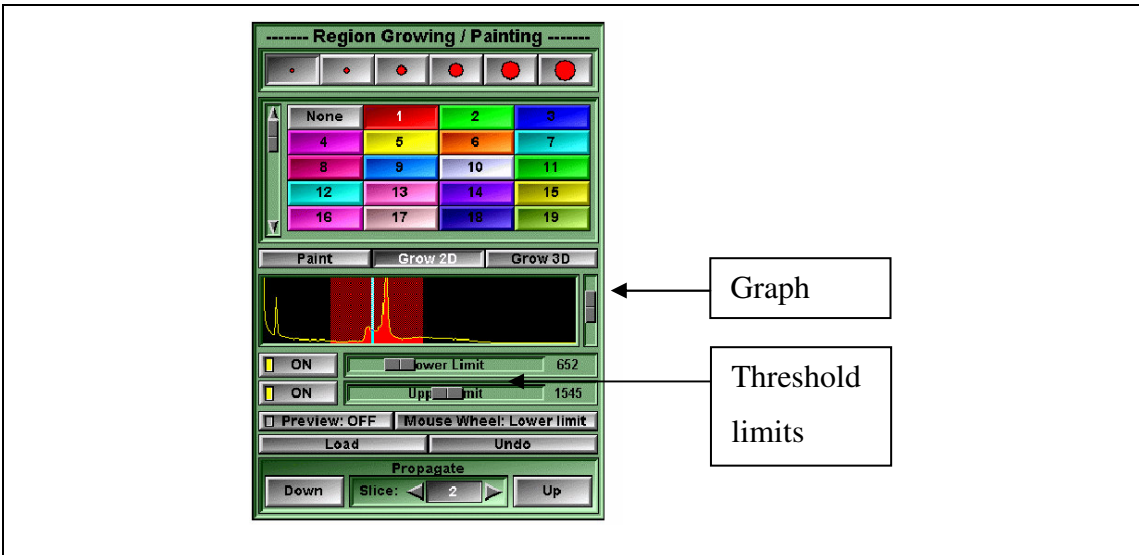
Figure 4-17: Threshold display

6. Set a lower and upper threshold value based on the grey level segmentation graph. Any HU value outside of these limits is discarded.

7. Click on "Grow 3D", to propagate the segmentation through all of the images.

8. Press the [space] bar and perform a visual inspection of the segmentation. Use a manual paintbrush to manually select new areas.

9. Use the 3D menu to save the object as an STL file. Figure 4-18 illustrates 3D models converted from DICOM (CT data) to STL.
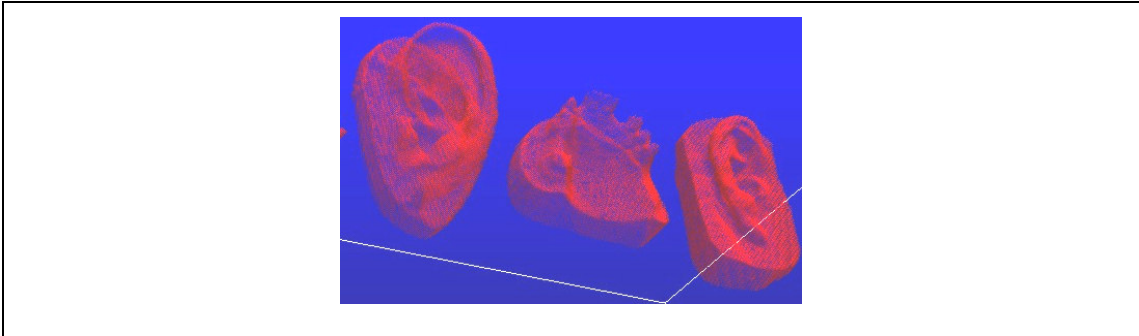
Figure 4-18: 3D view of the data for export

4.4 Design

This section describes firstly the method of removing errors and holes from STL files, and secondly the design of organic data. Hole filling and STL analysis is performed using Raindrop Geomagic Studio and Design is performed using the Freeform system.

4.4.1 Raindrop Geomagic

Use the following steps to create a watertight STL model. A watertight STL model is one with no holes or STL errors described in sub-section 2.5.2.

1. Start the Raindrop Geomagic Studio application and open the merged STL file.
2. Select the hole filling operation menu.
3. Deselect the curvature based hole filling option and select the fill small holes only option. This fills any small holes with less than the specified number of triangles around its edges.
4. Examine the model visually and make sure the holes filled correctly.
5. Select the fill all holes command using the curvature based hole filling option.
6. Click on any holes with simple geometry and no excessive curvature to fill them.
7. Fill large or complex holes using partial hole filling and bridges. This is performed by selecting a portion of the hole on a complex surface and filling it a small portion at a time. Typical hole filling results are illustrated in Figure 4-19.
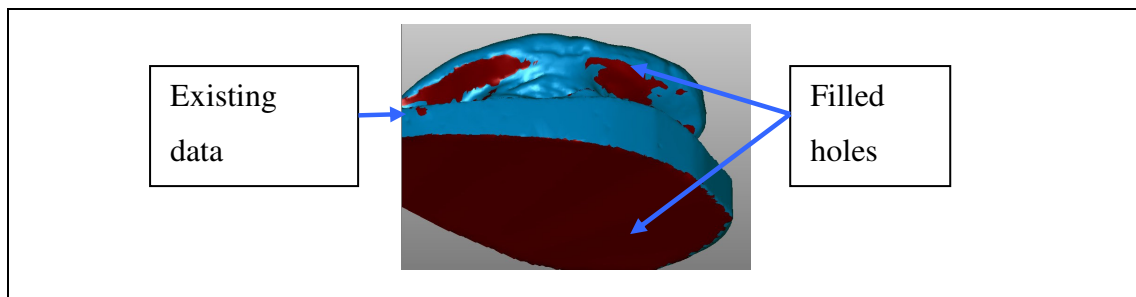
Figure 4-19: Hole filling using Raindrop Geomagic

8. Analyse the STL file for errors discussed in sub-section 2.5.2 using the "check intersections" command.
9. Save the model as an STL file.

4.4.2 Freeform system

Use the Freeform system for editing and designing with organic data.

1. Start the Freeform system and grasp the Phantom device like a pen with the first jointed section pointing downwards.
2. The Phantom device functions as a mouse and design tool.
3. Import the STL file into the Freeform system.
4. Set the clay coarseness. A low value requires more computing resources, but provides greater accuracy.
5. If green areas appear such as those displayed in Figure 4-20 then the model is not watertight and must be edited further in Raindrop Geomagic using the steps in sub-section 4.4.1.
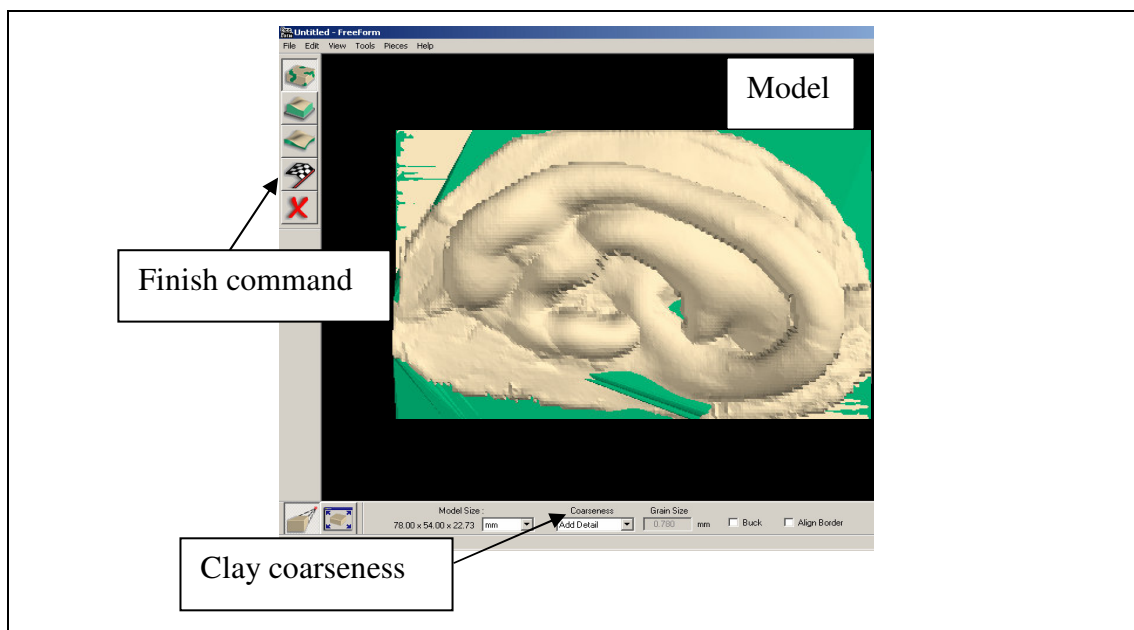
Figure 4-20: Freeform import screen

6. Select the finish command to convert the model into the voxel format.
7. The default tool is a ball shaped carving tool.
8. When the tool is moved around the screen, the phantom exerts a force if the tool comes into contact with the model and provide haptic interaction.
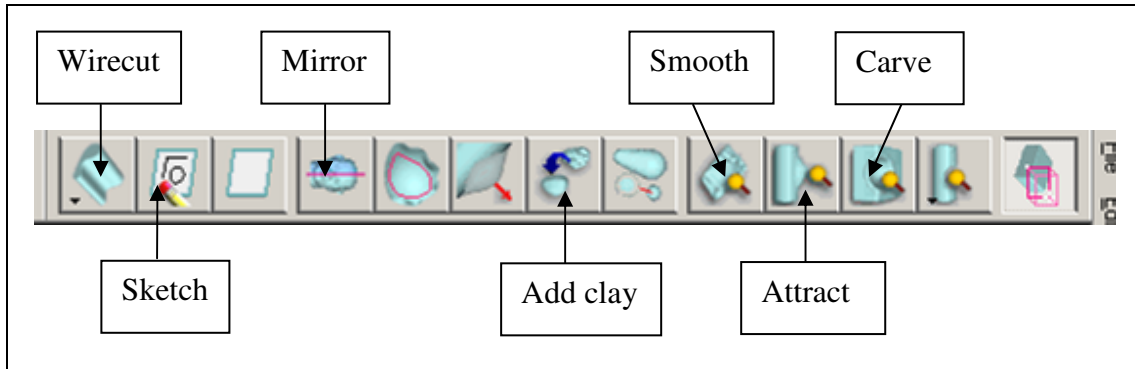
Figure 4-21: The basic Freeform commands

9. Figure 4-21 shows the basic Freeform commands, used during the investigation. Additional commands become available when the wire cut or sketch command is used.

10. Activate tools using the stylus to move the cursor over the tool and pressing the button located on the stylus with the index finger as illustrated in Figure 4-22.
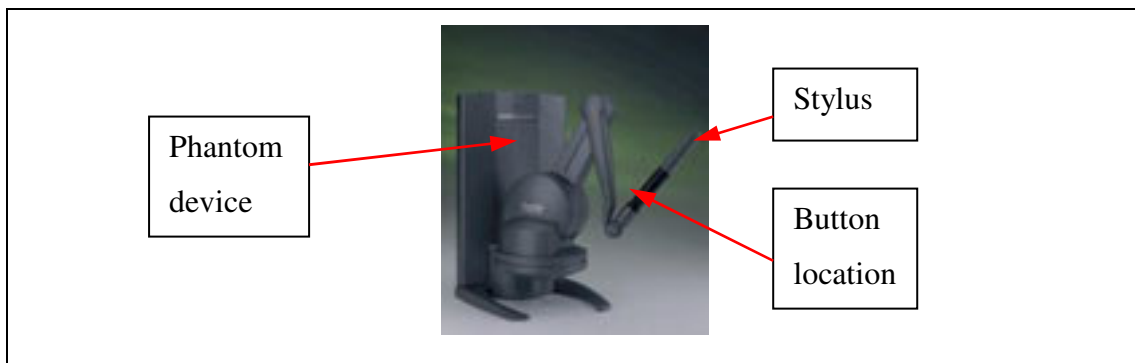
Figure 4-22: The Phantom device and button location

11. Use the carving tools and a light brushing motion to remove clay. Modify the tool size when more accuracy is required. The default tool size is ten times the diameter of the clay coarseness selected in step 4.

12. Use the attract command to raise and add clay.

13. Use the smoothing with a light brushing motion to smooth models, or use the tool globally by selecting an area.

14. Add additional clay primitives (spheres, cubes and cones) using the add clay command.

15. Use the mirror command to mirror a model through a plane.

16. Use the sketch tool to draw on a two dimensional plane for wire cutting .

17. Use the wire cutting tool toad or remove clay based on a sketch.
18. The "tools" menu, located at the top of the screen, contains the boolean operations and clay positioning tools.
19. Use the "pieces" menu to import additional files into the workspace.
20. View model properties by pressing the [o] key on the keyboard. This function creates a small window where model properties are displayed and altered.
21. Use the "File export" command to export and decimate models into the STL file format.

4.5 Rapid prototyping

The method used for RP on a Thermojet printer located at Rapid design technologies, Olivedale, South Africa is described in this section. The interface software for the Thermojet printer is the Thermojet print preview software version 1.00 (3D Systems, Valencia, CA).

4.5.1 Thermojet Printer

1. Start the Thermojet Print Preview software and import the required STL file.
2. Examine the model to ensure it fits on the virtual platform with the Thermojet printer dimensions, if the model is red in colour, it does not fit on the platform.
3. Orient the model in space and place it in an orientation so that the wax supports are on a side where a smooth surface is not required.
4. Use non uniform scaling and apply the wax shrinkage factor to the model.
5. Press the submit button with the mouse and turn the Thermojet printer on.
6. Place a clean platform in the Thermojet printer and print a test pattern to check for wax blockages.
7. Press the start button on the Thermojet printers control panel.
8. Building starts automatically, and the LCD shows the remaining build time.
9. Remove the part from the printer and cool to room temperature.
10. Brush off the wax supports using a blade and toothbrush.

4.6 Casting techniques

The casting for this investigation is performed at the school of prosthetic dentistry, University of the Witwatersrand. The casting methods use the investment casting or lost wax processes, discussed in section 2.7. A plaster model of patient anatomy is created to prevent the need of multiple patient visits and is also stored for future reference. This plaster model is known as a "master model" in this research to prevent confusion between other plaster models. Casting is also required to convert wax models to a different material such as silicone or acrylic.

Master model

A master model is cast from patient impressions. The method presented here uses a two part mould described in sub-section 2.8.3 by Kubon, Kurtz and Piro (2000, pp. 648-651).

1. Place the patient in a dental examination chair with the required anatomy facing the prosthodontist.
2. Mix a dental lab plaster mixture, (Kalabhai Parson, PVT, Ltd, 256 Sardar V Patel Road, Bombay, India), using 1 part plaster to 1 part water in a container.
3. Rub Vaseline onto the patient in the area surrounding the required anatomy and especially the hair.
4. Mix Coltene Lab Putty and a catalyst (Coltene AG, Feldwiesenstrasse 20, CH-9450, Altstatten, Switzerland) together in a ratio of 1 measure of catalyst to 2 scoops of putty.
5. Mould the mixture onto the underside of the patients anatomy (The underside of the pinna in the case of an ear impression) to create a base for the impression.
6. Mix an alginate mixture (Dentsply, Detrey Gmbh D-78467, Konstan Z), using a ratio of 1 part alginate to 1.5 parts water.
7. Pour the mixture over the top of the putty.
8. Remove the two parts to the impression after five minutes and wrap a damp paper towel around the impression.

9. Place the impression on a working surface and pour the plaster mixture from step 2 into the impression.

10. Leave the plaster to set for one hour.

Lost wax process

Use the lost wax process to convert a wax model into another material such as silicone or acrylic.

1. Mix a dental lab plaster mixture, (Kalabhai Parson, PVT, Ltd, 256 Sardar V Patel Road, Bombay, India), using 1 part plaster to 1 part water in a container.

2. Pour the plaster mixture into the flask base.

3. Place the wax model in the plaster, and submerge to a chosen split line.

4. Allow the plaster to set for 45 minutes.

5. Place the flask top over the flask base using the pins for alignment and remove the lid. Figure 4-23 illustrates the dental flask assembly.
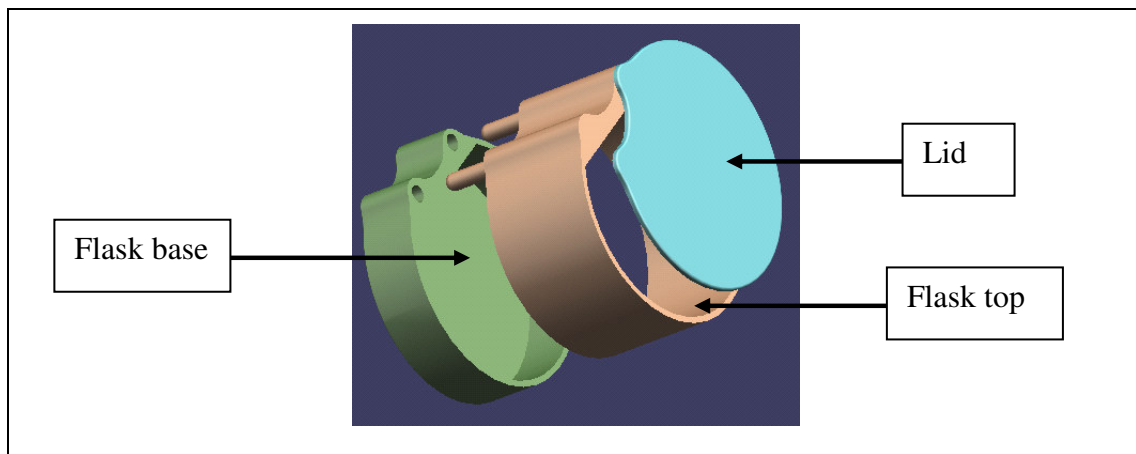
Figure 4-23: Dental flask assembly

6. Mix a second batch of dental lab plaster mixture, (Kalabhai Parson, PVT, Ltd, 256 Sardar V Patel Road, Bombay, India), using 1 part plaster to 1 part water in a container.

7. Pour the second batch of plaster mixture into the flask top.

8. Place the lid on the flask top.

9. Place the dental flask into a vice and apply 3 bars of pressure for 15 minutes, using the gauge on the vice to determine pressure.

10. Remove the dental flask from the vice and place it into the hot water bath for 30 minutes.

11. Use insulated gloves and remove the flask from the hot water bath and allow to cool for 10 minutes.

12. Open the flask and remove any excess wax using a sharp tool, care must be taken not to damage the plaster mould with the tool.

13. The resulting plaster model is a two piece mould that is used to cast the required products (implants and prostheses).

4.7 Process Evaluation

The process evaluation section consists of four sub-sections (4.7.1 to 4.7.4). Each sub-section uses a case study to evaluate either a partial or full generic reverse engineering process illustrated in Figure 2-1.

Sub-section 4.7.1 uses four anatomical models to investigate and compare imaging systems and software using the methods discussed from sub-section 4.2 to 4.3. Sub-section 4.7.2 illustrates a cranioplasty case study using the methods described from sub-section 4.2 to 4.6. Sub-section 4.7.3 illustrates a prosthesis design case study using the methods described from sub-section 4.2 to 4.6. Sub-section 4.7.4 illustrates a prosthesis duplication case study using the methods described from sub-section 4.2 to 4.6.

4.7.1 Anatomical models

The anatomical models are made using impressions taken from patients for the purposes of student training at the department of prosthetic dentistry, University of the Witwatersrand. The models are all yellow in colour and made of plaster.
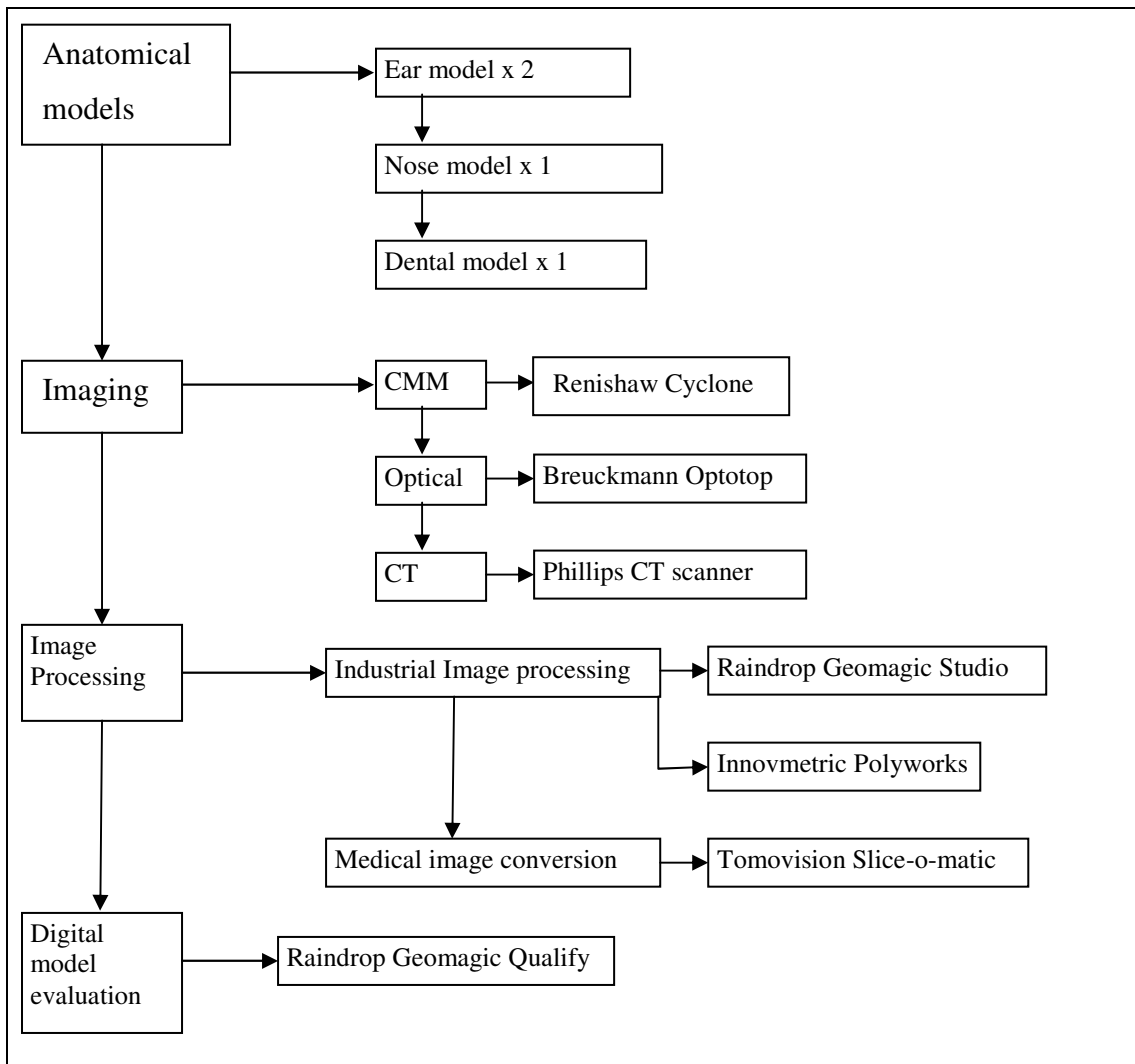
Figure 4-24: Flowchart for the anatomical models

Figure 4-24 shows the steps followed with the anatomical models. The steps provide digital models that are compared to one another using different imaging hardware and software. The anatomical models case study uses two steps in the digital process and an evaluation step.
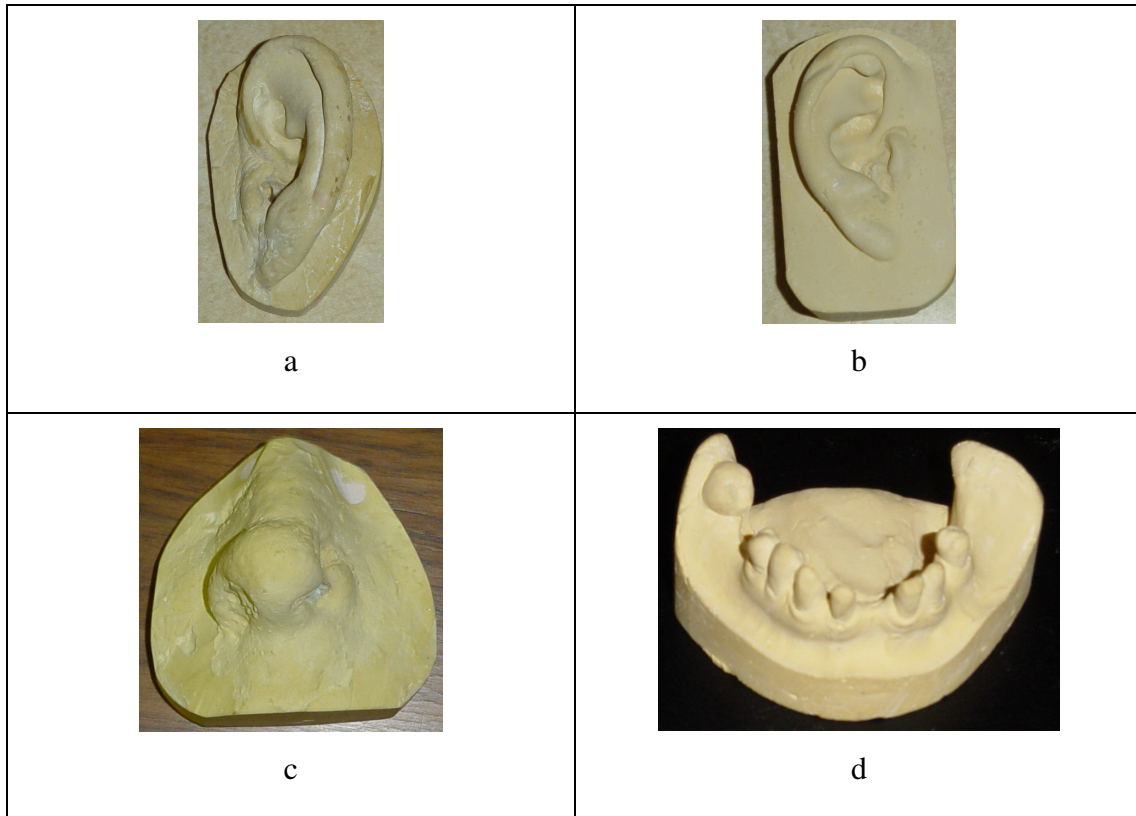
Figure 4-25: The anatomical models

Figure 4-25 (a-d) consists of the following: a larger ear (ear 1), a smaller ear (ear 2), a nose model (Nose 1) and a dental model (teeth 1). The anatomical models provide a method of evaluating the different scanners and image processing software using the following method:

Renishaw Cyclone

1. Scan ear 1, ear 2 and Nose 1 using the Renishaw Cyclone with a 2mm ball probe and the method presented in sub-section 4.2.1. Use several orientations to obtain a full geometric description.

2. Scan Teeth 1 using the Renishaw Cyclone with a 1mm ball probe and the method presented in sub-section 4.2.1. Use several orientations to obtain a full geometric description.

3. Obtain as many features as possible on the first scan.

4. Overlap data sets by a minimum of 2mm to assist with the local registration process.

Breuckmann Optotop

1. Calibrate the Breuckmann Optotop using the method presented in sub-section 4.2.2 and the HF-160 base bar.

2. Scan ear 1, ear 2 and nose 1 using the method presented in sub-section 4.2.2.

3. Calibrate the Breuckmann Optotop using the HF-80 base bar.

4. Scan teeth 1.

5. Obtain as many features as possible with the first scan to improve local registration.

6. Remove as much of the unwanted environmental data as possible with the masking tool in the Optocat software.

Phillips CT scanner

1. Place ear 1, ear 2, nose 1 and teeth 1 on the patient bed with the orientation presented in Figure 4-26 where the horizontal lines show the CT slice orientation.

Figure 4-26: Orientation of the anatomical models on the patient bed

2. Select a slice distance of 1mm.

3. Scan the anatomical models using the method presented in sub-section 4.2.3.

4. Take the Optical disk to a Phillips Easyvision workstation and write the data to CD using the method presented in sub-section 4.2.3.

Raindrop Geomagic Studio

1. Import data (STL) from the Renishaw Cyclone for ear 1 into Geomagic Studio.

2. Remove the flash data and redundant triangles using the method presented in sub-section 4.3.1.

3. Save the edited scans for image processing with Innovmetric Polyworks, these scans are known as the edited Renishaw Cyclone scans.

4. Use the local registration method presented in sub-section 4.3.1 to align each of the scans.

5. If problems occur during registration, select three points on both the floating and fixed scans that are closer to being correct.

6. Globally register and merge the Renishaw Cyclone data for the anatomical model.

7. Close and save the edited file under a new file name.

8. Repeat steps 1 to 6 for ear 2, nose 1 and teeth 1.

9. Import data from the Breuckmann Optotop (Point cloud) for ear 1 into Geomagic Studio.

10. Use the local registration method presented in sub-section 4.3.2 to align each of the scans.

11. Use point sampling to increase the speed of local registration.

12. If the sampling causes large misalignment of the scans, use the global registration function to improve alignment to and then repeat step 9 until local registration is complete.

13. Use the global registration algorithm on all of the aligned scans.

14. Merge the globally registered model.

15. Close and save the merged model under a new file name.

16. Repeat steps 8 to 14 for ear 2, nose 1 and teeth 1.

Innovmetric Polyworks

1. Import the edited Renishaw Cyclone scans (STL) for ear 1 into IMEdit using the method presented in sub-section 4.3.1.

2. Convert each of the scans to a sampled point cloud.

3. Import each point cloud into IMAlign.

4. Use N-point alignment for local registration of the data.

5. Globally register the data and merge the resulting model.

6. Close and save the merged model under a new file name.

7. Repeat steps 1 to 6 for ear 2, nose 1 and teeth 1.

8. Import the Breuckmann Optotop data (point cloud) for ear 1 into IMAlign using the method presented in sub-section 4.3.2.

9. Use N-point alignment for local registration of the data.

10. Globally register the data and merge the resulting model.

11. Close and save the merged model under a new file name.

12. Repeat steps 8 to 11 for ear 2, nose 1 and teeth 1.

Tomovision Slice-o-matic

1. Import the DICOM files from the CD.

2. Segment the four anatomical models from the background using the segmentation techniques presented in sub-section 4.3.3.

3. Export the four anatomical models as STL files.

Anatomical model evaluation

1. Import ear 1, ear 2, nose 1 and teeth 1 from all scanner and software combinations into Raindrop Geomagic Qualify.

2. Use the data set combinations for ear 1 presented in Table 4-1 to compare models.

Table 4-1: Data set combinations

		Reference		
		Breuckmann Optotop	**Renishaw Cyclone**	**CT Scanning**
Test		**Innovmetric Polyworks**	**Innovmetric Polyworks**	**Tomovision**
Breuckmann Optotop	**Raindrop Geomagic**	a	d	g
Breuckmann Optotop	**Innovmetric Polyworks**	N/A	N/A	h
Renishaw Cyclone	**Raindrop Geomagic**	b	e	i
Renishaw Cyclone	**Innovmetric Polyworks**	c	f	j

3. Starting with comparison "a" in Table 4-1, set the reference model by right clicking and selecting "reference" and set the test model by right clicking and selecting "test".

4. Select "Best fit alignment" which performs alignment twice, once with a sample size of 300 points and once with a sample size of 1500 points.

5. Accept the alignment and select "3D compare" and a colour error map is generated similar to that illustrated in Figure 4-27.
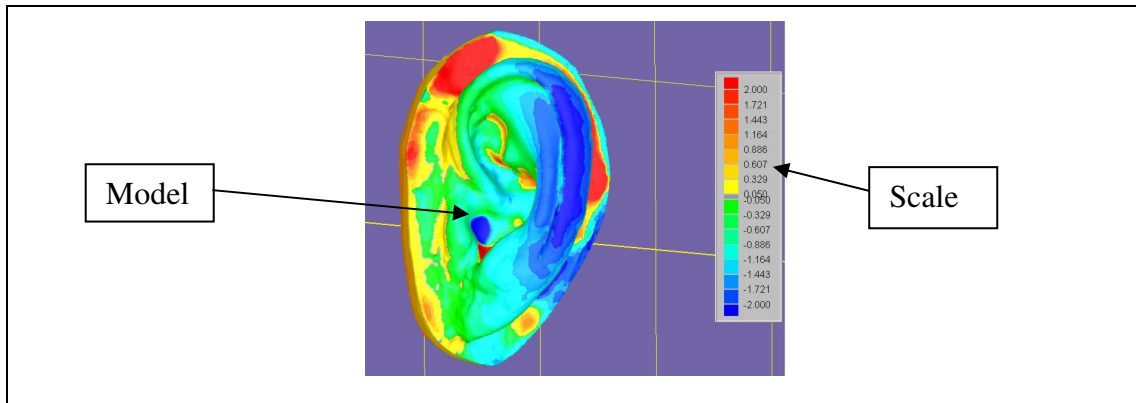
Figure 4-27: Colour error map

6. Repeat steps 2 to 5 with each of the remaining comparisons in Table 4-1.
7. Repeat steps 2 to 6 with ear 2, nose 1 and teeth 1.

4.7.2 Implant design

An implant case study uses a dry skull from the department of plastic surgery, University of the Witwatersrand.
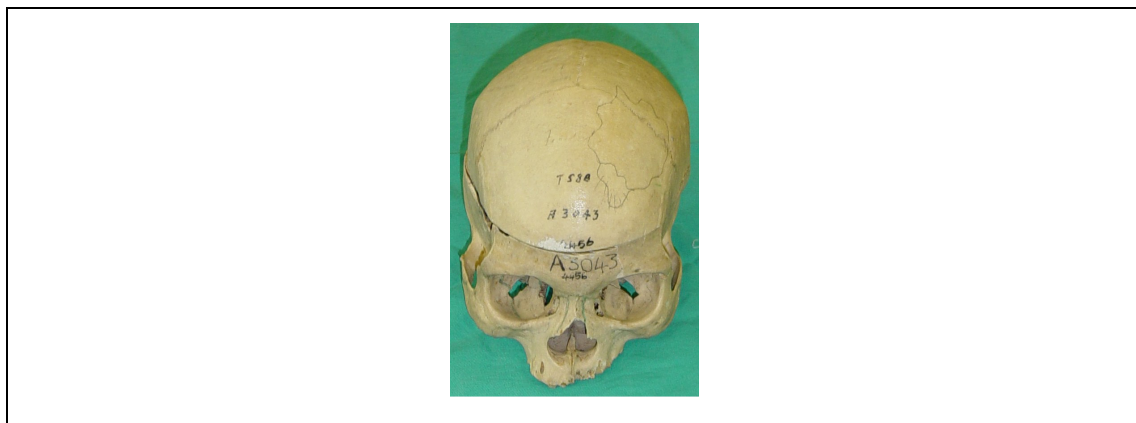
Figure 4-28: Dry human skull

Figure 4-28 shows the dry human skull for the cranioplasty case study. The cranium and lower portions of the skull are separated. The investigation uses the cranium for the case study.

Preparation

1. Scan the cranium using the Breuckmann Optotop and the HF-160 base bar, using the method presented in sub-section 4.2.2.

2. Use Innovmetric Polyworks for image processing and the method presented in sub-section 4.3.2.

3. Image the cranium using the Phillips CT scanner and the method presented in sub-section 4.2.3.

4. Draw a defect on one side of the cranium to simulate a unilateral defect with a pencil.

5. Place the cranium in a cardboard box with a vacuum system connected to the box to remove dust to prevent inhalation.

6. Mill the defect out of the cranium using a bone burr and dental drill at the department of prosthetic dentistry. Use a dust mask when milling to prevent inhalation of bone dust. Figure 4-29 shows the cranium in the box with a vacuum system and the dental drill.

Figure 4-29: The milling apparatus and vacuum system

Imaging

1. Place the cranium on the patient bed of the Phillips CT scanner.

2. Image the cranium using the Phillips CT scanner using the method presented in sub-section 4.2.3 and a slice distance of 1mm.

3. Transfer the data to a CD rom using the method presented in sub-section 4.2.3 and the Easyvision workstation.

Image Processing

1. Import the DICOM data from the CD rom to Tomovision Slice-o-matic.

2. Convert the DICOM to data to STL using the image segmentation techniques presented in sub-section 4.3.3.

3. A rendered image of the resulting cranium CT model is illustrated in Figure 4-30.
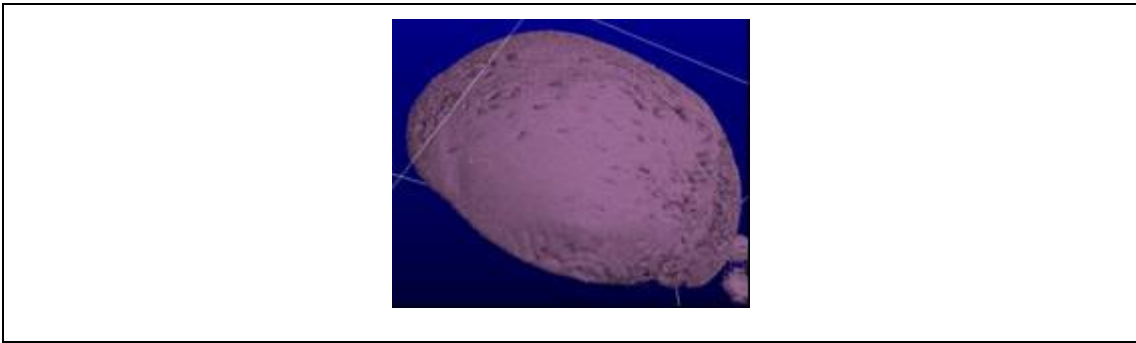
Figure 4-30: Digital cranial model

Design

1. Import the STL file into Freeform version 5 and use a clay coarseness of 300μm. If the Phantom vibrates then select a larger clay coarseness size.

2. Divide the cranium into three portions using the wire cut command and the sections illustrated in Figure 4-31.
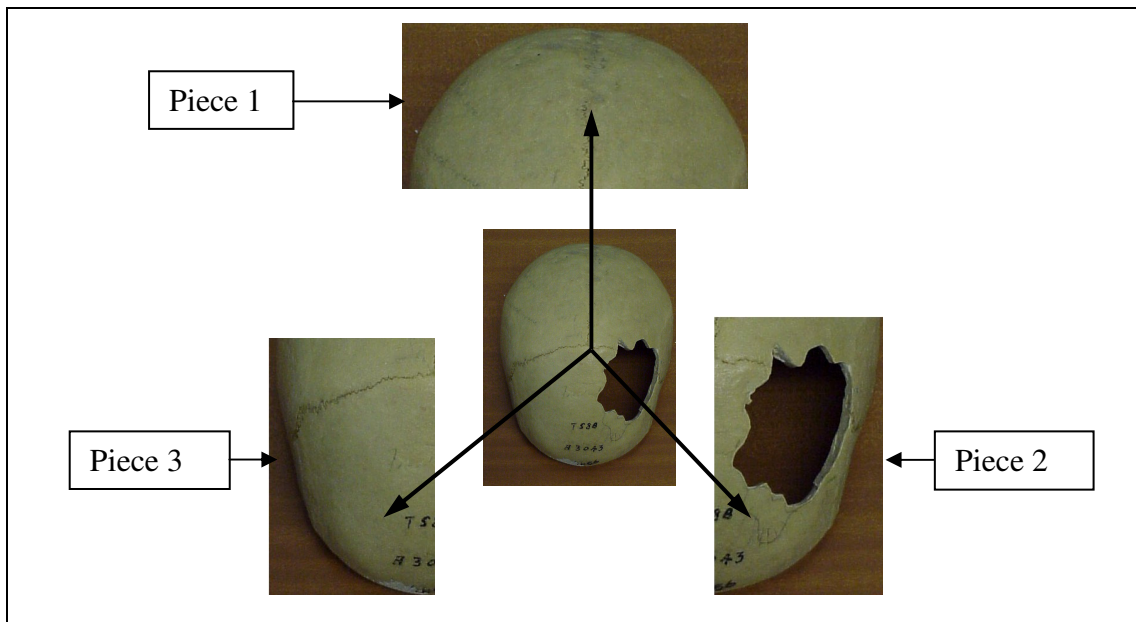
Figure 4-31: Dividing the cranium

3. Delete piece one to free up computing resources by reducing model size. Piece two contains the defect and piece three the anatomy that is to be mirrored.

4. Generate a mirror image of piece three using the mirror command to generate piece four.

5. Delete piece three illustrated in Figure 4-32.
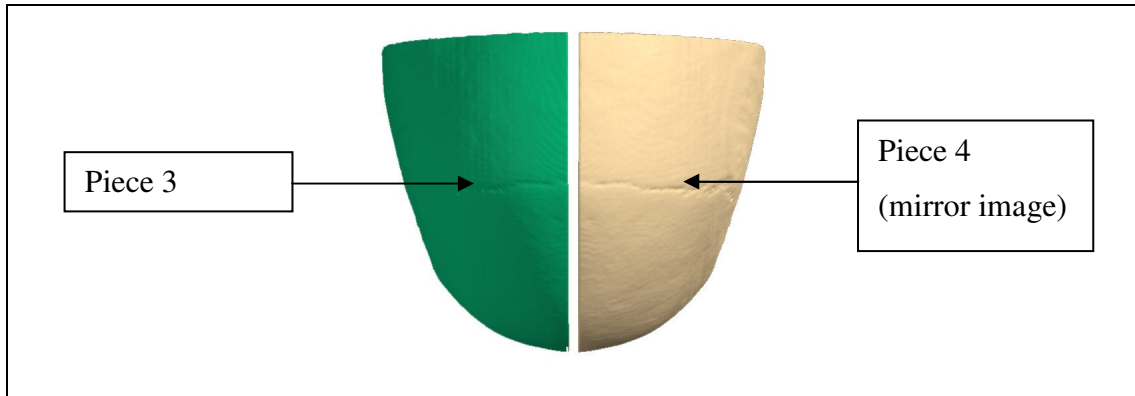
Figure 4-32: Mirroring a portion of skull

6. The remaining pieces are piece two (with the defect) and piece four (the mirrored anatomy).

7. Position piece four over piece two using the reposition command. Ensure the contours match as closely as possible. The repositioning of piece four is illustrated in Figure 4-33.
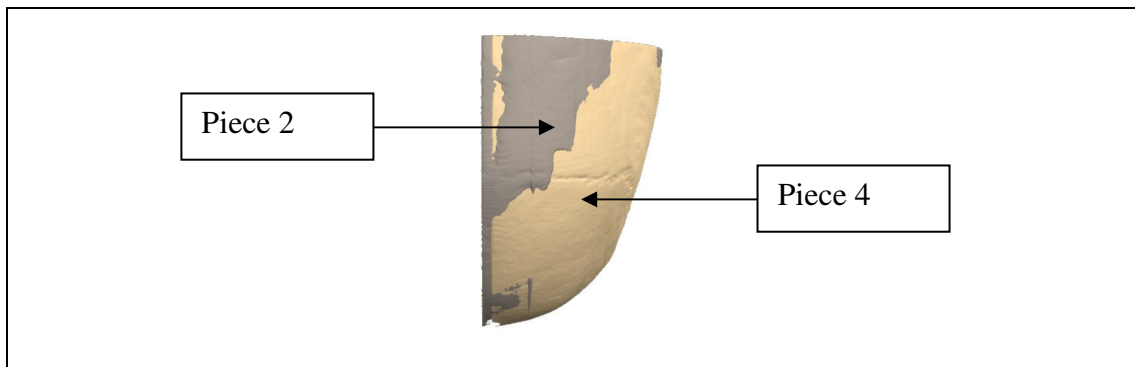
Figure 4-33: Results of positioning piece 2 and piece 4

8. Use the tools menu and a boolean subtraction of piece four subtract piece two.

9. The boolean subtraction results in piece two (with the defect being untouched), and a modified piece four that represents a rough implant.

10. Place a mask over piece two to prevent changes to this model. The mask colours piece two purple. Figure 4-34a and Figure 4-34b illustrate two views of piece two and piece four.
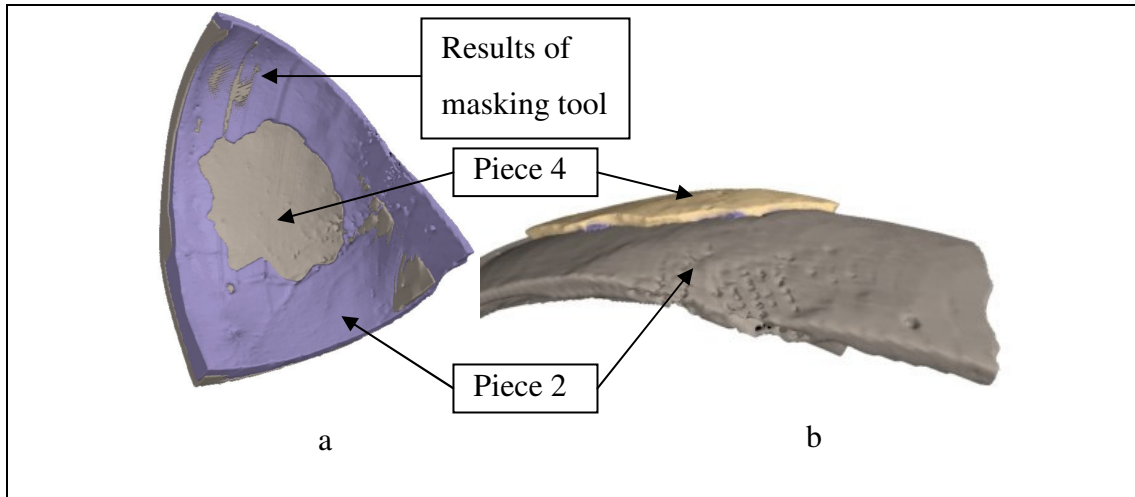
Figure 4-34: The rough implant and defect

11. Use the carving, smoothing and add clay commands described in sub-section
    4.4.2 to edit piece four. Remove any redundant digital clay from piece four
    using the select clay and delete commands. The implant can be protected from
    deleting by painting a mask on areas that are to be kept.

12. The implant is ready when it interfaces seamlessly with piece two to create a
    smooth surface between the pieces.
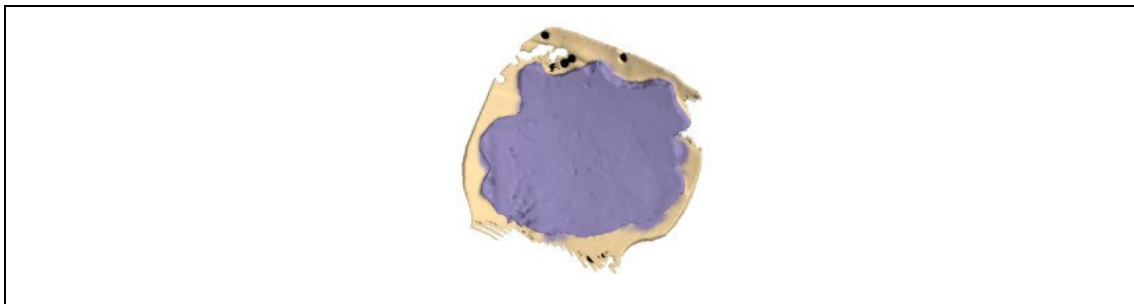
Figure 4-35: Digital implant

13. The resulting digital implant is illustrated in Figure 4-35 with some of the
    surrounding clay that is deleted.

14. Export the implant (Piece 4) as an STL file.

<u>Prototyping</u>

1. Import the implant STL file into the Thermojet print-preview software using
   the method described in sub-section 4.5.1.

2. Use the repositioning tools to place the top of the implant (Surface that contacts the skin) at the bottom. The rough surface created from prototyping supports is on the top surface.

3. Scale the model to compensate for wax shrinkage.

4. Prototype the implant. The wax implant and cranium are illustrated in Figure 4-36.
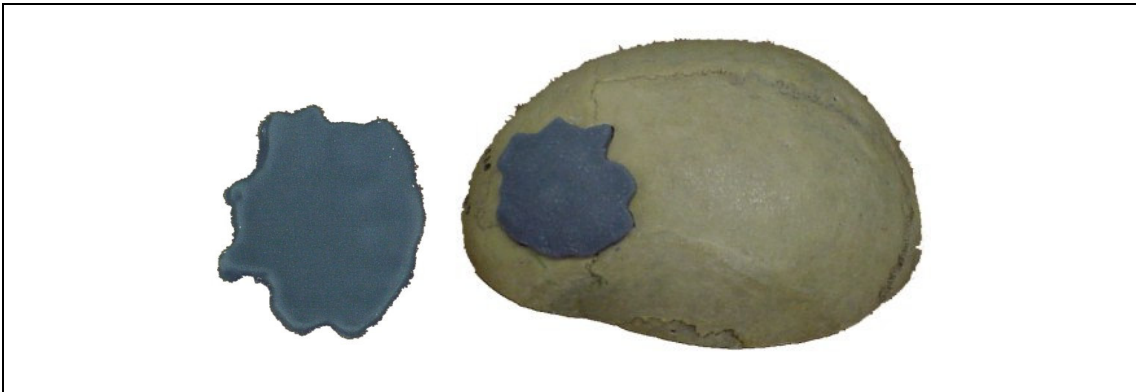
Figure 4-36: Wax implant prototype

Investment casting

1. Place a thin layer, ±100µm thick, of model release agent (MRA), (Dentsply International Inc., York, PA 17406, USA), over the wax implant using the supplied brush.

2. Prepare a dental flask base with plaster using the method presented in section 4.6.

3. Make three small indentations in the plaster to assist in any future alignments using the back of a pencil.

4. Place the wax implant in the plaster mixture, with the rough side facing into the plaster.
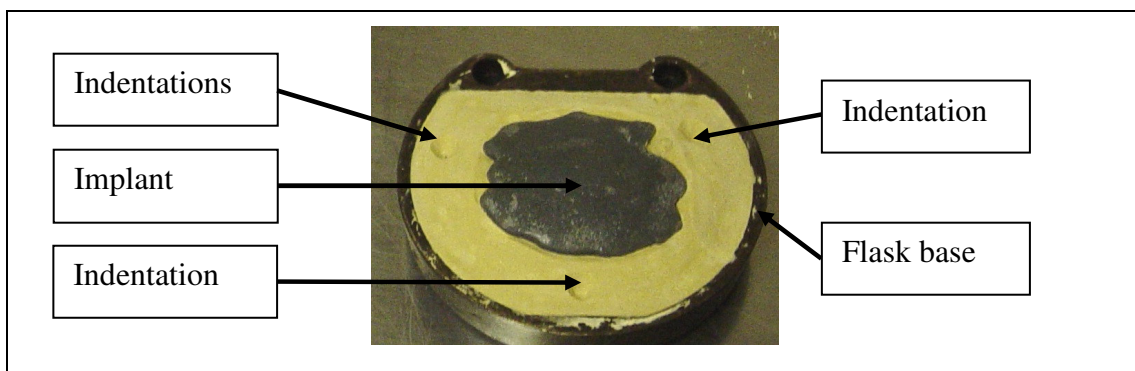
Figure 4-37: Implant in flask base

5. Place the top half of the dental flask over the base using the pins for alignment and pour in the second batch of plaster.

6. Follow the remaining steps of the investment casting process illustrated in section 4.6, including placing the flask in a vice and boiling out the wax.

7. Remove the remaining wax from the dental flask.

PMMA

1. Brush a thin layer of Divosep (Vertex-Dental, P.O. Box 10, 3700, AA Zeist, The Netherlands), an algenate insulation liquid, onto each half of the plaster mould shown in Figure 4-38. Divosep is a blue liquid and prevents the acrylic sticking to the plaster.

Figure 4-38: Brushing on the algenate insulation liquid

2. Use a container to mix Surgical Simplex P (Howmedica International Inc., Shannon Industrial Estate, Co. Claire, Ireland). Surgical simplex P is acrylic PMMA used in cranial repair and consists of a packet of white powder and a glass container of clear liquid catalyst.

3. Pour 40g of the fine white powder the container.

4. Pour 20cc of the clear liquid into the powder

5. Mix immediately with a spatula until putty, off-white in colour, forms after approximately 5 minutes. The mixture is highly exothermic and the heat from the putty can be felt. Figure 4-39 shows the container and mixing process.

Figure 4-39: The PMMA mixture

6. Mould the putty into the base of the dental flask, ensuring there is enough excess for the top of the flask.
7. Seal the dental flask and place it into the dental vice for 5 minutes.
8. Remove the dental flask from the vice and the implant from the flask.
9. Use a dental burr and a scalpel to remove the flash from the implant as illustrated in Figure 4-40.

Figure 4-40: Removal of flash from the implant

10. Figure 4-41 shows the implant placed in the cranium.

Figure 4-41: Implant placed in cranium

4.7.3 Prosthesis design

The prosthesis design case study uses a patient requiring a right ear prosthesis. The case study involves using both traditional and digital methods in the design and manufacture of a prosthesis. Sub-section 4.7.3 starts with the preparation of plaster models for both the traditional and digital process, followed by the traditional and digital processes respectively. Sub-section 4.7.3 ends with the evaluation of the two prostheses using the evaluation criteria presented in section 2.9.
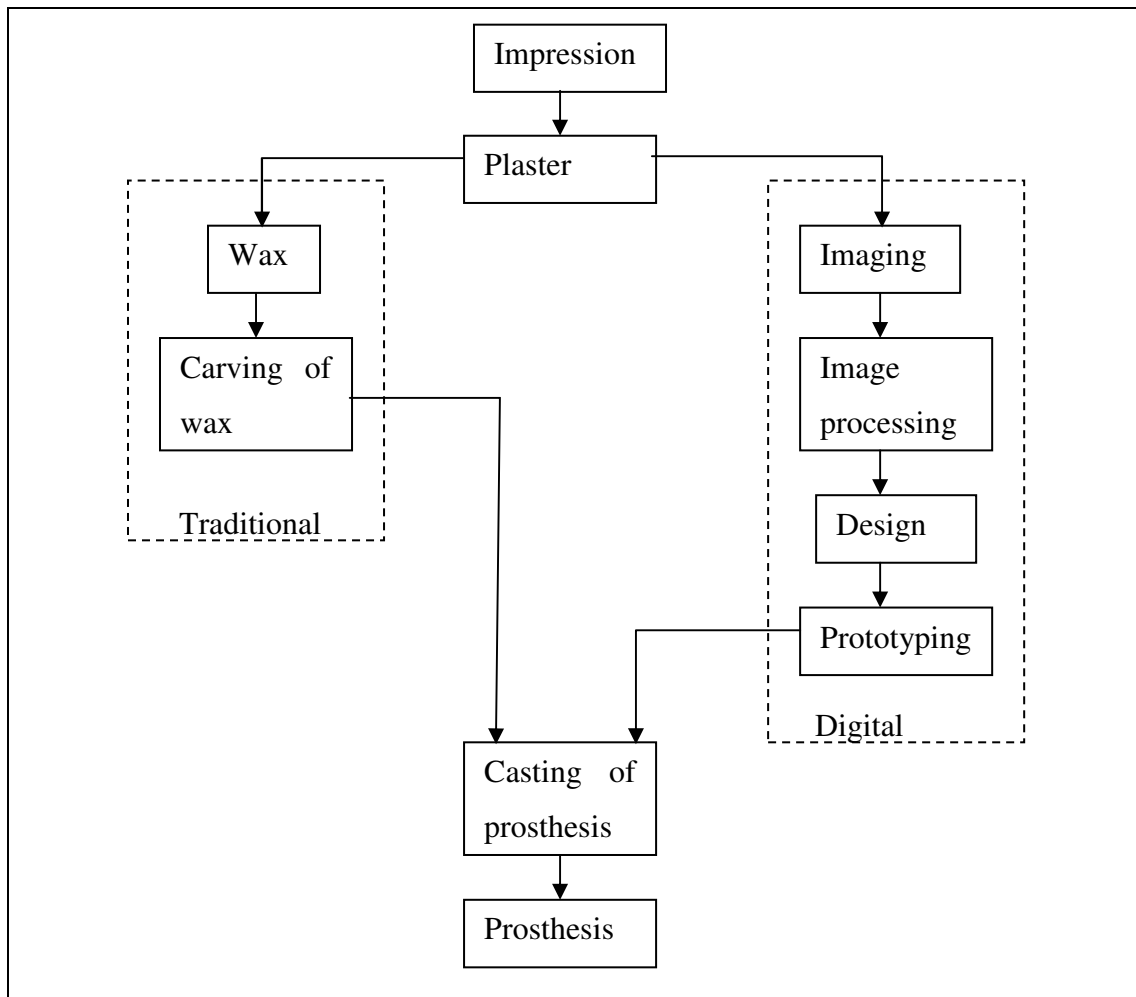
Figure 4-42: Prosthesis design method overview

Figure 4-42 shows an overview of the methods for both traditional and digital prosthesis design. The portion where the two methods differ is illustrated by "Traditional" and "Digital". The traditional method is based on the literature and method presented in sub-section 2.8.3 and section 4.6 respectively.

Preparation

The preparation presented here refers to both the traditional and digital processes for auricular prosthesis design.

1. Place the patient in a dental examination chair with the remaining ear facing towards the prosthodontist.
2. Use the method presented in section 4.6 to obtain a master model of the remaining ear.

3. Reposition the patient so the defective ear faces towards the prosthodontist.

4. Use the method presented in section 4.6 to obtain a master model of the defective ear.

	Helix	
	Tragus	
	Lobule	
Ear		Defective ear
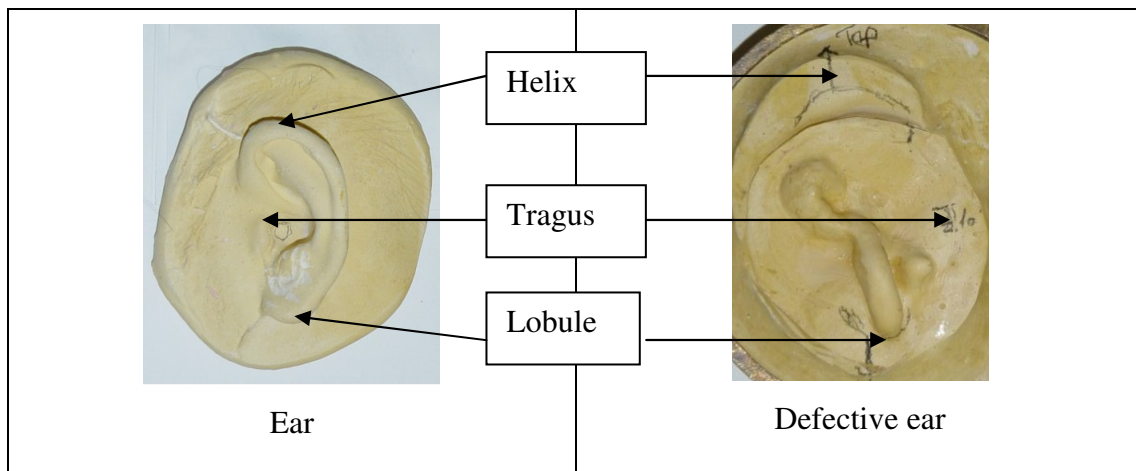
Figure 4-43: The master models

5. The master models are illustrated in Figure 4-43 with three anatomical features, helix, tragus and lobule.

6. Place the master model of the defective ear near the patients remaining ear.

7. Use a ruler and obtain measurements from both the patient and ear master model to indicate where anatomy should lie on the master model of the defective ear using a pencil. Label the helix, tragus and lobule on the model of the defective ear.

Traditional prosthesis design method

The following method illustrates the carving of a wax prosthesis by a prosthodontist using the traditional method.

1. Use the master ear model as a reference and carve a wax prosthesis using heated wax tools and a block of dental wax (Associated dental products LTD. Purton, Swindon, SN5 9HT, England).

2. The carving techniques may include methods described by Lemon *et al* (1996, pp. 292-293) and Nusinov and Gay (1980, pp. 68-71) in sub-section 2.8.3.

3. Create the interface to the defective ear by heating the base of the wax prosthesis and pressing it onto the master model of the defective ear. Use the impression created in the base of the wax to determine where wax is removed

with heated tools and then repeating the process until the wax prosthesis is easily replaced and removed from the master defective ear model.

4. Allow the wax prosthesis to cool for 45 minutes and place it on the defective ear master model. Smooth wax into the surrounding areas until a natural looking wax prosthesis is formed.

Figure 4-44: Dental wax ear

5. Figure 4-44 illustrates the wax prosthesis using the traditional method.

Digital prosthesis design method

The following four methods cover the digital portion of designing a prosthesis and include: imaging, image processing, design and rapid prototyping.

Imaging

1. Use the method presented in sub-section 4.2.2 to scan the master ear model using the Breuckmann Optotop with the HF-160 base bar and the Optocat software with a 0.4mm raster point size.

2. Use the method presented in sub-section 4.2.2 to scan the master defective ear model using the Breuckmann Optotop with the HF-160 base bar and the Optocat software with a 0.4mm raster point size.

Image processing

1. Locally register the scans for both models using Innovmetric Polyworks and the IMAlign module with the method presented in sub-section 4.3.2.

2. Globally register and merge both digital models using Innovmetric Polyworks and save the models as STL files.

3. Open both the ear and defective ear model using Raindrop Geomagic Studio. The two digital models are illustrated in Figure 4-45.
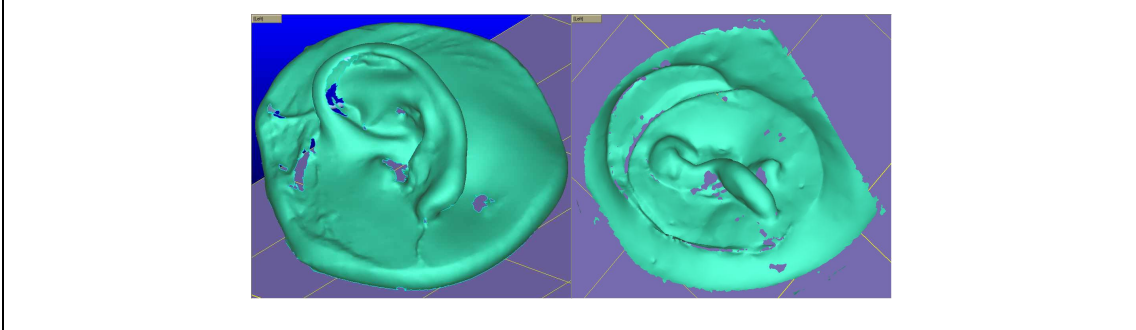
Figure 4-45: The digital models

4. Use the fill holes and test intersections command's and the method presented in sub-section 4.4.1 to create error free watertight STL files.

5. Export the model as an STL file.

<u>Design</u>

1. Start the Freeform system.

2. Import both the ear and defective ear model into Freeform using a clay coarseness of 0.16mm.

3. Use steps 4 to 9 and the method presented in sub-section 4.4.2 to design a digital ear prosthesis.

4. Mirror the ear model using a plane parallel to the base of the ear model.

5. Position the ear model over the defective ear model using the positioning tools and the pencil marks created on the master defective ear model. Place the mirrored ear in such an orientation that it covers as many of the ear remnants on the defective ear model as possible.

6. Use the ball shaped carving tool and remove the excess base from the mirrored ear and defective ear models. This size reduction frees up PC system resources. Figure 4-46 shows the repositioned ear models.
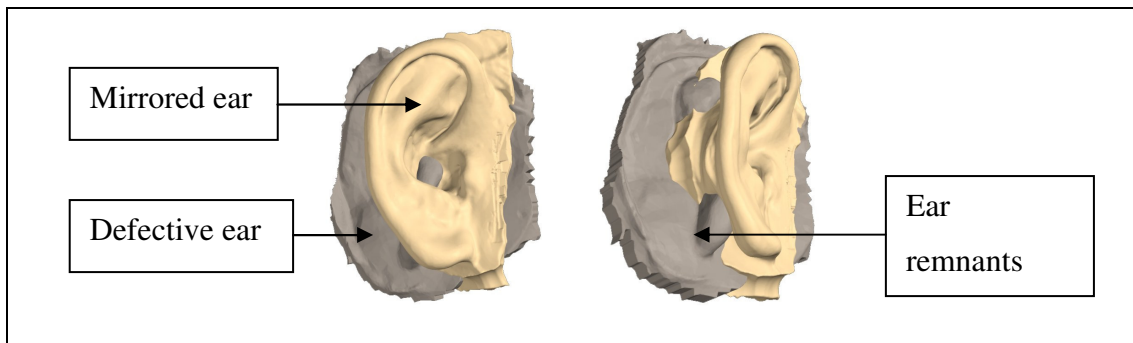
Figure 4-46: Repositioned ear models in Freeform

7. Place a mask over the defective ear model to prevent unwanted changes to the model.

8. Use the smoothing, carving and add clay tools in Freeform to edit the mirrored ear model to create a prosthesis. The mirrored ear model should cover all of the ear remnants and interface with the defective ear model.

9. Perform a boolean subtraction between the mirrored ear model and defective ear model to create a cavity for the mirrored ear model to fit over the ear remnants.

10. Export the designed digital prosthesis (mirrored ear model) as an STL file for rapid prototyping.

Rapid prototyping

1. Review the digital prosthesis using the Thermojet Print Preview software.

2. Orientate the underside of the prosthesis to the base of the Thermojet Printer, ensuring the rough surface is not visible on the final prosthesis.

3. Prototype the ear prosthesis on the Thermojet Printer.

4. Figure 4-47 shows the prototype of the prosthesis mounted on the defective master defective ear model, alongside the original plaster model of the patients remaining ear.

5. Use heated wax cutting tools to remove any excess wax preventing the mounting of the wax prosthesis.
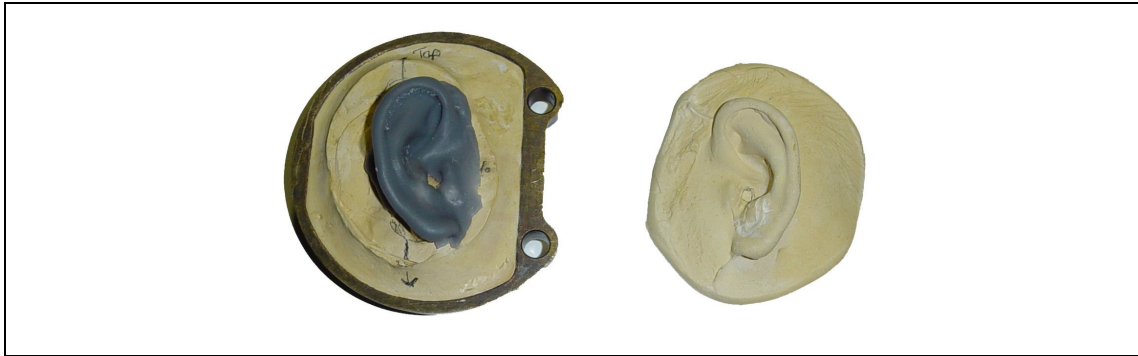
Figure 4-47: The Thermojet prosthesis and original plaster cast

<u>**Casting**</u>

The following method refers to both the traditional and digital process of creating a silicone ear prosthesis.

1. Prepare two dental flask bases using the lost wax process presented in section 4.6.
2. Place the traditionally made wax prosthesis in one base and the RP prosthesis in the other base.
3. Allow the plaster in both bases to set for 45 minutes.
4. Place the flask tops on both bases.
5. Pour in the remaining plaster in both bases and replace the lids.
6. Place both dental flasks in the dental vices and apply three bars of pressure for 15 minutes.
7. Boil out the wax using a heated water bath.
8. Prepare a silicone mixture (Cosmosil, Principality Medical Limited, Western valley road, Rogerstone, Newport, Gwent, South Wales, UK) using a silicone elastomer base (45/99/A) and crosslinker (K004) and a catalyst (4D:K007).
9. Use two drops of crosslinker per gram of base and one drop of catalyst per gram of base.
10. Add small amounts of pigment to the mixture to give the prosthesis a flesh tone colour, based on the patients skin colour and remaining ear.
11. Smooth the silicone into the moulds in the dental flasks using a spachelor.
12. Close and seal the dental flask.
13. Place the dental flask in a dental vice and apply two bars of pressure to the flask for 5 hours.

14. Remove each prosthesis from its flask using tools if necessary to pry it loose.

15. Remove the flash from each prosthesis using a pair of scissors and scalpel. Care must be taken not to mark the surface of the prosthesis, as this removes the shine and smooth surface.
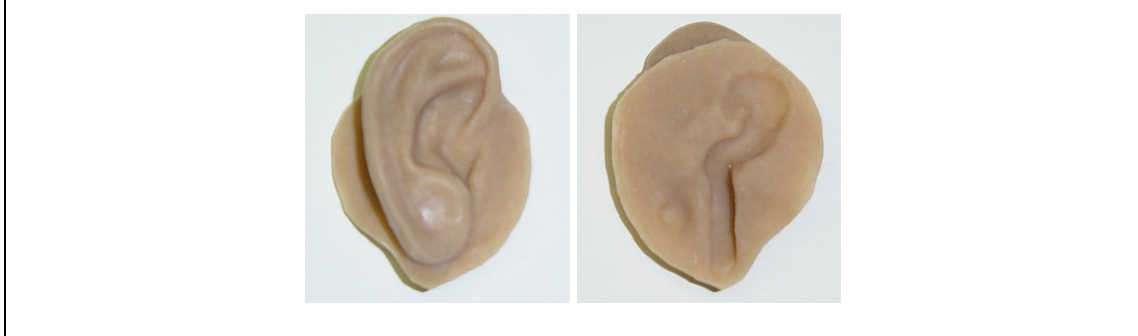
Figure 4-48: The traditionally made ear prosthesis

Figure 4-49: The digital process ear prosthesis

16. Figure 4-48 and Figure 4-49 show the hand carved and digital prosthesis respectively.

Evaluation of the Prostheses

The two prostheses are evaluated using a survey. The survey asks the respondents to compare each ear prosthesis to the master model of the patients ear. The respondent rates each prosthesis using five questions and an ordinal scale from 1 to 5 where 1 is excellent and 5 is poor.

The five questions on the survey are:

1. Shape
2. Anatomy
3. Size
4. Aesthetic appeal
5. Similarity to the cast model.

<u>Survey method</u>

1. Do not initially tell each respondent about the processes evaluated in the research.
2. Explain to each respondent that they must compare two prostheses to a cast model of an ear.
3. Refer to the traditionally made prosthesis as "prosthesis A".
4. Refer to the digitally made prosthesis as "prosthesis B"
5. Refer to the master model of the ear as "model C".
6. Hand a respondent prosthesis A and model C.
7. Ask the respondent to rate the shape of prosthesis A to the shape of model C on a scale from 1 to 5 where 1 is poor and 5 is excellent.
8. Repeat step 3 for the questions of anatomy, size, aesthetic appeal and similarity to model C.
9. Hand the patient prosthesis B and repeat steps 3 and 4, by comparing prosthesis B to model C.
10. Ask the respondent if he/she has any comments about the two prostheses they looked at.

4.7.4 Prosthesis duplication

The following case study deals with the duplication of an oral prosthesis. The case study uses both the traditional and digital methods of prosthesis duplication.
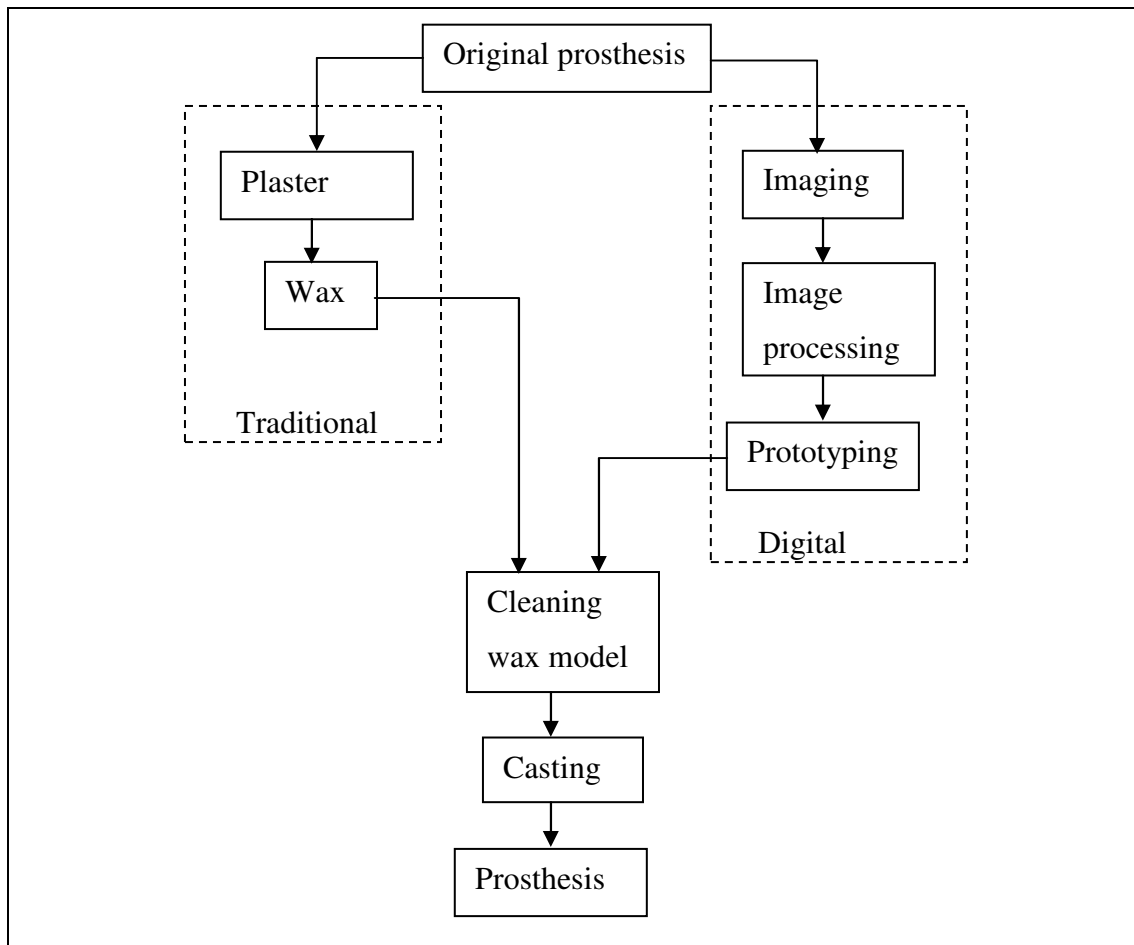
Figure 4-50: Prosthesis duplication method

Figure 4-50 shows a flowchart of both the traditional and digital methods of prosthesis duplication. The steps that differ are illustrated in the traditional and digital boxes respectively.

Traditional Method

The following steps outline the method for traditional prosthesis duplication.

1. Heat dental wax in a suitable metal or ceramic container.
2. Mix Coltene Lab Putty and a catalyst (Coltene AG, Feldwiesenstrasse 20, CH-9450, Altstatten, Switzerland) together in a ratio of 1 measure of catalyst to 2 scoops of putty.
3. Mould the mixture onto the underside of the oral prosthesis.
4. Mix an alginate mixture (Dentsply, Detrey Gmbh D-78467, Konstan Z), using a ratio of 1 part alginate to 1.5 parts water.

5. Pour the mixture over the top of the putty and the oral prosthesis.

6. Remove the two parts to the impression after 5 minutes and wrap a damp paper towel around the impression.

7. Place the impression on a working surface and pour the heated wax into the impression.

8. Leave the wax to harden for 45 minutes.

9. Place the ceramic teeth in the wax prosthesis using heated dental tools.

10. Image the wax prosthesis using the Breuckmann Optotop and a raster point size of 0.2mm, use the method presented in sub-section 4.2.2.

Digital method

The following steps outline the method for digital prosthesis duplication.

1. Image the original prosthesis using the Breuckmann Optotop and a raster point size of 0.2mm, using the method presented in sub-section 4.2.2.

2. Locally and globally register the scans using Innovmetric Polyworks and the method presented in sub-section 4.3.2. Merge the file and export as an STL file type.

3. Open the STL file in Geomagic Studio.

4. Fill the holes using curvature based hole filling and the method presented in sub-section 4.4.1.

5. Export a new STL file for prototyping.

6. Review the STL file using the Thermojet Print Preview program.

7. Orient the model on the prototyping platform so that the supports are placed at the top of the oral prosthesis, indicated in Figure 4-51.

Wax supports
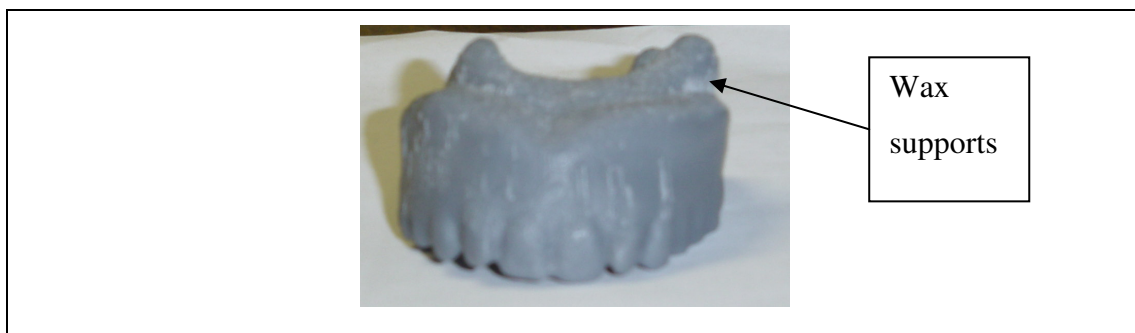
Figure 4-51: The prototyped oral prosthesis.

8. Image the wax oral prosthesis using the Breuckmann Optotop and a raster point size of 0.2mm. Use Innovmetric Polyworks and the method presented in sub-section 4.3.2 for image processing.

Casting of the acrylic oral prostheses

The following steps relate to both the traditional and digital methods and investment casts both of the wax prostheses into acrylic.

1. Prepare a plaster mixture using the method presented in section 4.6.
2. Pour plaster mixture into two dental flask bases.
3. Place each wax prosthesis in the plaster mixture in the dental flask bases and set for 45 minutes.
4. Place the flask tops on the flask bases, using the pins for alignment.
5. Pour in the remaining plaster mixture into each flask.
6. Place the lid on each dental flask.
7. Place each dental flask in a dental vice with three bars of pressure for 15 minutes.
8. Remove each dental flask from the vice and place both in a heated water bath for 10 minutes.
9. Remove the dental flask and use sharp tools to remove the wax remnants, leaving the ceramic teeth in place.
10. Pour dental acrylic mixture into each of the plaster moulds and place the flasks into a dental vice under three bars of pressure and allow to set for 24 hours.
11. Open the flask and remove the duplicated oral prostheses with the mounted ceramic teeth.

Oral prosthesis evaluation

Evaluate the traditional digital oral prostheses in the following manner.

1. Start Geomagic Qualify.
2. Import the models of the original, traditional and digital oral prostheses.
3. Set the original oral prosthesis as a reference model, this model is called "original".

4. Set the traditionally made oral prosthesis as a test model. This model is called a "traditional prosthesis".

5. Compare the original and traditionally made prostheses and create a colour error map.

6. Set the digital prosthesis as the test model and compare it to the original prosthesis. Create a colour error map of this comparison.

7. Set the digital prosthesis as the reference model and the traditional prosthesis as the test model and compare them. Create a colour error map of this comparison.

8. Table 4-2 illustrates the reference and test models for the comparison.

Table 4-2: Reference and test models

Reference	Test
Original	Traditional prosthesis
Original	Digital prosthesis
Digital prosthesis	Traditional prosthesis

With the apparatus and methods explained the results of the investigation are next given in chapter 5.

Chapter

5   **Results**

Chapter 5 presents the results of the investigation using the methods presented in chapter 4. Section 5.1 illustrates the digital process based on the generic process of reverse engineering illustrated in Figure 2-1. Section 5.2 displays the results of five case studies using the method presented in section 4.7.

5.1 Digital Process

Section 5.1 presents the overall digital process used in this investigation. The digital process consists of all steps for the generic reverse engineering process illustrated in Figure 2-1. Sub-section 5.1.1 presents estimated capital costs for the digital process. Section 5.2 presents the process evaluation results which consists of four case studies. The first case study using anatomical models (sub-section 5.2.1) follows only two steps in the digital process, namely imaging and image processing. The remaining three case studies (implant design in sub-section 5.2.2, prosthesis design in sub-section 5.2.3 and prosthesis duplication in sub-section 5.2.4) follow the full process illustrated in Figure 5-1.
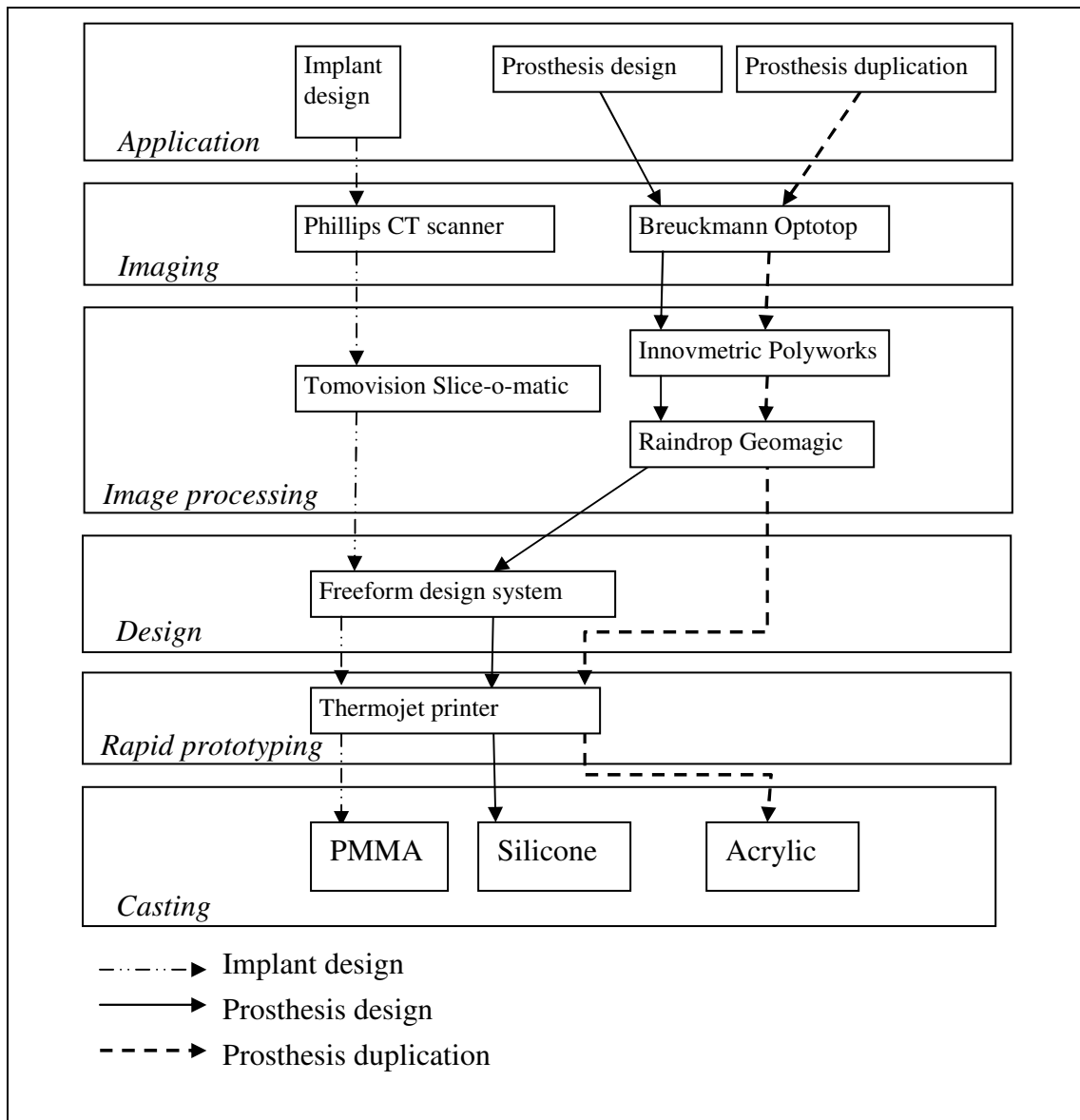
Figure 5-1: The digital process

Figure 5-1 shows the digital process steps for use in three applications, namely: implant design, prosthesis design and prosthesis duplication. The process utilises different apparatus for the three different case studies.

Imaging consists of the Breuckmann Optotop for prosthesis design and duplication, and a Phillips CT scanner for implant design. Image processing for prosthesis design and duplication requires both Innovmetric Polyworks and Raindrop Geomagic. Implant design, and in particular any study using internal medical imaging requires Tomovision slice-o-matic.

The design and editing step uses the Freeform system and the Phantom haptic device for both implant and prosthesis design. A Thermojet printer is used for all case studies and provides a wax model suitable for investment casting.

5.1.1 Digital process cost

The digital process has several costs associated with the purchase and running of equipment and software. The costs vary depending on the application selected in Figure 5-1. Because of different locations, accounting conventions and the age of some equipment, comparable costs are difficult to obtain. Cost estimations a provide an indication of the capital expenditure required. The Equipment and software costs are estimated in Table 5-1 and are assumed to be a commercial licence and correct to within 25% of the cost illustrated. Table 5-1 illustrates the capital, operator and running costs. The capital cost of equipment is estimated in rands (R). The operator and running costs are comparative with the assumption that a medical operator is significantly more expensive than an industrial operator. The running costs depend on the work environment and whether additional hardware is required, such as a compressed air supply for a Renishaw Cyclone.

Table 5-1: Estimated capital cost

Description	Capital cost	Operator cost	Running cost
Renishaw Cyclone	R500 000	Medium[1]	Medium
Breuckmann Optotop	R500 000	Medium	Low
Phillips CT	R5 million	High	High
Innovmetric Polyworks	R200 000	Medium	Low
Raindrop Geomagic	R200 000	Medium	Low
Freeform	R250 000	Medium	Medium
Thermojet Printer	R500 000	Medium	High

(1) R300 p/h

The Breuckmann and Renishaw systems are cheaper than a CT scanner in the three cost divisions. CT scanning requires a team of radiologists, and requires scheduled maintenance. It is assumed that an industrial or medical lab technician can be trained to use the Breuckmann Optotop and Renishaw Cyclone. The running costs of the Breuckmann Optotop is lower than that of the Renishaw Cyclone as it does not need the additional air supply, and the projector lamp is illuminated for a few seconds during the digitising process.

Freeform has a higher running cost than Innovmetric Polyworks and Raindrop Geomagic as it requires high end computing recourses. The Freeform system also has physical equipment expenditure in terms of the Phantom. The Thermojet Printer running costs are high due to proprietary material costs.

5.2 Process evaluation

The digital process is evaluated using case studies and both the traditional and digital process methods. The digital process is evaluated using the four quality evaluation factors presented in Table 2-4. The evaluation factors are: accuracy, aesthetics, cost and speed.

5.2.1 Anatomical models

Sub-section 5.2.1 provides the results of the anatomical models case study using the evaluation criteria presented in Table 2-4. The evaluations include accuracy and speed factors.

The anatomical models use the image and image processing steps of the digital process. The anatomical models are scanned using the parameters presented Table 5-2, Table 5-3 and Table 5-4 for the Renishaw Cyclone, Breuckmann Optotop and Phillips CT scanner respectively.

Table 5-2: Renishaw Cyclone scanning parameters

Model	No. of scans	Probe type	Scanning speed [mm/min]	Step over [mm]	Nominal pitch [mm]
Ear 1	6	2mm ball probe	500	0.5	0.5
Ear 2	3	2mm ball probe	500	0.5	0.5
Nose 1	3	2mm ball probe	500	0.5	0.5
Teeth 1	5	1mm ball probe	300	0.5	0.5

Table 5-2 shows the Renishaw Cyclone scanning parameters. The models refer to the anatomical models presented in sub-section 4.7.1. A full digital model is acquired using the number of scans illustrated in column two, using the probe type and size

illustrated in the "probe type" column. Teeth 1 use the smallest probe size illustrated due to the fine detail present between the teeth. The digitising process uses the scanning speed, step over and nominal pitch parameters presented in the last three columns for each model.

Table 5-3: Breuckmann Optotop scanning parameters

Model	No. of scans	Base bar	Resolution [mm]	Number of intensities	Phase banding removal used
Ear 1	8	HF-160	0.5	4	Yes
Ear 2	12	HF-160	0.6	3	No
Nose 1	10	HF-160	0.6	3	Yes
Teeth 1	18	HF-80	0.4	3	Yes

Table 5-3 shows the Breuckmann Optotop scanning parameters when digitising the four anatomical models. Table 5-3 illustrates the number of scans used and base bar size to digitise each of the models. The resolution, number of intensities and whether or not phase banding removal is used is also illustrated. Teeth 1 use the smallest scanning volume (HF-80) and resolution due to the small features in between the teeth. Each model requires multiple lighting intensities for digitising, depending on environmental lighting conditions, and model colour. Using multiple lighting intensities reduces the number of holes in each model, as the best intensity is selected by the Optocat software.

Table 5-4: CT scanning parameters

Description	Unit	Value
Number of scans	number	109
Time per slice	seconds	2
Slice distance	millimetres	1
Image size	pixels	512 x 512
Pixel dimension	millimetres	0.8
Tube voltage	kilovolts	120
Tube current	milliamps	150
Exposure	milliamp seconds	300

Table 5-4 shows the CT scanning parameters for the anatomical models. The models are scanned simultaneously using the same parameters. The parameters include the overall number of scans, the time taken to obtain each slice and the slice distance. Other parameters relating to CT accuracy include the image size and pixel dimension.

Accuracy

The evaluation of accuracy results for the anatomical models are obtained by comparing them to one another using a combination of the Renishaw Cyclone,

Breuckmann Optotop and Phillips CT scanner, using both Innovmetric Polyworks and Raindrop Geomagic for image processing.

Table 5-5: Global registration results

Model	Scanner	Raindrop Geomagic		Innovmetric Polyworks	
		Average distance [mm]	Standard deviation [mm]	Average distance [mm]	Standard deviation [mm]
Ear 1	Renishaw	1.9×10^{-2}	2.7×10^{-2}	3×10^{-4}	5.8×10^{-2}
	Breuckmann	9×10^{-3}	1.5×10^{-2}	1.9×10^{-6}	2.3×10^{-3}
Ear 2	Renishaw	3.3×10^{-2}	3.4×10^{-2}	3.2×10^{-5}	2.4×10^{-2}
	Breuckmann	2.5×10^{-2}	2.1×10^{-2}	2.8×10^{-5}	1.4×10^{-3}
Nose 1	Renishaw	1.2×10^{-2}	1.2×10^{-2}	1.2×10^{-3}	4.3×10^{-2}
	Breuckmann	6×10^{-3}	1.2×10^{-2}	3.4×10^{-4}	6.2×10^{-3}
Teeth 1	Renishaw	1.4×10^{-2}	1.3×10^{-2}	8.15×10^{-4}	4.2×10^{-2}
	Breuckmann	3.8×10^{-2}	3.6×10^{-2}	4.2×10^{-5}	2.1×10^{-2}

Table 5-5 shows the global registration results using the Renishaw Cyclone and Breuckmann Optotop. The average distance is the average distance between each scan, and the standard deviation is the distribution about this average. Raindrop Geomagic provides an overall average and standard deviation, whilst Innovmetric Polyworks provides averages for each scan. For consistency, the arithmetic average of the mean errors are calculated for the average distance, and the maximum of the standard deviations are used for the Innovmetric Polyworks results.

The model comparison results using Geomagic Qualify are presented in Table 5-6 to Table 5-9 and show the deviations using hardware and software combinations for ear 1, ear 2, nose 1 and teeth 1. Each table consists of a reference section along the columns and a test section down the rows for the different combinations. Each cell consists of two values, the first is the average error and the second is the standard deviation. Measurements are relative to the reference model. Colour error maps for several comparisons are displayed in Appendix E.

Table 5-6: Comparison error of ear 1

Test	Reference	Breuckmann Optotop Innovmetric Polyworks	Renishaw Cyclone Innovmetric Polyworks	CT Scanning Tomovision
Breuckmann Optotop	Raindrop Geomagic	0.133mm 0.126mm	0.162mm 0.210mm	0.207mm 0.203mm
Breuckmann Optotop	Innovmetric Polyworks	N/A N/A	N/A N/A	0.154mm 0.157mm
Renishaw Cyclone	Raindrop Geomagic	0.269mm 0.189mm	0.259mm 0.190mm	0.292mm 0.295mm
Renishaw Cyclone	Innovmetric Polyworks	0.798mm 0.647mm	N/A N/A	0.197mm 0.332mm

Table 5-7: Comparison error of ear 2

Test	Reference	Breuckmann Optotop Innovmetric Polyworks	Renishaw Cyclone Innovmetric Polyworks	CT Scanning Tomovision
Breuckmann Optotop	Raindrop Geomagic	0.247mm 0.174mm	0.240mm 0.275mm	0.340mm 0.214mm
Breuckmann Optotop	Innovmetric Polyworks	N/A N/A	N/A N/A	0.242mm 0.178mm
Renishaw Cyclone	Raindrop Geomagic	0.093mm 0.157mm	0.056mm 0.078mm	0.160mm 0.170mm
Renishaw Cyclone	Innovmetric Polyworks	0.049mm 0.082mm	N/A N/A	0.219mm 0.149mm

Table 5-8: Comparison error of teeth 1

Test	Reference	Breuckmann Optotop Innovmetric Polyworks	Renishaw Cyclone Innovmetric Polyworks	CT Scanning Tomovision
Breuckmann Optotop	Raindrop Geomagic	0.095mm 0.067mm	0.119mm 0.086mm	0.417mm 0.349mm
Breuckmann Optotop	Innovmetric Polyworks	N/A N/A	N/A N/A	0.652mm 0.456mm
Renishaw Cyclone	Raindrop Geomagic	0.093mm 0.095mm	0.066mm 0.073mm	0.201mm 0.165mm
Renishaw Cyclone	Innovmetric Polyworks	0.049mm 0.049mm	N/A N/A	0.272mm 0.191mm

Table 5-9: Comparison error of nose 1

Test	Reference	Breuckmann Optotop Innovmetric Polyworks	Renishaw Cyclone Innovmetric Polyworks	CT Scanning Tomovision
Breuckmann Optotop	Raindrop Geomagic	0.164mm 0.131mm	0.057mm 0.118mm	0.216mm 0.302mm
Renishaw Cyclone	Innovmetric Polyworks	N/A N/A	N/A N/A	0.251mm 0.267mm
Renishaw Cyclone	Raindrop Geomagic	0.084mm 0.151mm	0.040mm 0.056mm	0.104mm 0.293mm
Renishaw Cyclone	Innovmetric Polyworks	0.049mm 0.049mm	N/A N/A	0.361mm 0.304mm

The average values and maximum standard deviations for all models are calculated and displayed in Table 5-10 .

Table 5-10:Average deviations

Test	Reference	Breuckmann Optotop Innovmetric Polyworks	Renishaw Cyclone Innovmetric Polyworks	CT Scanning Tomovision
Breuckmann Optotop	Raindrop Geomagic	0.160mm 0.125mm	0.145mm 0.172mm	0.295mm 0.267mm
Breuckmann Optotop	Innovmetric Polyworks	N/A N/A	N/A N/A	0.325mm 0.265mm
Renishaw Cyclone	Raindrop Geomagic	0.135mm 0.148mm	0.105mm 0.099mm	0.189mm 0.231mm
Renishaw Cyclone	Innovmetric Polyworks	0.236mm 0.207mm	N/A N/A	0.262mm 0.244mm

Table 5-10 shows the overall registration accuracy of the imaging systems. The average and standard deviation are presented in the same manner as Table 5-6 to Table 5-9. The smallest deviation between models is 0.105±0.099mm using the Renishaw cyclone with Innovmetric Polyworks and Raindrop Geomagic for image processing. The largest deviation is 0.325±0.265mm, between the Phillips CT scanner and the Breuckmann Optotop using Innovmetric Polyworks for image processing.

Initially, a known and calibrated part was sought for comparing scanning systems, but this is not possible for the following reasons:

1.   A great deal of scattering (X-rays reflect off some particles) occurs if a metal calibration piece is placed in a CT scanner.
2.   A calibrated piece has a polished surface creates glare when scanning with the Breuckmann Optotop.

For these reasons, the following uncertainties per scanning system are calculated in Table 5-11 using the manufacturer's specifications, maximum registration uncertainty and average deviation from Table 5-10.

Table 5-11: Expected scanner uncertainty

System	Average scanner uncertainty
Renishaw Cyclone	0.16±0.20mm
Breuckmann Optotop	0.19±0.20mm
Phillips CT	1.25±0.27mm

Table 5-11 gives the expected uncertainty for each scanner for objects approximately the same size as the anatomical models. The largest system uncertainty is the CT scanner with an uncertainty of 1.25±0.27mm including a slice distance of 1mm.

Speed

The speed of the three imaging systems are evaluated using the average time taken to digitise all four anatomical models. The average scanning time is illustrated in Table 5-12. The Phillips CT scanner is capable of digitising multiple models and gives it a fast digitising speed. The Renishaw Cyclone's speed is affected by the scanning parameters illustrated in Table 5-2, and in particular the scanning speed parameter and the scanning area. The times illustrated in Table 5-12 include the image processing for the Renishaw Cyclone and Breuckmann Optotop, from registration to merging into the STL format, and both scanning and conversion to STL for the Philips CT scanner.

Table 5-12: Speed comparison of 3 scanning methods and software combinations

Description	Ear 1	Ear 2	Nose 1	Teeth 1	Average time
Renishaw Cyclone and Raindrop Geomagic	655 min	265 min	230 min	1020min	542 min
Renishaw Cyclone and Innovmetric Polyworks	665 min	265 min	220min	1000 min	537.5 min
Breuckmann Optotop and Raindrop Geomagic	80 min	105 min	100 min	80 min	91.25 min
Breuckmann Optotop and Innovmetric Polyworks	30 min	50 min	40 min	55 min	43.75 min
Phillips CT	40 min	40 min	40 min	40 min	40 min

In Table 5-12 the scanning time for the models is approximated to the nearest 5 minutes. The average time for the Breuckmann Optotop, using Innovmetric Polyworks and the Phillips CT scanner is very close at 40 and 43 minutes respectively. Using Raindrop Geomagic with the Breuckmann Optotop doubles the processing time. The Renishaw Cyclone's speed can be increased but adversely affects data accuracy.

5.2.2 Implant design

The cranioplasty results using the method presented in sub-section 4.7.2 are presented in this sub-section. The results include the evaluation factors of accuracy, speed and cost.

<u>**Accuracy**</u>

The accuracy of the cranioplasty case study is determined by comparing the CT scan of the cranium to a Breuckmann Optotop scan of the cranium using Raindrop Geomagic Qualify. The deviation of the CT scan is 0.73±0.87mm from the Breuckmann Optotop scan. For a conservative estimate on the expected uncertainty of the implant, this is added to the CT scan system error presented in Table 5-11 this gives a total deviation in the CT scan data of 1.98±1.14mm. There is some deviation in the physical PMMA implant when placed in the cranium creating a rocking motion. The deviation is removed using a dental burr.

Aesthetics

The aesthetic feature of a cranial implant is the external curvature, which if incorrect, can show disfigurement in a patient. The surface curvature is generated in Freeform by mirroring the non-defective portion of skull to create a symmetrical implant. The mirroring and use of symmetry increases the aesthetic result of the design.

Cost and speed

The estimated cost and time for a digital cranioplasty application are illustrated in Table 5-13. The running costs are indicated and exclude the capital costs displayed in Table 5-1. Some costs are dependant on time, and as such the estimated duration is included.

Table 5-13: Cranioplasty cost estimation

Digital process	Description	Cost	Duration
Imaging	Phillips CT scanner	R1000	40 minutes
Image processing	Tomovision	R100	20 minutes (R300 p/h)
Design	Freeform	R600	2 hours (R300 p/h)
Prototyping	Thermojet printer	R300	3 hours
Casting	Casting labour	R150	30 minutes (R300 p/h)
	Casting materials	R100	
	PMMA material	R200	
TOTAL		R2450	6 hours 30 minutes

5.2.3 Prosthesis design

The results of the prosthesis design case study are illustrated here. The results include the evaluation criteria of: accuracy, aesthetics, cost and speed.

Accuracy

The accuracy of the two ear prostheses is determined by a discussion of the anatomical features of each prosthesis and the available quantitative information. The registration accuracy using Innovmetric Polyworks is presented in Table 5-14.

Table 5-14: Prosthesis design case study registration accuracy

Model	Registration Type	Average distance	Standard deviation
Ear	N-Point	1.8×10^{-6} mm	2.23×10^{-2} mm

The globally registered digital model of the remaining ear is illustrated in Figure 5-2
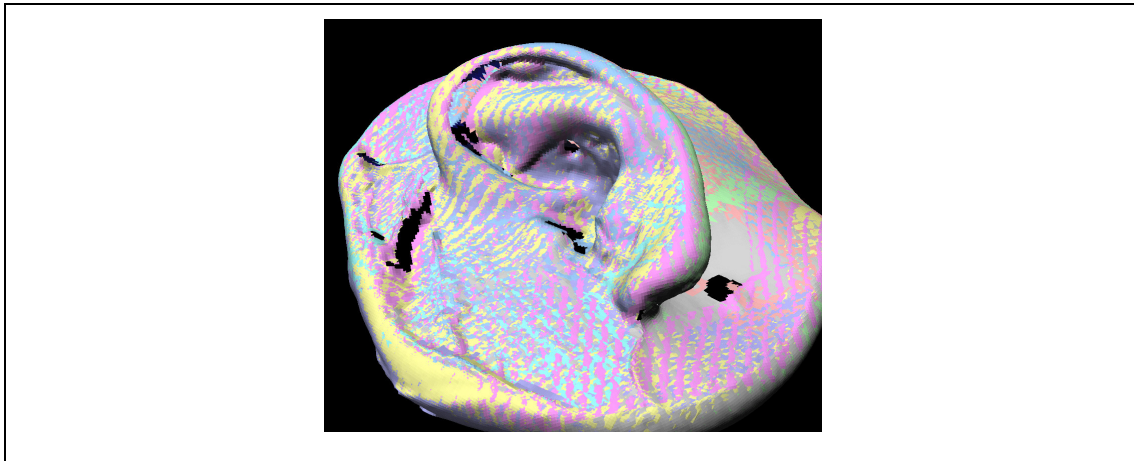
Figure 5-2: The globally registered ear prosthesis

The anatomical comparison sites are illustrated in Figure 5-3, along with both the digitally and traditionally made ear prostheses.

Casting   Digital   Traditional
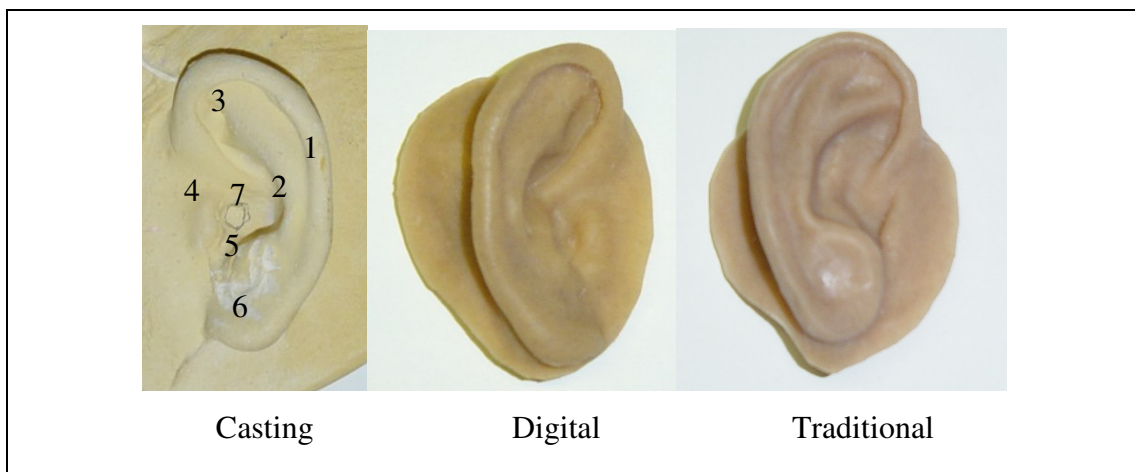
Figure 5-3: Anatomical comparison sites

The anatomical comparison sites are base on those discussed in literature in Figure 2-29. The helix (1) is similar in both prostheses, but the digital prosthesis has a smaller undercut underneath the helix. The helix of the traditional prosthesis is square in shape, compared to the round helix of the digital prosthesis. The antihelix (2) is smaller in the digital prosthesis and accentuated in the traditional prosthesis. The triangular fossa (3) in the traditional prosthesis is accentuated and follows a different path. The tragus (4) looks more accentuated in the traditional prosthesis, whilst the digital prosthesis has less definition, but this is similar to the cast model. The antitragus (5) meets with the base of the ear irregularly in the traditional prosthesis.

The lobule (6), joins at the base of the ear differently in the traditional prosthesis, and has a vertical curvature as it moves into the helix. The external acoustic meatus (7) looks more accurate in the traditional prosthesis, as the scanner is unable to digitise this area fully.

Aesthetics

The aesthetics of each prosthesis are judged using the survey results and the evaluation method described in sub-section 4.7.3. In the survey, respondents are asked to judge and compare the two ear prostheses to a cast model of the remaining ear.

The prostheses are judged using ordinal ratings from 1 to 5 where "1" is "excellent" and "5" is "poor" on: shape, anatomy, size, aesthetics and resemblance to model C. The χ^2, discussed in section 2.9, is used to determine whether a significant difference in respondents opinion exists between the two prostheses. The overall results of the survey for prosthesis A (traditional method) are presented in Figure 5-4.
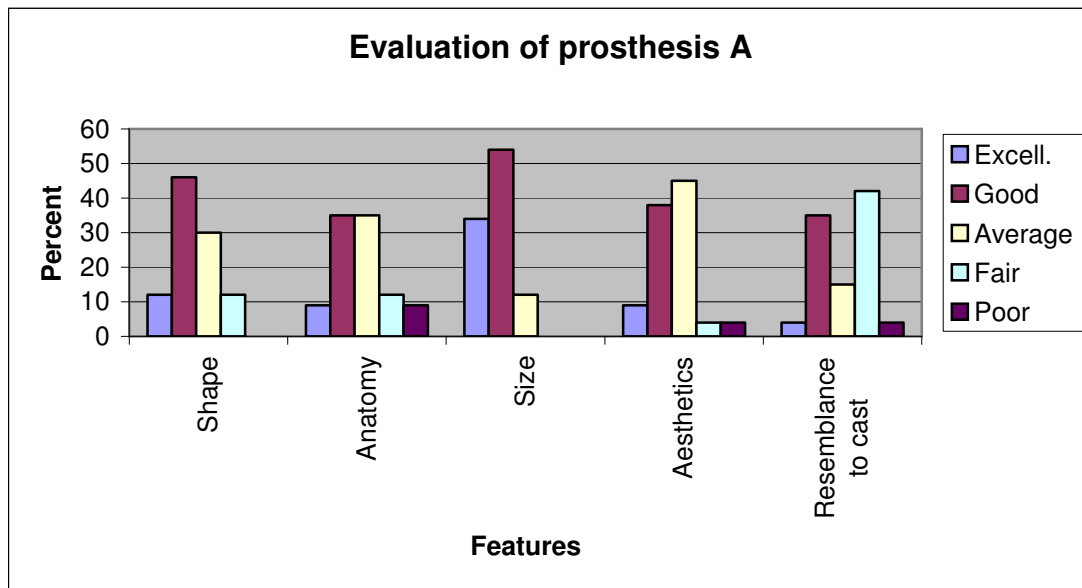
Figure 5-4: Evaluation of prosthesis A

The overall results of the survey for prosthesis B (digital method) are presented in Figure 5-5.
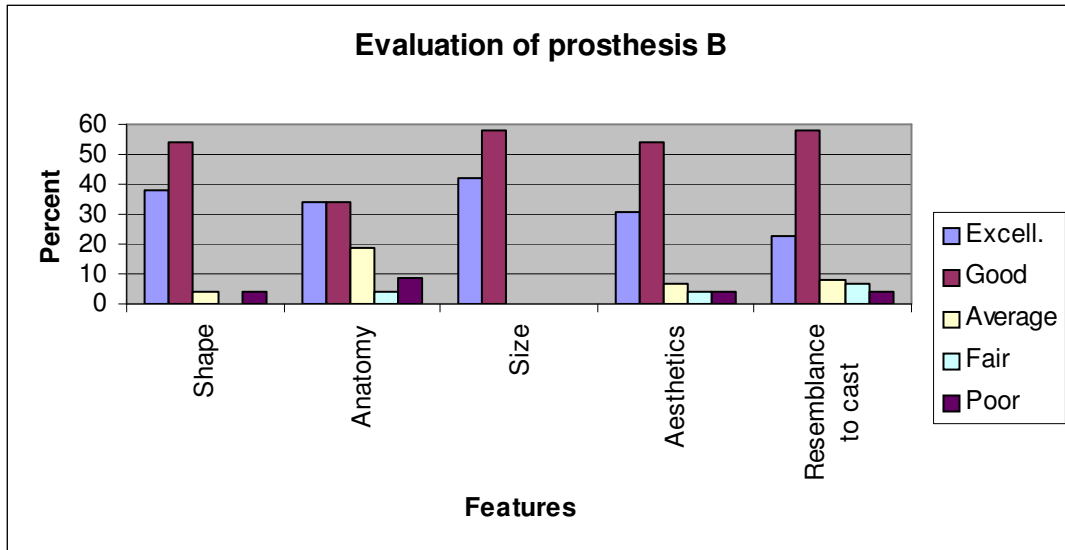
Figure 5-5: Evaluation of prosthesis B

The statistical analysis uses a level of significance of α=0.05. There is a significant difference of opinion for both shape and aesthetic appeal. There is no significant difference of opinion for the other factors with α = 0.05. The calculations for the χ^2 test and unprocessed results of the survey are presented in Appendix C.

Eleven or 42% of respondents rate prosthesis A (traditional) as fair to poor, compared to two or 8% of respondents for prosthesis B (digital) in terms of shape. Fourteen or 54% of respondents rate prosthesis A as fair to poor, compared to four or 15% for prosthesis B in terms of aesthetic appeal.

Figure 5-6 shows the percentage of respondents that chose a particular rating for all of the comparison factors combined. Figure 5-6 shows a greater number of respondents selecting "Excellent" for prosthesis B (digital) and a greater number of respondents using "Fair" to "Average" for prosthesis A (traditional).
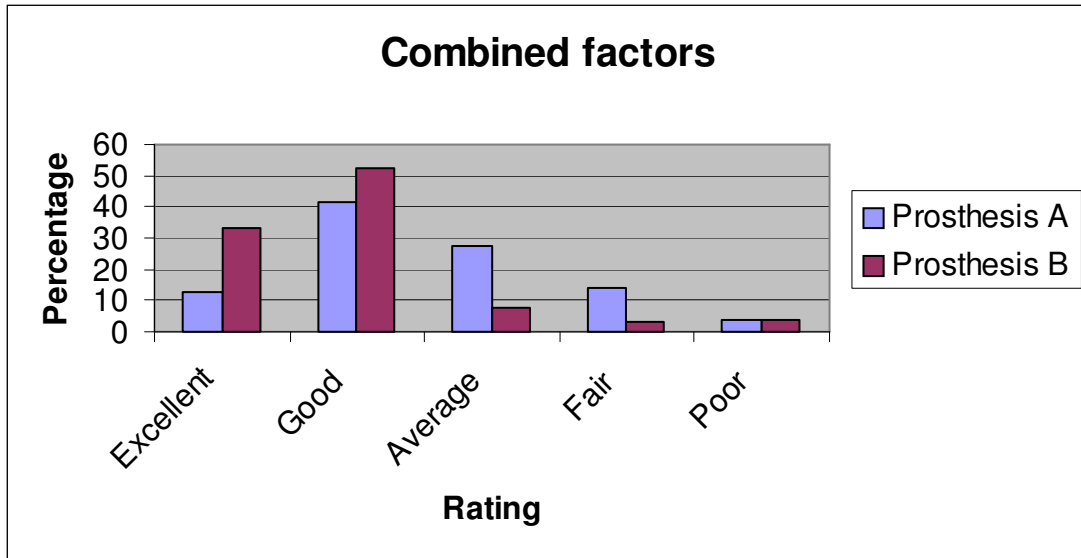
Figure 5-6: Combined factors response for the survey

Cost and speed

The cost and speed results for prosthesis design are grouped together because of the time-cost relationship with hourly rates. Table 5-15 illustrates the costs and associated times using the traditional method of prosthesis design. The times are all estimated to the nearest 5 minutes, with the wax carving having an assumption that no breaks are taken, and carving is continuous.

Table 5-15: Traditional prosthesis design cost estimation

Process	Description	Cost	Duration
Carving			
	Carving a wax prosthesis	R1800	6 hours (R300p/h)
Casting			
	Casting labour	R150	30 minutes (R300 p/h)
	Casting materials	R100	
	Silicone	R200	
TOTAL		**R2250**	**6 hr 30 minutes**

Table 5-16 illustrates the times and associated costs for prosthesis design using the digital method. The times are estimated to the nearest five minutes.

144

Table 5-16: Digital prosthesis design cost estimation

Process	Description	Cost	Duration
Imaging	Breuckmann Optotop	R200	40 minutes (R300 p/h)
Image processing	Innovmetric Polyworks	R125	25 minutes (R300 p/h)
Design	Raindrop Geomagic	R200	40 minutes (R300 p/h)
	Freeform design	R225	45 minutes (R300 p/h)
Prototyping	Thermojet printing	R300	2 hours 40 minutes
	Prototype cleaning	R100	20 minutes (R300p/h)
Casting			
	Wax model adjustments	R150	30 minutes (R300 p/h)
	Casting labour	R150	30 minutes (R300 p/h)
	Casting materials	R100	
	Silicone	R200	
TOTAL		**R1750**	**6hr 00 minutes**

5.2.4 Prosthesis duplication

The results of the prosthesis duplication case are presented in this section. The prosthesis duplication is evaluated on accuracy, cost and speed and is compared to the traditional process. The original prosthesis is the original acrylic prosthesis, the traditional prosthesis is the prosthesis duplicated using traditional methods and the digital prosthesis is the duplicated prosthesis made using the digital process.

<u>Accuracy</u>

The accuracy of the oral prostheses are determined by imaging the wax models using the Breuckmann Optotop and comparing this to the model of the original acrylic prosthesis. The imaging parameters for the Breuckmann Optotop are displayed in Table 5-17.

Table 5-17: Breuckmann Optotop parameters

Prosthesis	Base bar	Feature size	No. of intensities	Scan time [Min]
Original	HF-160	0.5	3	45
Traditional	HF-160	0.4	4	25
Digital	HF-160	0.4	4	25

Table 5-18: Global registration error

Prosthesis	No. of scans	Software	Mean error [mm]	Standard deviation[mm]
Original	19	Polyworks	7.5×10^{-5}	4.4×10^{-2}
Traditional	11	Polyworks	1.50×10^{-5}	4.32×10^{-2}
Digital	6	Polywork	3.34×10^{-4}	3.35×10^{-2}

Table 5-18 illustrates the average global registration error for each model and shows both the mean error and maximum standard deviation. The number of scans for the original and traditional prosthesis in Table 5-18 is greater than the digital method as both the acrylic (original prosthesis) and dental wax (traditional method) have a high reflectivity, compared to the grey wax from a Thermojet Printer.

Table 5-19 illustrates the deviations between the prostheses, the deviations are between the original prosthesis and the wax models for the duplication.

Table 5-19: Error between the duplicated prostheses

Reference	Test	Max error [mm]	Average error [mm]	Standard deviation [mm]
Original	Traditional	2.70	0.54	0.48
Original	Digital	2.57	0.33	0.36
Digital	Traditional	2.71	0.47	0.47

The comparisons in Table 5-19 are made using Raindrop Geomagic Qualify. The test measurements are relative to the reference model in each case. The greatest deviation is between the digital and traditional prostheses.
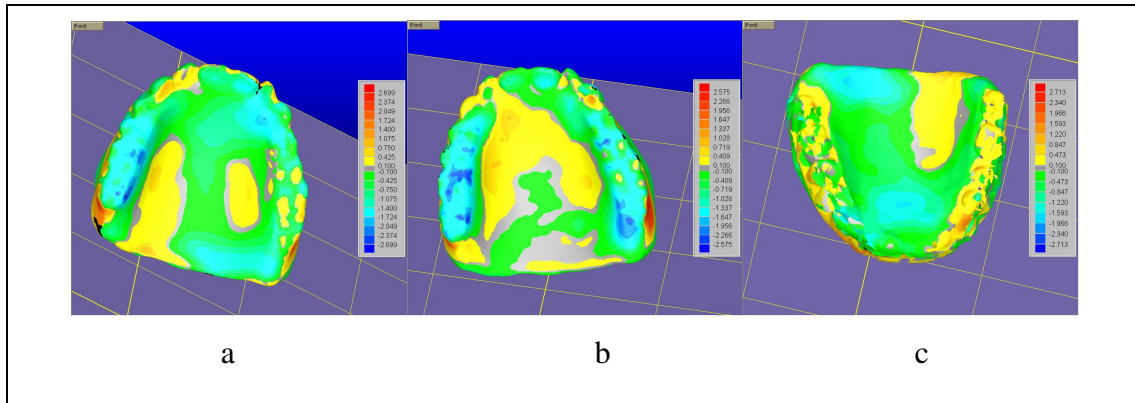
Figure 5-7: Duplicated prostheses colour error map

Figure 5-7a shows the traditional prosthesis compared to the original prosthesis. Figure 5-7b shows the digital prosthesis compared to the original prosthesis. Figure 5-7c shows the traditional prosthesis compared to the digital prosthesis.

Cost and speed

Table 5-20 and Table 5-21 show the estimated costs and time for the traditional and digital prosthesis duplication methods respectively.

Table 5-20: Cost estimation of traditional prosthesis duplication

Item	Cost	Duration
Impression of original prosthesis		
Impression labour	R150	30 minutes (R300p/h)
Impression materials	R100	
Casting		
Casting labour	R150	30 minutes (R300 p/h)
Casting materials	R100	
Acrylic	R200	
TOTAL	**R700**	**1 hr**

Table 5-21: Cost estimation of digital prosthesis duplication

Process	Description	Cost	Duration
Imaging	Breuckmann Optotop	R225	45 minutes (R300 p/h)
Image processing	Innovmetric Polyworks	R125	25 minutes (R300 p/h)
	Raindrop Geomagic	R200	40 minutes (R300 p/h)
Prototyping	Thermojet printing	R400	4 hours 20 minutes
	Prototype cleaning	R100	20 minutes (R300p/h)
Casting	Casting labour	R150	30 minutes (R300 p/h)
	Casting materials	R100	
	Acrylic	R200	
TOTAL		**R1500**	**6hr 55 minutes**

Table 5-20 shows the cost of duplicating prostheses traditionally is over half that of using digital methods. A large cost in digital prosthesis duplication is the prototyping costs which are R500 in total or 1/3 of the overall cost.

Discussion

Chapter 6 discusses the results presented in chapter 5 with respect to the objectives of the investigation presented in section 1.5. Section 6.1 discusses the digital process in general, following the steps of the generic reverse engineering process. Section 6.2 discusses the process evaluation, following the evaluation criteria of accuracy, aesthetics, cost and speed.

6.1 The digital process

The digital process follows all of the steps presented by Cooper (2001, pp. 166-167) and includes: imaging, image processing, design, rapid prototyping and casting. The digital process provides a digital solution for implant and prosthesis design and prosthesis duplication.

6.1.1 Imaging

CT scanning is traditionally selected when using RP for medical applications, (D'urso *et al,* 2000, pp. 200-204), (Petzold, Zeilhofer and Kalender, 1999, p. 277), (Winder *et al*, 1999), (Sailer *et al,* 1998) and (Mankovich *et al*, 1994) and this investigation uses three scanning methods. CT scanning provides the ability for internal imaging, a requirement for any implant study, but is not for external studies such as prosthetics.

The Renishaw Cyclone is an accurate scanning system by manufacturer's specifications and the results of the investigation, but lacks on speed. The Cyclone's discrete method of scanning, where only one data point is obtained per time interval, is the primary factor in its slow speed. The high accuracy of the Renishaw Cyclone is expected from its metrology applications in the automotive and aerospace industries. The scanning speed can be increased, but the geometric complexity of the anatomical models makes the overall time decrease minimal in this project. The Renishaw

Cyclone data is not designed for ICPM registration, due to the sparseness of the point clouds. Dense point clouds can be generated, but at the expense of time. The registration problem is overcome by resampling the point cloud in Innovmetric Polyworks. The Renishaw Cyclone can use an indexing system, but anatomical models require multiple axis rotation making this method impractical. Model orientations pose a problem on the Renishaw, especially in the case of anatomical models, such as the ear. A lot of time is spent orientating the model, and if a mistake is made it is costly by lost time. The selection of probe geometries is not critical, and the ball shaped probes used in the investigation proved easier to use, as the assumption is made that no undercut is digitised. The Renishaw Cyclone, although capable of digitising medical models proves tedious for applications where low accuracy (less than 0.5mm) is required.

The Breuckmann Optotop offers high resolution, accuracy and speed when scanning. The Breuckmann generates a denser point cloud, in the hundreds of thousands to millions of points, compared to the Renishaw in the tens of thousands. The Breuckmann Optotop is mounted on a tripod, making the system portable, this is useful for scanning a feature directly from the patient if the need arises.

The Breuckmann System is suited for contour matching of scans using the ICPM algorithm. The base bar size does not affect scanning speed, which is an advantage for customised anatomy. If a larger scan volume is selected, thus preventing the need for calibration, it is more difficult to ensure that one can see the entire scan area with both the projected light and the camera. Visualisation is sometimes difficult with models such as the ear with high curvature when using a large scanning volume. The selection of the 153 x 113 x 100mm (HF-160) scanning volume is sufficient in decreasing the required number of scans, whilst digitising most of the models. This is evident with Teeth 1 requiring 18 scans compared to Ear 2 requiring 12 scans in sub-section 5.2.1. The phase error issue with the Breuckmann is not critical and the ripples are small and less than 20µm in size. The downstream design and manufacture applications such as Freeform and the Thermojet Printer smooth the surface, removing this error being lower resolution systems.

The slice distance of the CT scanner is a limiting factor in accuracy using CT scanning. Newer CT scanners have a slice distance as small as 0.5mm, this may cause harm to a patient due to increased X-ray dosage. It is also difficult to justify the need for a CT scan for an external prosthesis if the same result may be obtained using industrial scanning. The use of a 1mm slice distance prolongs X-ray tube life, compared to shorter slice distances and hence reduces cost. A major advantage of CT scanning over the other scanners is the ability to scan multiple models, without affecting time and hence speed.

6.1.2 Image processing

Image processing software provides an interface between scanning and downstream applications such as design. Both Innovmetric Polyworks and Raindrop Geomagic Studio are used in the digital process, both with different advantages.

Innovmetric Polyworks offers the user a high level of control for all aspects of image processing, requiring longer time and training requirements. The ability to have full control in image registration is an advantage, as scans with little overlap can be registered accurately and quickly. The sparse data from the Renishaw Cyclone isn't easily registered and requires additional import routines. The dense Breuckmann Optotop data is easily imported and visual sampling is offered. Visual sampling reduces the number of points displayed on a screen, and does not physically reduce the number of points. This makes image processing faster and in real time. Editing in Innovmetric Polyworks is a complicated process involving manipulation of control points, and requires more time to create an aesthetic result in hole filling. The editing with control points is similar to that in traditional CAD packages with NURBS surfaces.

Raindrop Geomagic does not offer control over all image processing parameters and is easier to use. This lack of parameter control means that several attempts are often required for local registration. It is faster than Innovmetric Polyworks in registering Renishaw Cyclone data and the default settings perform satisfactory in this regard. Raindrop Geomagic is slow when importing the Breuckmann data and no visual

sampling method is offered, making manipulation of data during registration tedious and physical point sampling is required. This speed difference with Polyworks is evident in the average scanning times using the Breuckmann Optotop and Raindrop Geomagic with an average time of 91 minutes compared to using Innovmetric Polyworks with an average time of 43 minutes. Only 1 and 3-point registration options are available in Raindrop Geomagic, and this requires that the points are placed in very close proximity to being correct.

Geomagic offers both flat and curvature based hole filling. A difference between these two methods is that curvature based hole filling makes adjustments to the border of the hole to blend in with the surrounding curvature. This technique may cause data to bulge in large holes and create lumps. This problem is solved using the partial hole filling technique, whereby the user selects two points along the boundary of the hole and fills in one side of the hole. The flat based hole filling does not alter the hole border, and will generally satisfy the criteria of closing the shortest distance around the edges.

The "point and click" approach to hole filling in Geomagic is quicker when a data set contains many sub-millimetre size holes. It was found that if scanning digitised most of the object, the need for filling large holes is eliminated making Raindrop Geomagic a faster method of editing. The digital ear from the prosthesis design case study has a polygonal surface area of $15902mm^2$ after merging and a polygonal area of $16739mm^2$ after hole filling, this means that approximately 94% of the model surface is digitised, and only 6% consists of holes.

Both Innovmetric Polyworks and Raindrop Geomagic are purchased in modules, so the use of Innovmetric Polyworks for image registration, and Raindrop Geomagic for editing is possible. This split increases the capital cost somewhat but provides the user with the benefits of each software package.

Tomovision provides a method of converting from DICOM to STL rapidly. The 3D segmenting technique where the mask propagates through all of the scans increases the working speed. Generating an STL mesh from segmented data is relatively simple, and no STL file problems occurred in design software. CT conversion software such

as Tomovision offer many unnecessary functions that are not required in this investigation. The software cost may be reduced by removing the unnecessary functions and offering a simple segment and export package.

6.1.3 Design

The slow speed of design experienced by Fadel and Kirschmann (1996, p. 5) is almost negligible using the Freeform system. The use of touch in a computing environment requires additional training, but adds a degree of realism to design and can be compared to the traditional "hands on approach" in medicine. Digital design offers several advantages over the traditional approach such as: saving work progress, undo command, scaling and mirroring. All of these advantages cannot easily be replicated physically. The handle of a digital tool does not interfere with the model surface which is impossible with physical tools.

Much time is spent by prosthodontists making mirror images of anatomy that still require modifications from the source model. The longest time in the digital process is spent positioning and editing, with a mirror image taking seconds to generate. The Freeform system uses a three dimensional workspace, but positioning is difficult and requires multiple views.

Using the Phantom device to reposition digital models is easier than the trial and error approach of typing in coordinates. The ear prosthesis is the most difficult to position as a few positions seemed satisfactory in one view, and then unsatisfactory in another view (e.g. the ear was "floating" above the defect in the side view, but directly overhead in the top view). The cranial implant is easier to position due to a simple curvature and lack of features.

The Freeform system's use of digital sculpting allows quick editing of a model in exact areas using the sense of touch for positioning. This ability is superior to non-touch enabled systems as it is similar to sculpting in reality with digital advantages. Design attempts in Raindrop Geomagic and Innovmetric Polyworks are

unsatisfactory, taking many hours of work to achieve similar design results to the Freeform system.

Importing STL data into Freeform is a simple process and the clay coarseness selection of 0.16mm for the prosthesis design case study (ear prosthesis) ensures enough computing resources are available for updating the haptic device preventing the vibrations described in sub-section 2.5.2. The 0.16mm clay coarseness is finer than the scanning resolution of 0.4mm selected and does not generate significant inaccuracies in the prosthesis, evident from the evaluation.

6.1.4 Rapid prototyping

Medical modelling uses rapid prototyping in several applications and are discussed in detail in sub-section 2.8.5. Thermojet printing is faster and cheaper than SLA, which builds more durable and higher resolution acrylic prototypes. Greater durability and higher resolution are not core requirements for implant and prosthesis design. The Thermojet printer is suitable for an office or medical environment and is used as a network printer from standard PC's. Both surgeons and prosthodontists can use and control the same system over a standard PC network. The Thermojet system is easy to operate, has few controls and a simple LCD display indicates which task is required to produce a prototype.

The direct investment casting ability of the Thermojet wax speeds up the process and is integrated with traditional medical casting methods. There were few negative comments regarding the Thermojet wax from the prosthodontist involved in the study. Two notable comments were the wax viscosity and colour. The wax required hotter tools to work with and was more viscous than traditional dental wax. Dental wax is pink in colour to prevent a patient being "put off" by the wax prosthesis colour during fitment trials. The Thermojet wax is dark grey in colour, but is not considered as a critical problem and more a preference.

6.1.5 Casting

The casting in the investigation uses the standard medical procedures including dental flasks, and heated water baths. Casting the Thermojet wax is similar to the dental wax currently used in medical facilities. The PMMA and silicone materials used in this investigation show no negative effects from the use of Thermojet wax instead of traditional dental wax.

6.2 Process evaluation

The digital process is evaluated and compared to traditional processes using four case studies. The case studies highlight imaging and image processing with the anatomical models, and illustrate the overall digital process potential with the implant and prostheses.

Table 6-1: Case study overview

Case study	*Traditional comparison*	*Accuracy*	*Aesthetics*	*Cost*	*Speed*
Anatomical models	N/A	√			√
Implant design	No	√		√	√
Prosthesis Design	Yes	√	√	√	√
Prosthesis duplication	Yes	√		√	√

Table 6-1 shows the evaluation factors related to each case study. The ticks indicate whether a particular evaluation factor is used in a case study. The prosthesis design case study using an ear prosthesis is the only case study with quantitative results regarding the aesthetic qualities of the product. The prosthesis design and prosthesis duplication case studies use a parallel traditional method for evaluation purposes.

The anatomical models illustrate the advantages and disadvantages of each scanning and image processing system. The anatomical models present a variety of geometry including: undercut regions, high curvature, convex and concave contours. These models provide a suitable method for highlighting the advantages and disadvantages

of each scanning and image processing system in a digital process investigating medical applications.

The implant design case study does not use a parallel traditional method, as meaningful results would not be obtained. Every cranioplasty case is unique with time and cost being variables. The prosthesis design case study designs a complex ear prosthesis using both traditional and digital methods. The digital and traditional methods produce unique products that are evaluated using a survey. The prosthesis duplication case study highlights an area where digital design is more expensive and does not necessarily offer overwhelming benefits.

6.2.1 Accuracy

Quantifying the accuracy of a product requires a specification. The medical case studies in this investigation consist of unique and patient specific products without a standard specification. Medical doctors were asked what they felt the specifications should be and the following list explains this:

1. A cranial implant should be accurate to within 2mm to 5mm, based on the literature in sub-section 2.8.1 with similar case studies. This assumption is further substantiated as there are typically many bone fragments from head trauma that are removed, but not visible on a CT scan. The contours of the implant must match the surrounding anatomy, so that the implants geometry looks natural when fitted.

2. In facial prosthetics, aesthetics are more important than accuracy. For the design of an ear prosthesis, it should be accurate to within two millimetres, compared to the patients remaining ear.

3. Oral applications are more stringent on fit, in the prosthesis duplication case study, the required interface must fit into the oral cavity. This means that a suitable accuracy is 0.5mm, minimising post manufacturing modifications.

The accuracy of the data from the Renishaw Cyclone, Breuckmann Optotop and Phillips CT scanners are determined from a combination of:

1. The manufacturers specification
2. The registration error
3. The average error between models using a particular scanner.

The conservative uncertainty estimation is assumed for similar shaped and sized anatomical models using these scanners. The registration uncertainty is used as it is assumed that any object using the digital process requires multiple scans. The estimated uncertainty shows that the Renishaw Cyclone is the most accurate method (0.16±0.21mm), with a manufacturers specification of 7µm. The Breuckmann Optotop (0.19±0.21mm) has a larger manufacturers specification of 20µm using the HF-160 base bar, but still shows promising results when compared to the Phillips CT scanner uncertainty of 1.25±0.27mm. Although the Renishaw Cyclone and Breuckmann Optotop show a low average uncertainty, the standard deviation illustrates that it is not suited for oral prosthesis applications (specification of 0.5mm). From these uncertainties, both external prosthesis design and cranial implant design applications are within the specifications.

a   b   c
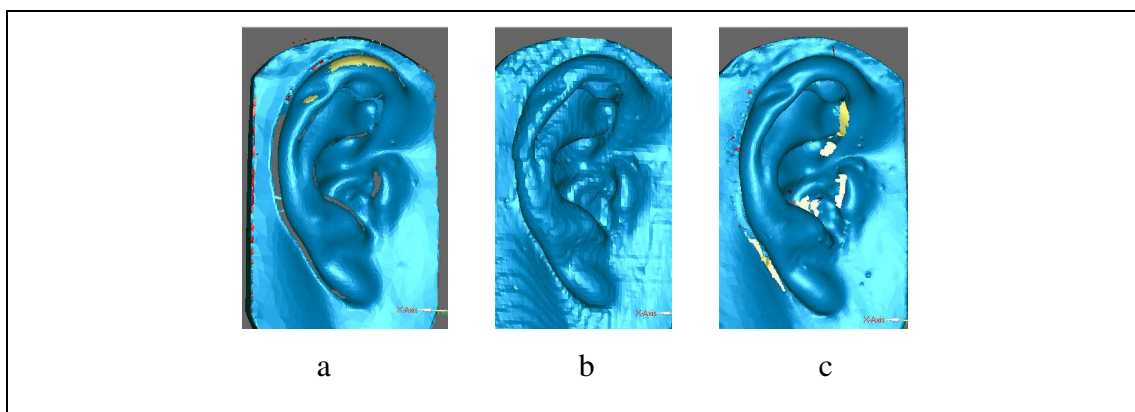
Figure 6-1: Renishaw(a), CT (b) and Breuckmann Scans (c)

Figure 6-1 shows the three digital models of Ear 2 using the Renishaw (a), CT (b) and Breuckmann scanner. The Renishaw (a) and Breuckmann (c) look similar, whereas the CT scan (c) looks rough from less resolution. This will also affect accuracy, but the Freeform system is capable of smoothing such data.

The implant design case study images the dry skull using the Breuckmann Optotop and compares it to the CT scan of the skull. The overall deviation, including

uncertainty is 1.98±1.14mm. Using 2 standard deviations (approx 95% of the image), the error is 4.253mm, close the maximum 5mm specification. During the implant testing there is a rocking motion caused by two edges that are too long and require milling with a dental burr. There are also two areas that are shorter than required. The deviations create a rocking motion of the implant and are illustrated in Figure 6-2 by the two "longer" areas.
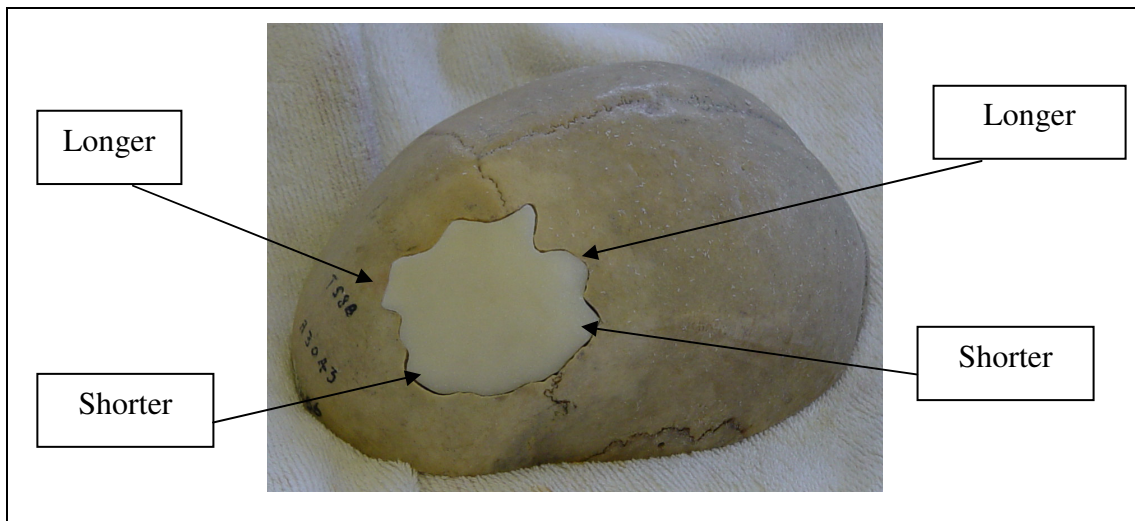
Figure 6-2: Implant placement in the skull

There are also two areas where the implant is too short and this is also indicated in Figure 6-2. These errors are caused by design errors rather than manufacturing. This error when shown to a plastic surgeon was not deemed as serious, and some visible error will be expected.

The ear prostheses cannot be compared using imaging and digital comparison, as they are two independently designed objects. The accuracy of the prosthesis is discussed based on the survey using respondents. The traditional prosthesis has accentuated features, in areas such as the anti-helix and lobule. The digital prosthesis differs in areas that are difficult to scan, such as the undercut in the helix, especially where it meets up with the triangular fossa. The tragus and acoustic meatus are also difficult areas to scan and some hole filling is used there. It is believed that the prosthesis uncertainty is within the 2mm specification. This estimate is substantiated by the design method using a mirrored model and the results of the prosthesis duplication case study. Minimal editing is performed on the mirrored prosthesis with the focus being the placement over the ear remnants.

The accuracy of the prosthesis duplication case study is judged by digitally comparing the prostheses. The duplicated acrylic prostheses are not compared as the wax models are modified for improved patient fit. This results in a prosthesis which won't compare to the original prosthesis. A shrinkage factor for acrylic is not applied and the digital wax prosthesis should match the acrylic prosthesis. White dye penetrant is used when scanning the oral prostheses to reduce glare and lighten the model colours. The large number of scans used, (19 for the original, 11 for the traditional wax and 6 for the digital wax prostheses) provides an indication of how the original glossy acrylic prosthesis produces a lot of glare when scanning. The glare from the model causes the system to discard much of the data, except in areas that are almost normal (90 degrees) to the camera. The high degree of curvature on both the top and bottom of the prostheses makes local registration easy. The registration errors are also minimal (3.34 x 10^{-4}mm for the digital wax prosthesis).

The colour error maps show the maximum deviations between the original prosthesis and the traditional prosthesis of 2.70mm. The average error of this comparison is 0.54±0.48mm, indicating two standard deviations, (95%) of the deviations are under 1.5mm. This is not suitable for the specification of 0.5mm, and also why the wax models are adjusted to fit the patient. The deviations between the original and digital prostheses with two standard deviations is 1.05mm. This result is also indicative that an assumption of less than 2mm uncertainty for an ear prosthesis is adequate.

The teeth are not imaged properly during the oral prosthesis scanning using the HF-80 volume around the teeth. CT scanning digitises all areas around and in between the teeth, but the 1mm slice distance yields similar inaccurate results based on the specification.

6.2.2 Aesthetics

The aesthetic value of the implant design case study is not quantified numerically, but it is believed that mirroring anatomy improves or matches current methods. This statement is based on the traditional process using hand instruments to mould the acrylic PMMA into the required form. Although the human body is not 100%

symmetrical, the use of mirroring the undamaged portion of the skull achieves better results than starting from scratch in the traditional method. During surgery, focus now needs to be placed on the boundary interface and not the aesthetic curvature.

The prosthesis design case study uses 26 respondents to evaluate five comparison factors. Shape and aesthetic appeal show a significant difference between opinions using the χ^2 test and a confidence level of 95%.

Figure 5-6 highlights the overall results of the survey and it is interesting to note how prosthesis B (digital method) rates higher on the "good" and "excellent" ratings and prosthesis A (traditional method) rates higher on the lower end of the scale from poor to average.

Although respondents are asked specifically on the aesthetics of each prosthesis, other factors namely: shape, anatomy, size and resemblance to cast model all contribute to the aesthetics. The anatomy question, generated excellent and good ratings for both prostheses, it is believed that the accentuated anatomy of the traditional prosthesis highlights the anatomy of the ear.

6.2.3 Cost

Both the capital and running costs are estimated for the digital process. The costs provide an estimation and comparison of the digital process cost, compared to the traditional process.

The implant design case study provides an overall cost of R2450, excluding capital costs. If it is assumed that a patient requires a CT scan and that the same casting costs are used in the traditional process, then the digital process increases costs by R1000. If operating room costs are R30 per minute, then this cost equates to 30 minutes. If digital implant design can save at least 30 minutes, then it is financially viable depending on capital costs. The capital costs, although high must be compared with the perceived financial value of aesthetics when making a decision. A further

financial incentive is that less operating rooms are required, as the throughput is increased.

The prosthesis design case study shows the greatest difference in costs with the traditional method costing 22% more than the digital process at R1750. The largest cost associated with the traditional prosthesis is the wax carving. The largest cost associated with the digital process is the prototypes at R300.

The cost of prosthesis duplication case study shows little support for the digital process as it costs almost double. The major cost is the prototyping costs. The oral prosthesis costs R400 to prototype, compared to the ear prosthesis of R300 to prototype. This is due to the large model volume; prototyping costs are independent of geometry, apart from cleaning and are dependant on the volume of material used and the prototyping time.

6.2.4 Speed

The speed of imaging systems with the anatomical models show that CT scanning is the fastest. The Breuckmann Optotop provides a similar average speed with the anatomical models of 43 minutes compared to the CT speed of 40 minutes. The doubling of time when using Raindrop Geomagic for image processing with the Breuckmann Optotop justifies a closer inspection on the purchase of both packages, or at least the relevant modules discussed in sub-section 6.1.2.

The largest uncertainty in the time estimates is that of the carving time for the traditional prosthesis. This can vary from hours to days, depending on the skill of the prosthodontist. The digital process relies on a mirror image and adapting it to fit over the remnants, a process taking 45 minutes. The equivalent task in the traditional process is carving and a conservative estimate of 3 or more hours is not unrealistic. Digital implant design will also have time savings using mirrored anatomy.

A time saving in manufacturing technique is that multiple prototypes add a short duration when prototyped. It takes 2 hours and 42 minutes for one ear prosthesis, but

3 hours and 20 minutes for 10 ear prostheses. It is recommended that the prototyping be done overnight and that multiple models are manufactured at once. This effectively removes between 2 and 3 hours from the comparison, as it is assumed this time is not normally used, resulting in the digital process taking under 4 hours per prototype, and is a significant improvement on the traditional process.

The cleaning of the prototypes is a task adding a variable amount of time to any prototype and is geometry dependant. A prototype with thin cross sections (<2mm) requires care when removing the supports. For this reason it is important that one chooses an optimised orientation for prototyping to reduce the cleaning time. If thin cross sections exist, they should be placed vertical, reducing the cleaning requirements, but this will add to building time.

The wax ear prosthesis does not fit over the remnants immediately and requires localised heating and then forcing over the remnants. This additional work ensures a tight fit on the patient. An analysis of the draft angles after design will foresee this problem, but it is far quicker to heat the base and place it over the remnants than to analyse the model. This process is described as wax model adjustments in Table 5-16 and takes approximately 30 minutes.

The prosthesis duplication case study shows the least support for the digital method in terms of both time and cost. The digital method takes nearly 7 hours and the traditional method 1 hour. Even with the prototyping times removed for the purposes of prototyping overnight, the process still takes at least two hours.

6.2.5 Process improvements

A digital process offers several advantages that are not immediately apparent. Sub-section 6.2.5 describes these general improvements.

Digital information can be stored indefinitely and take up very little space. This is advantageous as additional prostheses or implants can be made without the patients presents and posted to another medical facility. A database of anatomy can be formed,

for patients that have bi-lateral defects, such as two ears missing. Traditionally prosthodontists use a compatible family member or a member of public. The patient can choose the required ears off a database.

Doctors can be trained digitally using anatomy imported into the Freeform system, and this can be used as virtual pre-operative planning. Screenshots can be emailed to colleagues across the world for advice on difficult cases.

Prototyping allows many models to be created at once, increasing the throughput and also provides a standard for doctors to use, essentially any software that will output an STL file.

6.2.6 Digital process summary

A summary of the digital process is provided in this sub-section in Table 6-2. The summary highlights each step in the process and compares the equipment in terms of the evaluation criteria. The apparatus in each process step are compared using the terms: low, medium and high, indicating the performance ratings in this investigation.

Table 6-2: Digital process summary

Process step	Apparatus	Accuracy	Aesthetics	Cost	Speed
Imaging					
	Renishaw Cyclone	High	Low	Medium	Low
	Breuckmann Optotop	Medium	High	Medium	Medium
	Phillips CT	Low	Medium	High	High
Image processing					
	Raindrop Geomagic	Medium	High	High	Low
	Innovmetric Polyworks	High	Medium	High	High
	Tomovision	Low	Low	Medium	Medium
Design					
	Freeform	Low	High	High	High
Rapid prototyping					
	Thermojet	Medium	High	Medium	High

The remainder of the section discusses the ratings illustrated in Table 6-2.

The accuracy of imaging apparatus is the ability to accurately present data. The additional data from the Renishaw and slice distance of the Phillips CT lower the aesthetics ratings. The Phillips CT scanner has the highest cost and speed, with the ability for multiple models.

The accuracy of image processing software is the ability to replicate missing data and registration of individual scans. Innovmetric Polyworks offers the highest degree of control making the system the most accurate, but Tomovision uses manual methods in image segmentation, making it offer the lowest accuracy. Image processing aesthetics is the ability to generate smooth surfaces on the models when processing and hole-filling. Raindrop Geomagic has the highest aesthetics value, with the single click approach, compared to Polyworks which requires a lot of user input to generate a smooth surface. The fast local and global registration algorithms make Polyworks the

fastest software, and one can register while scanning as it adds on almost no time. Geomagic lacks visual sampling and makes the processing time longer and require physical sampling of data for fast results.

The accuracy of the Freeform system is considered to be medium as the system recources dictate resolution, and the freedom of motion with the Phantom device also lowers it's accuracy. The freedom of design using the Phantom device makes the system an aesthetic choice rather than one based on accuracy. The speed is rated as high, and it is doubtful whether the aesthetic design changes made using the Freeform system can be made rapidly in a traditional CAD system. The cost is considered to be high, when compared to other design methods, but this includes both hardware (Phantom) and software (Freeform).

The Thermojet printer is not the most accurate system and its manufacturer's accuracy specifications are lower than that of SLA. The smooth surface gives it a high rating for aesthetic value. The wax may also be smoothed using heated implements, enahancing aesthetics. The Thermojet system is very fast, and build times greater than 10 hours would be recorded if SLA was used to prototype the models used in the investigation. The cost is considered to be high, especially when including material costs.

Conclusion

Chapter 7 presents the conclusions of the investigation with respect to the objectives illustrated in section 1.5.

All of the objectives of the investigation are achieved and are stated below:

1. A digital process is created and tested for the design and duplication of prostheses and implants. The digital process consists of imaging, image processing, design, fabrication and casting.

2. A cranioplasty case study is used for implant design, an ear prosthesis case study is used for prosthesis design and an oral prosthesis case study is used for prosthesis duplication.

3. The evaluation criteria of accuracy, aesthetics, cost and speed are used to evaluate the case studies.

Industrial imaging systems are included in the digital process and prevent the need for costly and inaccurate CT scans when external human anatomy is reverse engineered. The Breuckmann Optotop can accurately and rapidly obtain images, and when used with Innovmetric Polyworks can produce digital anatomy in under an hour.

Haptic design using the Phantom and Freeform improves a digital reverse engineering process and makes it possible to use industrial external imaging with human anatomy.The Phantom enables the user to interact with the model through the sense of touch and adjust a model's size and shape. The Freeform software with its smoothing ability generates aesthetic designs and enhances a patients appearance when facial prosthetics are required.

RP manufactures any geometry in little time compared to traditional manufacturing processes. The wax build material of the Thermojet makes direct casting for implants and prostheses possible reducing time and cost.

The digital process reduces patient involvement and the overall medical procedures remain the same with the difference being manufacturing in an external environment. This process similarity assists in its adoption in the medical field and for further testing in other applications.

The digital process can create both implants and prostheses for human patients in less time than traditional methods. The traditional method for the design of an ear prosthesis takes hours to days depending on the skill of the prosthodontist, compared to the digital process requiring just over two hours to obtain the digital design. If the full potential of the digital process is used by prototyping multiple models, a single prosthodontist can create three or more ear prostheses a day, and prototype them overnight. Custom implants for unilateral defects are also feasible using a digital process, and the design capabilities using haptic methods generate a smooth interface, increasing the aesthetics of an implant.

Further cost savings with both RP and haptic technology can be expected in future when more companies enter the market place. If a digital process is used commercially, then economies of scale apply to prototyping, reducing costs and mass producing custom products. A centralised facility or bureau using this digital process will in the meantime prove sufficient for several departments or clinics. The Thermojet Printer is suitable for use in a clinical environment and is simple to use.

The use of a digital process will result in the following benefits when compared to a traditional process:

1. Digital models can be saved for future reference or replacement prostheses.
2. Preoperative planning can be performed on the digital models using the Freeform software instead of large costly prototypes for implants.
3. Implants can be manufactured outside the operating room in a cheaper environment.
4. The hazards of using PMMA in a patient discussed by D'Urso *et al* (2000, p. 201), are negligible if the implant is manufactured preoperatively.

Further Research

There are a variety of medical applications that can use the ability of both haptic modelling and RP as many of the traditional procedures still rely on the artistic aptitude of the medical technician. Internal implants can benefit greatly from these processes as much of the work at present is done with pre-made implants that come in certain sizes. These implants could be customised and manufactured rapidly, ready for use in the operating theatre. More work is required in terms of biomaterials for RP processes. Also several patient based case studies should be performed using digital comparison techniques such as Raindrop Qualify to quantify the error of such prototypes. This information can be used later if an implant fails and may help determine the cause. Other materials e.g. hydroxyappatite (HA) (Thomas *et al*, 1999, pp. 359-362, D'Urso *et al*, 2000, pp. 200-201), and polymer coated calcium phosphate (Vail *et al,* 1999, p. 130) are currently used in cranial applications. The advantages of these ceramics include osteoinductivity, (stimulate new bone growth), under certain conditions. This research excludes the use of such ceramics due to casting difficulties. Research is being performed in using bio-medical ceramics in RP systems, but currently only simple geometries are created (Richter, Thomas and Deventer, 1999, pp. 325-326 and Vail *et al*, 1999, p. 130). The use of a full digital process with these exotic materials may further enhance results.

The scope of this investigation limits it to traditional RP systems, but the process may be expanded further to any manufacturing process using STL as data input. Industrial imaging systems are continuously being updated, and the use of colour scanning systems in prosthetics may enhance a digital process.

References

Abovitz, R. (2001) Digital surgery: the future of medicine and the human-robot symbiotic interaction, *Industrial robot: An international journal,* vol. 28, no. 5, pp. 401-405.

Allen P.F., Watson G., Stassen L. and McMillan A.S. (2000) Peri-implant soft tissue maintenance in patients with craniofacial implant retained prostheses, *The international journal of oral and maxillofacial surgery,* vol. 29, pp. 99-103

Anonymous, 3D systems home page; www.3dsystems.com, 22 August 2002

Anonymous, Breuckmann home page, www.breuckmann.com, April 2002

Anonymous, http://rpdrc.ic.polyu.edu.hk/content/rp_for_arch_short_guide_4.htm; 5 May 2004

Anonymous; Imaginis, http://www.imaginis.com, 01 August 2001

Anonymous; Medical College of Winsconsin, www.mcw.edu, 28 August 2001

Anonymous; Molson Medical Informatics, http://sprojects.mmi.mcgill.ca/braintumor/section2/subsection4/default.htm, 11 January 2004

Anonymous, Sensable Technologies, http://www.sensable.com, 29 August 2001

Anonymous, Siemens, http://www.siemens.com, 28 August 2001

Anonymous, Renishaw home page www.renishaw.com; April 2002

Asher E.S., Evans J.H., Wright R.F. and Wazen J.J. (1999) Fabrication and use of a surgical template for placing implants to retain an auricular prosthesis, *The journal of prosthetic dentistry,* vol. 81, no. 2, pp. 228-233

Bardell R., Balendran V. and Sivayoganathan K. (2003) Accuracy analysis of 3D data collection and free-form modelling methods, *Journal of materials processing technology,* vol. 133, pp. 26-33

Bernardini F and Rushmeier H (2002) The three D model acquisition pipeline, *Computer Graphics Forum,* vol. 21, no. 2, pp. 149-172

Beumer J (1996) *Maxillofacial rehabilitation: Prosthodontic and surgical considerations*; Ishiyakyu EuroAmerica Inc., pp 383 – 385; 443-467

Bholat OS, Haluck R.S, Murray W.B., Gorman P.J and Krummel T.M. (1999) Tactile feedback is present during minimally invasive surgery, *Journal of the American college of surgeons,* vol. 189, no. 4, pp. 349-355

Bicheno J (2002) *The quality 75*, PICSIE books, Buckingham, UK, pp. 16-17

Bless C. and Higson-Smith C. (1995) *Social research methods: an African perspective*, Juta and company, Cape Town, South Africa, pp. 100-101

Bless C. and Kathuria (1993) *Fundamentals of social statistics: An African perspective*, Juta & Co. Cape Town, South Africa, pp. 185-238

Bradley C., (1998) The application of reverse engineering in rapid product development, *Sensor Review,* vol. 18, no. 2, pp. 115-120

Bronzino *et al*. (2000) The Biomedical Engineering Handbook, *Computed Tomography*, CRC Press, IEEE Press UK, pp. 62-4, 62-5, 63-2, 64-10, 67-7

Brown N.J.G., Britton K.E., Plummer D.L. (1998) Standardisation in medical image management, *International Journal of medical informatics,* vol. 48, pp. 227-238

Buckingham, R.A. and Buckingham, R.O. (1995) Robots in operating theatres, *British medical journal*, vol. 311, pp. 1479-1482

Catafau A.M. (2001) Brain SPECT in clinical practice: Part 1: Perfusion, *Journal of Nuclear medicine,* vol 42, pp. 259-271

Chang T.C., Wysk R.A. and Wang H.P. (1998) *Computer aided manufacturing*, Prentice Hall, Upper Saddle River, New Jersey, pp. 92-130, 460-462

Chen F., Brown G.M. and Song M. (2000) Overview of three-dimensional shape measurement using optical methods, *Optical engineering,* vol. 39, no. 1, pp. 10-22

Choi, S.H. and Samavedam, S. (2001) Visualisation of rapid prototyping, *Rapid prototyping journal,* vol. 7, no. 2, pp. 99-114

Choi J.Y., Choi J.H., Kim N.K., Kim Y., Lee J.K., Kim M.K., Lee J.H.,
Kim M.J. (2002) Analysis of errors in medical rapid prototyping models, *International Journal of Oral and Maxillofacial Surgery* Vol. 31 pp. 23–32

Cooper K.G. (2001) *Rapid Prototyping technology: Selection and application*, Marcel Dekker Inc., Basel, New York, pp. 44-48, 166-167, 214

Cooper R.A. and Weekes A.J. (1983) *Data models and statistical analysis*, Phillip Allan publishers limited, Oxford, UK, pp. 38-39

Corvera C.U. and Kirkwood, K.S. (1997) Recent advances: General surgery, *British medical journal,* vol. 315, pp. 586-589

Curless B. and Levoy M. (1996) A volumetric method for building complex models from range images, *Proceedings of SIGGRAPH '96* , pp. 303-312

Cutting C., Bookstein F.L., Grayson B., Fellingham L. and McCarthy J.G. (1986) Three-dimensional computer assisted design of craniofacial procedures: optimisation and interaction with cephalometric and CT-based models, *Plastic and reconstructive surgery,* vol. 77, no. 6, pp.877-885

D'Urso, P.S., Earwalker, W.J., Barker, T.M., Redmond, M.J., Thompson, R.G., Effeney, D.J. and Tomlinson, F.H. (2000) Custom cranioplasty using stereolithography and acrylic, *British journal of plastic surgery,* vol. 53, pp. 200-204

D'Urso, P.S., Thompson, R.G., Atkinson, R.L., Weidmann, M.J., Redmond, M.J., Hall, B.I., Jeavons, S.J., Benson, M.D. and Earwalker, W.J.S. (1999) Cerebrovascular biomodelling: a technical note, *Surgical neurology,* vol. 52, pp. 490-500

Dachille F., Qin H. and Kaufman A. (2001) A novel haptics based interface and sculpting system for physics based geometric design, *Computer aided design,* vol. 33, pp. 403-420

Dolenc A. and Makela I. (1996) Rapid prototyping from a computer scientists point of view, *Rapid prototyping journal,* vol. 2, no. 2, pp. 18-25

Fadel G.M., Kirschman C. (1996) Accuracy issues in CAD to RP translation, *Rapid prototyping journal,* vol. 2, no. 2, pp. 4-17

Garvin D. (1988) *Managing quality: The strategic and competitive edge*, The Free press , New York, NY, pp 49-68

Gibson S., Fyock, C., Grimson, E., Kanade, T., Kikinis, R., Lauer, H., McKenzie, N., Mor, A., Nakajima, S., Ohkami, H., Osborne, R., Samosky, J. and Sawada, A. (1998) Volumetric modelling for surgical simulation, *Medical image analysis,* vol. 2, no. 2, pp. 121-132

Girod S., Teschner M., Schrell U., Kevekordes B. and Girod B. (2001) Computer aided 3-D simulation and prediction of craniofacial surgery: a new approach, *Journal of cranio-maxillofacial surgery,* vol. 29, pp. 156-158

Gregory A., Lin M.C., Gottschalk S. and Taylor R. (2000) Fast and accurate collision detection for haptic interaction using a three degree of freedom force feedback device, *Computational geometry,* vol. 15, pp. 69-89

Hassfield, S. and Mühling, J. (2001) Computer assisted oral and maxillofacial surgery, *International journal of oral and maxillofacial surgery*, vol. 30, pp. 2-13

Horton K.M., Sheth S., Corl F. and Fishman E.K. (2002) Multidetector row CT: Principles and clinical applications, *Critical reviews in computed tomography,* vol. 43, no. 2, pp. 143-181

Jee, H.J. and Sachs, E., (2000) A visual simulation technique for 3D printing, *Advances in engineering software,* vol. 31, pp. 97-106

Kai, C.C. and Fai, L.K. (1997a) Rapid prototyping in Singapore: 1988 to 1997, *Rapid prototyping journal,* vol. 3, no. 3, pp. 116-119

Kai C.C. and Fai L.K. (1997b) *Rapid prototyping: principles and applications in manufacturing,* John Wiley and sons (Asia) Pte Ltd, Singapore, pp. 221-224

Kai C.C., Meng C.S., Ching L.S., Teik L.S. and Aung S.C. (2000) Facial prosthetic fabrication using rapid prototyping tools, *Integrated manufacturing systems,* vol. 11, no. 1, pp. 42-53

Katz, Z. and Smith, P.E.S. (2001) On process modelling for selective laser sintering of stainless steel, *Proceedings for the institution of mechanical engineers,* vol. 215, part B, pp. 1497-1504

Kubon T.M., Kurtz K.S. and Piro J.D. (2000) Impression procedure for creating a partial auricular prosthesis, *Journal of prosthetic dentistry,* vol. 83, pp. 648-651

Lawler L.P., Fishman E.K. (2002) Three dimensional CT angiography with multidetector CT data: Study optimization, Protocol design, and clinical applications in the abdomen, *Critical reviews in computed tomography,* vol. 43, no. 2, pp. 77-141.

Lee S.H., Kim H.C., Hur S.M. and Yang D.Y. (2002) STL file generation from measured point data by segmentation and delaunay triangulation, *Computer aided design,* vol. 34, pp. 691-704

Lee S.J., Jung I.Y., Lee C.Y, Choi S.Y. and Kum K.Y (2001) Clinical application of computer aided rapid prototyping for tooth transplantation, *Dental traumatology,* vol. 17, no. 3 pp. 114-119

Lemon J.C., Chambers M.S., Wesley P.J. and Martin J.W. (1996) Technique for fabricating a mirror image prosthetic ear, *Journal of prosthetic dentistry,* vol. 75 pp. 292-293

Liu G.H., Wong Y.S., Zhang Y.F. and Loh H.T. (2002) Error based segmentation of cloud data for direct rapid prototyping, *Computer aided design,* vol. 35, pp. 633-645

Lopponen H., Holma T., Sorri M., Jyrkinen L., Karhula V., Koivula A., Hikko J., Laitinen J., Koivukangas J., Oikarinen J. and Alamaki O. (1997) Computed tomography data based rapid prototyping model of the temporal bone before cochlear implant surgery, *Acta otolaryngology,* vol. 529, pp. 47-49

Lumley J. (1996) *Surface anatomy*; Churchill Livingstone, pp. 16

Mankovich, N.J., Samson, D., Pratt, B.S., Lew, D. and Beumer, J. (1994) Surgical planning using three-dimensional imaging and computer modelling, *Otolaryngologic clinics of North America,* vol. 27, no. 5, pp. 875-889

McGovern, K. (1994) Applications of virtual reality to surgery, *British medical journal*, vol. 308 pp. 1054-1055

McGurk, M., Potamianos, P., Amis, A.A. and Goodger, N.M. (1997) Rapid prototyping techniques for anatomical modelling in medicine, *Annals of the royal college of surgeons in England,* vol. 79, pp. 169-174

Meier, A.H., Rawn, C.L. and Krummel, T.M. (2001) Virtual reality: surgical application – challenge for the new millennium, *Journal of the American college of surgeons*, vol. 192, no. 3, pp. 372-384

Meinzer H.P., Thorn M., Vetter M., Hassenpflug P., Hastenteufel M. and Wolf I. (2002) Medical imaging: examples of clinical applications, *ISPRS journal of photogrammetry & remote sensing,* vol. 56, pp. 311-325

Miguel P.A.C., King T.G. (1994) Co-ordinate measuring machines: Concept, classification and comparison of performance tests, *International journal of quality and reliability managements,* vol. 12 No.8, pp. 48-63.

Miller I. and Freund J.E. (1985) *Probability and statistics for engineers*, Prentice-Hall, Eaglewood cliffs, NJ, USA, pp. 255-260

Mullineux G. (2002) Improvement of free-form surfaces for product styling applications, *Computer aided design,* vol. 34, pp. 871-880

Nusinov N.S. and Gay W.D. (1980) A method for obtaining a reverse image of an ear, *The journal of prosthetic dentistry,* vol. 44, no. 1 pp. 68-71

Parel S.M. (1980) Diminishing dependence on adhesives for retention of facial prostheses, *The journal of prosthetic dentistry,* vol. 43, no. 5, pp. 552-560

Parel S.M., Branemark P.I., Tjellstrom A. and Gion G. (1986) Osseointegration in maxillofacial prosthetics Part II: Extraoral applications, *The journal of prosthetic dentistry,* vol. 55, no. 5, pp. 600-606

Park C (2000) Subfascial expansion and expanded two-flap method for microtia reconstruction, *Plastic and reconstructive surgery,* vol. 106, no. 7, pp. 1473-1487

Parrott A. and Machet A. (2001) Medical applications of rapid prototyping: The Auricular prosthesis, *RAPDASA proceedings*, 14-15 November 2001, pp. 66-72

Penkner K, Santler G., Mayer W., Pierer G., and Lorenzoni M. (1999) Fabricating an auricular prosthesis using three-dimensional soft tissue models, *The journal of prosthetic dentistry*, vol. 82, no. 4, pp.482-484

PettiJohn T.F. (1999) Psychology: A connecText, http://www.dushkin.com/connectext/psy/ch02/pet.mhtml, Fourth edition, McGraw Hill

Petzold, R., Zeilhofer, H.F. and Kalender, W.A. (1999) Rapid prototyping technology in medicine – basics and applications, *Computerised medical imaging and graphics,* vol. 23, pp. 277-284

Potamianos, P., Amis, A., Forester, A.J., McGurk, M. and Bircher, M. (1998) Rapid prototyping for orthopaedic surgery, *Proceedings of the institute for mechanical engineers,* vol. 212, part H, pp. 383-393

Prasad B. (1998) A method for measuring total value towards designing goods and services, *The TQM magazine,* vol. 10, no. 4, pp. 258-275

Priest J.W. and Sanchez J.M. (1988) *Product development and design for manufacturing*, Marcel Dekker, New York, NY, USA, p. 17

Richter P.W., Thomas M.E. and van Deventer T. (1999) Macroporous hydroxyapatite by solid freeform fabrication: towards custom implants, *South African Journal of Science*, vol. 95, pp. 325-326

Sailer H.F., Haers P.E., Zollikofer C.P.E., Warnke T., Carls F.R. and Stucki P. (1998) The value of stereolithographic models for preoperative diagnosis of craniofacial deformities and planning of surgical corrections, *International journal of oral and maxillofacial surgery,* vol. 27, pp. 327-333

Sanghera, B., Naique, S., Papaharilaou, Y. and Amis, A. (2001) Preliminary study of rapid prototype medical models, *Rapid prototyping journal,* vol. 7, no. 5, pp. 275-284

Santler, G. (2000) 3-D COSMOS: a new 3-D model based computerised operation simulation and navigation system, *Journal of cranio-maxillofacial surgery*, vol. 28, pp. 287-293

Schroeder W.J., Zarge J.A. and Lorensen W.E. (1992) Decimation of triangle meshes, *ComputerGraphics,* Vol. 26 No. 2, pp. 65-70

Sebastianelli R., Tamimi N., (2002) How product quality dimensions relate to defining quality, *International journal of quality and reliability management,* vol. 19, no. 4, pp. 442-453

Siebert J.P., and Marshall S.J. (2000) Human body 3D imaging by speckle texture projection and photogrammetry, *Sensor review,* vol. 20 no. 3, pp. 218-226

Slack N. (1991) *The manufacturing advantage*, Mercury books, Gold arrow publications limited, London, UK.

Thomas, G., Johnson, L., Dow, S., Stanford, C. (2001) The design and testing of a force feedback dental simulator, *Computer methods and programs in biomedicine,* vol. 64, pp. 53-64

Thomas M.E., Richter P.W., van Deventer T, Crooks J. and Ripamonti (1999) Macroporous synthetic hydroxyapatite bioceramics for bone substitute applications, *South African journal of science,* vol. 95, pp. 359-362

Thurfjell, L., McLaughlin, J., Mattsson, J., Lammertse, P. (2002) Haptic interaction with virtual objects: the technology and some applications, *Industrial robot: an international journal,* vol. 29, no. 3, pp. 210-215

Vail N.K., Swain L.D., Fox W.C., Aufdlemorte T.B., Lee G. and Barlow J.W. (1999) Materials for biomedical applications, *Materials and design,* vol. 20, pp. 123-132.

Varaday T., Martin R.R. and Coxt J. (1997) Reverse engineering of geometric models – an introduction, *Computer aided design*, vol. 29, no. 4, pp. 255-268

Wang C.C.L., Chang T.K.K. and Yuen M.M.F. (2003) From laser-scanned data to feature human model: a system based on fuzzy logic concept, *Computer aided design,* vol. 35, pp. 241-253

Wang R.R., Andres C.J. (1999) Hemifacial microsomnia and treatment options for auricular replacement: A review of literature, *The journal of prosthetic dentistry,* vol. 82, no. 2, pp. 197-204

Wang R. (1999a) Presurgical confirmation of craniofacial implant locations in children requiring implant-retained auricular prosthesis, *The journal of prosthetic dentistry,* vol. 81, no. 4, pp. 492-495

Wang, R. (1999b) Preoperative wax pattern duplication for surgical template fabrication, *The journal of prosthetic dentistry,* vol. 81, no. 5, pp. 634-637

Webb, P.A. (2000) A review of rapid prototyping (RP) techniques in the medical and biomedical sector, *Journal of medical engineering and technology,* vol. 24, no. 4, pp. 149-153

Werner A., Lechniak Z., Skalski K. and Kedzior K. (2000) Design and manufacture of anatomical hip joint endoprostheses using CAD/CAM systems, *Journal of materials processing technology*, vol. 107, pp. 181-186

Wickham, J. E. A. (1994) Minimally invasive surgery: Future developments, *British medical journal*, vol. 308, pp. 193-195

Winder J., Cooke R.S., Gray J., Fannin T. and Fegan T. (1999) Medical rapid prototyping and 3D CT in the manufacture of custom made cranial titanium plates, *Journal of medical engineering and technology,* vol. 23, no. 1, pp 26-28

Wohlers T. (1995) Future potential of rapid prototyping and manufacturing around the world, *Rapid prototyping journal,* vol. 1, no. 1, pp. 4-10

Wright P. K. (2001) *21st Century Manufacturing*, Prentice Hall

Xu Z.Q., Ye S.H. and Fan G.Z. (2002) Colour 3D reverse engineering, *Journal of materials processing technology,* vol. 125, pp. 495-499

Young, Y.Y., Yu, K.M. and Kwong, C.K. (2001) Layer manufacture of jewel ring by volume efficient methodology, *Proceedings of the institute of mechanical engineers,* vol. 215, part B, pp. 1035-1049

Zhang Q. (2001) Quality dimensions, perspectives and practices: A mapping analysis, *International journal of quality and reliability management,* vol. 18, no. 7, pp. 708-721

Zhang Z. (1994) Iterative point matching for registration of free-form curves and surfaces, *International journal of computer vision,* vol. 13 no. 2, pp. 119-152

Appendix A

Appendix A lists manufacturer's specifications for the Renishaw Cyclone, Breuckmann Optotop and Thermojet Printer.

Apparatus specifications

Renishaw Cyclone

Table A-1: Renishaw Cyclone specifications

Item	Description
Axis travel	600mm x 500mm 400mm nominal
Maximum work piece weight	200 kg
Repeatability	5μm
Axis Resolution	7μm
Scanning speed	Up to 3 metres per minute
Rapid speed	6 metres per second
Scanning rate	400 points per second
Scale type	Renishaw RG2
Probe type	Renishaw 3 axis SP620 Analogue scanning probe
Probe range	±1.0mm
Probe rate	1.2N/mm nominal
Standard stylus	M4, 100mm ceramic x ∅6mm ruby ball tip
Working range (Z axis)	391 ±5mm with a 100mm stylus
Crash protection	Detachable magnetic stylus holder
Controller	Custom controller with optical PC interface
Software	Renishaw TraceCut
Weight	162kg
Colour	Royalite grey and black
Table	Composite granite tile with grid of 14 M8 holes
Operating temperature	+10°C to +38°C
Storage temperature	-10°C to +50°C
Electrical supply	90 – 265VAC, 47 – 60 Hz
Air supply	0.55 to 1.0 Mpa
Power consumption	80 watts
Air consumption	40 litres per minute

(Renishaw specifications: www.renishaw.com; April 2002)

Breuckmann Optotop-HE

Table A-2: Breuckmann Optotop specifications

Image processing	Specification
Host computer	Intel Pentium III / IV, > 1 GHz, > 256 MB Ram > 20 GB, Open GL Graphic adaptor, CD Writer
Image data interface	IEEE 1394 (Fire Wire)
Operating system	Windows 2000
Measurement software	OPTOCAT for Windows
Data interface	ASCII, Binary, optional STL
Sensor	
Principle of operation	Miniaturised projection technique (MPT)
Light source	100 W halogen
Sensor weight	1.5 – 2.5kg
Camera	High resolution digital black/white
Digitisation	1280 x 1024 pixel
Operating distance	From approx. 50mm
Min. depth resolution	2µm
Acquisition time	Approx. 1 second
Standard measuring areas	
HF-80	FOV 80 x 60 mm
HF-160	FOV 160 x 120 mm
HF-320	FOV 320 x 240 mm
HF-480	FOV 480 x 360 mm

(Breuckmann technical data, www.breuckmann.com, April 2002)

3D Systems: Thermojet Printer

Table A-3: Thermojet printer specifications

Machine	Description
Technology	Multi-jet modelling (MJM)
Resolution	300 x 400 x 600 DPI (xyz)
Maximum model size	250 x 190 x 200mm
Available build materials	Thermojet 2000 and Thermojet 88 thermoplastic build material
Material colour options	Neutral, gray or black
Material capacity	5.9kg
Material loading	2.3kg cartridge
Interface	TCP / IP prototcol; Ethernet 10/100 base-TX network; RJ-45 connector required
Platform support	Silicon Graphics IRIX v6.5.2 (open GL required) Hewlett Packard HP-UX v10.2 ACE (Open GL required) Sun Microsystems Solaris v2.6.0 (Open GL required) IBM RS/6000 AIX v4.3.2 (Open GL required) Windows NT v4.0, 98, 2000, Millenium edition
Warranty	90-day on-site
Power consumption	100VAC, 50/60 Hz, 12.5 amps 115 VAC, 50/60 Hz, 10 amps 230 VAC, 50/60 Hz, 6.3 amps
Dimensions	W1.37 x D0.76 x H1.12 m
Weight	Without crate – 375kg
Shipping weight	499kg with crate and accessory kit
Shipping dimensions	W1.58 x D1.02 x H1.60m
Build material properties	**Thermojet 2000**
Melt temperature	70 – 75°C
Softening temperature	55°C
Density (g/cubic cm)	@140°C: 0.865 @130°C: ------ @110°C: 0.883 @23°C: 0.982
Volumetric shrinkage	From 140°C to Room temperature: 11.7%
Linear shrinkage	From 140°C to Room temperature: ≈ 2.3%

(3D systems; www.3dsystems.com, 22 August 2002)

Appendix B

Appendix B contains specifications on materials used during the investigation.

Material specifications

Name: **Dental Lab Plaster**

Manufacturer: Kalabhai Parson

                            PVT Ltd

                            256 Sardar V Patel Road

                            Bombay

                            India

Description: Dental grade plaster of paris, a yellow powder indicating a medium hardness, the product is supplied in 20kg bags

Additional information:

               Water/powder ratio: 58 cc's to 100 grams

               Mixing manually: 60 seconds

               Mixing mechanically: 30 seconds

               Setting time: 5 – 7 minutes

               Linear expansion: 0.10%

Name: **Model release agent (MRA)**

Manufacturer: Dentsply International Incorporated

                            York

                            PA

                            17406

                            USA

Description: A highly viscous fluid, that is clear and used to prevent sticking of master models when investment casting. The product is supplied in a bottle and is 120 grams

Name:	**Divosep**
Manufacturer:	Vertex Dental B.V.
	PO Box 10
	3700
	AA Zeist
	The Netherlands
Description:	A blue liquid, that has a greasy feel to it that is commonly brushed on plaster moulds when using algenate impressions.

Additional information:

The product is supplied in 1000ml bottles.

Name:	**Surgical Simplex P**
Manufacturer:	Howmedica International Inc.
	Shannon Industrial Estate
	Co. Clare
	Ireland
Description:	A white powder and colourless liquid (monomer). The mixture of the powder and liquid produce a white acrylic suitable for the creation of implants in bone

Appendix C

Appendix C contains the χ^2 results for the prosthesis design survey.

χ^2 test and survey questionnaire results

The χ^2 test determines whether the observed or actual frequency of a phenomenon corresponds to an expected frequency if the hypothesis under study is correct. The χ^2 test is a test of significance of the observed differences. Being a non-parametric test, the χ^2 test does not assume a normal distribution of the population nor require any other parametric properties to be fulfilled (Bless and Kathura, 1993, pp. 186).

The general expression of the χ^2 test is (Miller and Freund, 1985, pp 263):

$$X^2 = \sum_{i=1}^{r} \sum_{j=1}^{c} \frac{(O_{ij} - E_{ij})^2}{E_{ij}} \qquad \text{(D-1)}$$

Where:

χ^2 = Chi squared value

O_{ij} = observed frequency in row i and column j; where i and j are indices.

E_{ij} = expected frequency in row i and column j; where i and j are indices.

r = row

c = column

The expected value is calculated using (Bless and Kathura, 1993, p. 189):

$$E_{ij} = \frac{R_i * C_j}{T} \qquad \text{(D-2)}$$

Where:

E_{ij} = expected frequency in row i and column j; where i and j are indices.

R_i= the total frequency of all items in the ith row; where i is an index.

C_j = the total frequency of all items in the jth column; where j is an index.

T = a grand total of all frequencies.

The observed values for the χ^2 test are compared to critical values of χ^2 (χ^2_{crit}) obtained from statistical tables of the χ^2 test.

The data from a survey is presented in an r x c table, or contingency table, in which data is tallied into a two-way classification having *r* rows and *c* columns (Miller and Freund, 1985, p. 262).

Each χ^2 contingency table has its degrees of freedom (df) which is the number of data points that can be arbitrarily chosen within the given constraints. The number of degrees of freedom is calculated using D-3, (Bless and Kathura, 1993, pp. 189).

$$df = (r-1)(c-1) \qquad \qquad \text{(D-3)}$$

If the expected frequency of a value is less than 5, then adjacent columns are merged, since the sampling distribution of the χ^2 statistic is only approximately the χ^2 distribution (Miller and Freund, 1985, p. 258).

If $\chi^2_{obs} < \chi^2_{crit}$, then H_0 is not rejected for the chosen level of significance α.

If $\chi^2_{obs} \geq \chi^2_{crit}$, then H_0 is rejected for the chosen level of significance α.

The processed results of a survey conducted between the 2 ear prostheses for the prosthesis design case study using 26 respondents are displayed in this section. A significant difference in opinion is found for the comparison factors of aesthetics and shape.

The categories of 1, 2 and 3 have been combined, as the expected values are less than 5 (Miller and Freund, 1985, pp 258).

Table D-1: Shape

Shape		1	2	3	4	5	Total
Prosthesis A	Observed	3	12	11			26
	Expected	6.5	13	6.5			
	CHI_SQR	1.885	0.077	3.115			
Prosthesis B	Observed	10	14	2			26
	Expected	6.5	13	6.5			
	CHI_SQR	1.885	0.077	3.115			
TOTAL		13	26	9	3	1	52

df = 2

α.= 0.05

χ^2_{crit} = 5.99

χ^2_{obs} = 10.154

In Table D-1, The observed value of χ^2, (χ^2_{obs}), is greater than χ^2_{crit}, thus there is a significant difference in opinions on shape between prosthesis A and B. In particular at the lower end of the scale prosthesis A was rated poorly by more respondents, 11 respondents compared to 2 respondents for prosthesis B.

Table D-2: Anatomy

Anatomy		1	2	3	4	5	Total
Prosthesis A	Observed	2	9	15			26
	Expected	5	9.5	11.5			
	CHI_SQR	1.8	0.026	1.065			
Prosthesis B	Observed	8	10	8			26
	Expected	5	9.5	11.5			
	CHI_SQR	1.8	0.026	1.065			
TOTAL		10	19	14	4	5	52

df = 2

α.= 0.05

X^2_{crit} = 5.99

X^2_{obs} = 5.783

In Table D-2, The observed value of χ^2, χ^2_{obs}, is less than χ^2_{crit}, and there is no significant difference in opinions on anatomy between prosthesis A and B. It is noted that 8 of the 26 respondents rated prosthesis B as having excellent anatomical detail compared to 2 for prosthesis A.

Table D-3: Size

Size		1	2	3	4	5	Total
Prosthesis A	Observed	9	17				26
	Expected	10	16				
	CHI_SQR	0.1	0.063				
Prosthesis B	Observed	11	15				26
	Expected	10	16				
	CHI_SQR	0.1	0.063				
TOTAL		20	29	3	0	0	52

df = 1

α.= 0.05

$X^2_{crit} = 3.84$

$X^2_{obs} = 0.325$

Table D-3 shows the observed value of χ^2 , χ^2_{obs}, is less than χ^2_{crit}, and there is no significant difference in opinions between prosthesis A and B on size.

Table D-4: Aesthetics

Aesthetics		1	2	3	4	5	Total
Prosthesis A	Observed	2	10	14			26
	Expected	5	12	9			
	CHI_SQR	1.8	0.333	2.778			
Prosthesis B	Observed	8	14	4			26
	Expected	5	12	9			
	CHI_SQR	1.8	0.333	2.778			
TOTAL		10	24	14	2	2	52

df = 2

α.= 0.05

$X^2_{crit} = 5.99$

$X^2_{obs} = 9.822$

Table D-4 shows the observed value of χ^2, χ^2_{obs}, is greater than χ^2_{crit}, and there is a significant difference in opinions between prosthesis A and B in terms of aesthetics. In particular the lower end of the scale shows prosthesis A rated poorly by more respondents, 14 respondents compared to the 4 respondents for prosthesis B.

Table D-5: Resemblance to model C

Resemblance		1	2	3	4	5	Total
Prosthesis A	**Observed**		14		12		26
	Expected		18.5		7.5		
	CHI_SQR		1.095		2.7		
Prosthesis B	**Observed**		23		3		26
	Expected		18.5		7.5		
	CHI_SQR		1.095		2.7		
TOTAL		7	24	6	13	2	52

df = 1

α.= 0.05

$X^2_{crit} = 3.84$

$X^2_{obs} = 2.189$

Table D-5 shows the observed value of χ^2, χ^2_{obs}, is less than χ^2_{crit}, there is no significant difference in opinions for resemblance to model C between prosthesis A and B.

Appendix D

STL File specifications

Table E-1: The STL file format

Entity	Described By
The Header	80 bytes
Number of Triangles	Unsigned long integer (4 bytes)
For Each Triangle the following information appears	See Below: (50 bytes)
Normal vector I	Floating point integer (4 bytes)
Normal Vector J	Floating point integer (4 bytes)
Normal Vector K	Floating point integer (4 bytes)
First Vertex X	Floating point integer (4 bytes)
First Vertex Y	Floating point integer (4 bytes)
First Vertex Z	Floating point integer (4 bytes)
Second Vertex X	Floating point integer (4 bytes)
Second Vertex Y	Floating point integer (4 bytes)
Second Vertex Z	Floating point integer (4 bytes)
Third Vertex X	Floating point integer (4 bytes)
Third Vertex Y	Floating point integer (4 bytes)
Third Vertex Z	Floating point integer (4 bytes)
Attribute	Unsigned integer (2 bytes)

(Wright, 2001, p. 141)

Appendix E
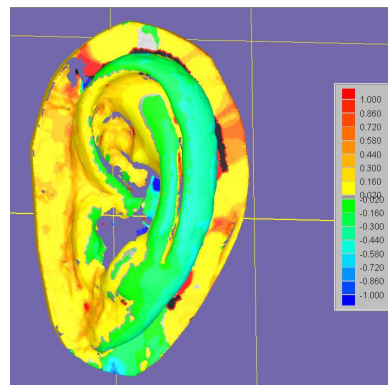
Digital comparisons

Additional figures illustrating the use of colour error maps is displayed in this appendix.
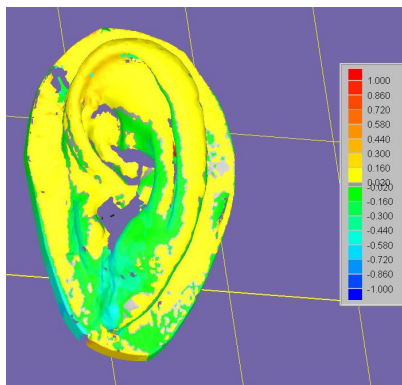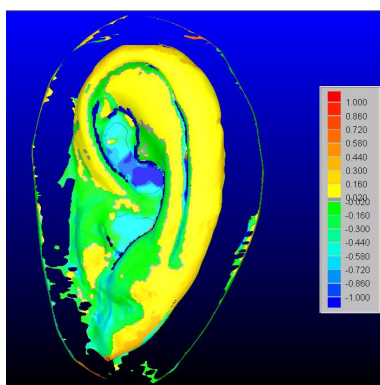

Ear 1

Reference: Breuckmann, Polyworks

Float: Breuckmann, Geomagic

Ear 1

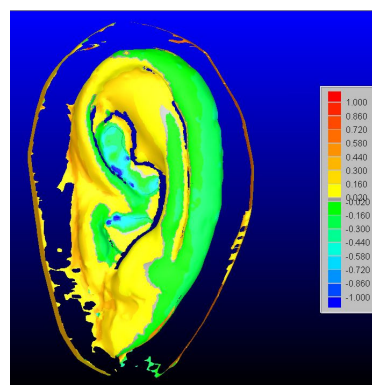Reference: Breuckmann, Polyworks

Float: Renishaw, Geomagic
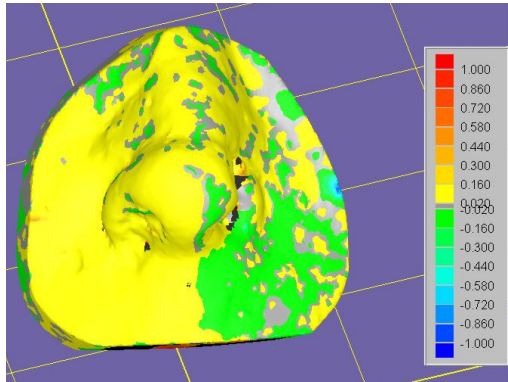

Ear 1

Reference: Renishaw, Polyworks

Float: Breuckmann, Geomagic
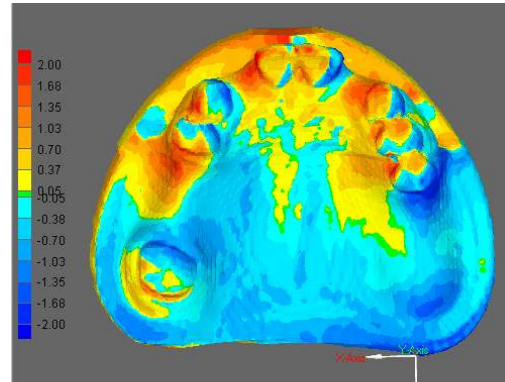

Ear 1

Reference: Renishaw Polyworks

Float: Renishaw Geomagic

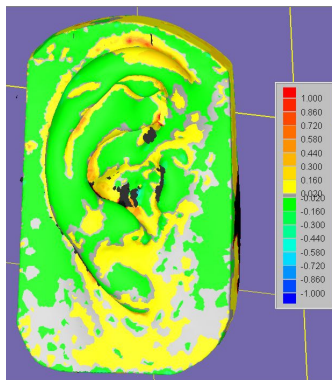Nose 1

Reference: Breuckmann, Polyworks

Float: Renishaw, Geomagic

Teeth 1

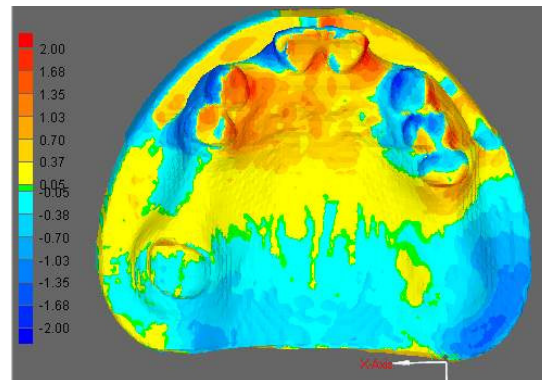Reference: Breuckmann, Polyworks

Float: Renishaw, Polyworks

Ear 2

Reference: Breuckmann, Polyworks

Float: Renishaw, Polyworks

Teeth 1

Reference: Breuckmann, Polyworks

Float: Phillips, Tomovision